AD-A050 000 GENERAL APPLIED SCIENCE LABS INC WESTBURY N Y F/G 20/4
UNSTEADY PLUME AND BLAST FIELD GENERATED BY A ROCKET LAUNCH.(U)
SEP 77 J I ERDOS F44620-76-C-0058
UNCLASSIFIED GASL-TR-246 AFOSR-TR-77-1302 NL

| OF |
AD A050000

END
DATE FILMED
3-78
DDC

AFOSR-TR- 77-1302

Approved for public release; distribution unlimited.

General Applied Science Laboratories inc.

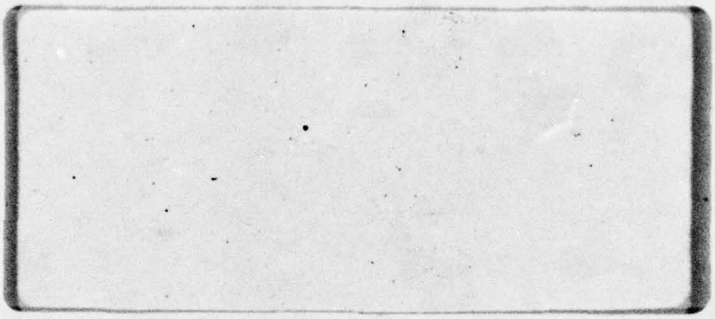

Conditions of Reproduction

Reproduction, translation, publication, use and disposal in whole or in part by or for the United States Government is permitted.

Qualified requestors may obtain additional copies from the Defense Documentation Center, all others should apply to the National Technical Information Service.

(18) AFOSR (19) TR-77-1302

(11) SEP 1977

(2)

(14) GASL-TR-246

(6) UNSTEADY PLUME AND BLAST FIELD GENERATED BY A ROCKET LAUNCH

By

(10) John I. Erdos

(12) 90 p.

(9) A FINAL REPORT, 15 JAN 76 - 14 APR 77

PREPARED FOR
AIR FORCE OFFICE OF SCIENTIFIC RESEARCH
BOLLING AIR FORCE BASE
WASHINGTON, D. C. 20332

(15) UNDER CONTRACT F44620-76-C-0058

(16) 2308

(17) A1

By

GENERAL APPLIED SCIENCE LABORATORIES, INC.
Merrick and Stewart Avenues
Westbury, New York 11590

146800

UNCLASSIFIED

SECURITY CLASSIFICATION OF THIS PAGE (When Data Entered)

REPORT DOCUMENTATION PAGE		READ INSTRUCTIONS BEFORE COMPLETING FORM
1. REPORT NUMBER AFOSR-TR- 77 - 1302	2. GOVT ACCESSION NO.	3. RECIPIENT'S CATALOG NUMBER
4. TITLE (and Subtitle) UNSTEADY PLUME AND BLAST FIELD GENERATED BY A ROCKET LAUNCH		5. TYPE OF REPORT & PERIOD COVERED FINAL 15 Jan 76 - 14 April 1977
		6. PERFORMING ORG. REPORT NUMBER GASL TR-246
7. AUTHOR(s) JOHN I ERDOS		8. CONTRACT OR GRANT NUMBER(s) F44620-76-C-0058 new
9. PERFORMING ORGANIZATION NAME AND ADDRESS GENERAL APPLIED SCIENCE LABORATORIES, INC MERRICK AND STEWART AVENUES WESTBURY, NEW YORK 11590		10. PROGRAM ELEMENT, PROJECT, TASK AREA & WORK UNIT NUMBERS 2308 A1 61102F (17) A1
11. CONTROLLING OFFICE NAME AND ADDRESS AIR FORCE OFFICE OF SCIENTIFIC RESEARCH/NA BLDG 410 BOLLING AIR FORCE BASE, D C 20332		12. REPORT DATE Sep 77
		13. NUMBER OF PAGES 89
14. MONITORING AGENCY NAME & ADDRESS (if different from Controlling Office)		15. SECURITY CLASS. (of this report) UNCLASSIFIED
		15a. DECLASSIFICATION/DOWNGRADING SCHEDULE

16. DISTRIBUTION STATEMENT (of this Report)

Approved for public release; distribution unlimited.

17. DISTRIBUTION STATEMENT (of the abstract entered in Block 20, if different from Report)

18. SUPPLEMENTARY NOTES

19. KEY WORDS (Continue on reverse side if necessary and identify by block number)

UNSTEADY AERODYNAMICS
PLUME TECHNOLOGY
BLAST WAVES
UNSTEADY TURBULENT MIXING

20. ABSTRACT (Continue on reverse side if necessary and identify by block number)

The basic fluid dynamic properties of the unsteady plume and blast field generated by ignition and launch of a rocket have been defined for the inviscid flowfield, both in terms of numerical and asymptotic solutions, subject to the assumption of spherical symmetry. The key role of the energy deposition rate in determining the boundary conditions controlling the subject problem has been discussed, as well as the general behavior of the principal structural features of the flowfield, i.e., the blast wave, contact surface and plume Mach disc. The effects of turbulent mixing in the steady exhaust stream of the rocket

DD FORM 1 JAN 73 1473 EDITION OF 1 NOV 65 IS OBSOLETE

UNCLASSIFIED

SECURITY CLASSIFICATION OF THIS PAGE (When Data Entered)

(prior to ground impingement) on the rate and duration energy disposition at the ground surface have been shown to be dominant for low acceleration rates, but negligible for very high acceleration rates; the net effect appears to desensitize the dependence of energy deposition on vehicle acceleration in the range of intermediate rates. Numerical examples are presented to illustrate the temperature, pressure and thermochemical characteristics of the unsteady flow region between the blast wave and Mach disc. The extreme temperature jump which presists across the contact surface has been emphasized as a possible cause of instability of this surface and a driving mechanism for production of turbulence (in the absence of a velocity jump across the contact surface). An unsteady turbulent mixing layer analysis has been formulated to describe conduction and diffusion across the contact surface. A two-equation second order closure model for the turbulent thermal energy (TTE) equation is postulated by analogy with Spaulding's two-equation model of the turbulent kinetic energy (TKE) equation. An integral method is used to reduce the analysis to solution of a system of coupled, first-order, ordinary differential equations. Numerical results show excellent agreement with observations of mixing layer growth in the muzzle blast of a M-16 rifle. Extension of the model to a chemically reacting system is outlined. Finally, it is pointed out that the present study has only addressed the initial formation of the propellant gas cloud at the ground surface following lift-off of the rocket. The ultimate motion and dispersion of the propellant gas cloud will be the result of buoyant forces and winds, which have not been included in this study.

TABLE OF CONTENTS

LIST OF FIGURES

LIST OF FIGURES (Continued)

LIST OF SYMBOLS

a	rate of acceleration
A	area
a_i, b_i, c_i	constants in the representation of $h_i(T)$
B	constant in the energy release power law
c	speed of sound
C_v	specific heat at constant volume
C_0, C_1, C_2, C_3	constants in the TKE and TTE closure model
e	specific internal energy
E	total energy
$\dot{E}$	total energy flux, in ground-fixed coordinates
$\langle\dot{E}\rangle$	total energy flux, in vehicle-fixed coordinates
g	acceleration due to gravity
h	specific enthalpy
I	total number of chemical species
I_{sp}	specific impulse
J_o	constant in the energy release power law
k	an integer which is 0 for planar summetry, 1 for cylindrical symmetry and 2 for spherical symmetry
$\bar{k}$	turbulent kinetic energy
k_T	eddy conductivity
ℓn	natural logarithm
L^*	characteristic length of the combustion chamber
m_o	lift-off mass of the rocket
$\dot{m}$	mass flow rate, in ground-fixed coordinates
$\langle\dot{m}\rangle$	mass flow rate, in vehicle-fixed coordinates

LIST OF SYMBOLS (Continued)

M	Mach number
M_i	molecular weight of the ith species
n	exponent in blast wave power law
p	static pressure
q	magnitude of the gas velocity vector
r	radius
R	gas constant, $R_o / \sum_{i=1}^{I} \alpha_i M_i$
R_o	energy related length scale for blast field; also universal gas constant
ΔS	specify entropy
t	time
T	static temperature
Th	thrust
u	axial component of gas velocity
u,v	tangential and normal velocity components in the mixing layer
U	tangential component of velocity at the outer edge of the mixing layer
V	rocket velocity
W	constant in the energy release power law
x,y	tangential and normal coordinates in the mixing layer
z	axial distance from nozzle exit
α_i	mass fraction of ith species
β	exponent in the energy power law
ε	dissipation term in the TKE closure model
ρ	gas density
ω_i	mass rate of production of the ith species by chemical reaction

LIST OF SYMBOLS (Continued)

μ_T	eddy viscosity
ν	laminar kinematic viscosity
ξ_i	stretched radial coordinate in ith sub-domain, i - 1 or 2
θ	temperature fluctuation , $\bar{T}$-T
ϕ	dissipation-type term in TTE closure model

SUBSCRIPTS

1,2	sub-domains of the mixing layer and of the unsteady shock layer; also break points in the E vs t curve
c	contact surface
e	exhaust stream averaged; also plume edge value; also nozzle exit
f	chemically frozen
i	ignition; also chemical species index
ℓ	lift-off
m	Mach disc
o	initial value; also at nozzle exit plane
r	reference value
s	shock or blast wave
∞	ambient, atmospheric condition

SUPERSCRIPTS

*	evaluated at sonic line
'	turbulent, fluctuating value
-	time averaged value

1. PROBLEM STATEMENT

1.1 Background - The unsteady exhaust plume and blast field generated by a rocket launch has been of concern in the past principally to those responsible for the structural integrity of the launch pad and/or adjacent structures. The transient thermal loads and forces may be conservatively estimated without recourse to detailed analysis of the plume flowfield. However, the steady exhaust plume flowfield has been studied in careful detail at both high and low altitude, since it may provide a trail of optically and/or electromagnetically observable gases suitable for remote detection and tracking of a launch vehicle, and possibly diagnostic information as well. The objective of early detection has pressed interest to the lowest practical altitudes, but the unsteady exhaust plume and blast field at ignition has not been addressed in this context since any signal (optical, electromagnetic or acoustic) is largely attenuated by the atmosphere near sea level. However, the plume technology base is nevertheless incomplete without an adequate description of the plume flowfield at ignition and lift-off.

1.2 General Description of the Flowfield - The unsteady flowfield at ignition of a rocket, as depicted in Figure (1) bears certain resemblances to the muzzle blast field of a gun or mortar, shown in Figure (2). Both share structural features common to the steady underexpanded rocket exhaust plume; principally, the now-familiar underexpanded supersonic core, barrel shocks and Mach disc. The steady exhaust plume is most frequently depicted in a vehicle-fixed frame of reference, with the vehicle far away from the ground surface. In this situation, the exhaust plume near the vehicle is, on the average, steady and predominately supersonic. Turbulent mixing eventually decelerates the plume to entirely subsonic conditions further from the vehicle, and asymptotically far from the vehicle to a randomly fluctuating field to be dispersed by prevailing winds, buoyant forces or simply dissipated by viscous stresses. However, the picture is considerably altered at launch, due to the interaction of the plume with the ground plane. In simplest terms, an unsteady plume spreads over the ground surface, displacing the air around it. The unsteady plume collapses as the vehicle leaves the vicinity of the ground plane, and the remaining propellant

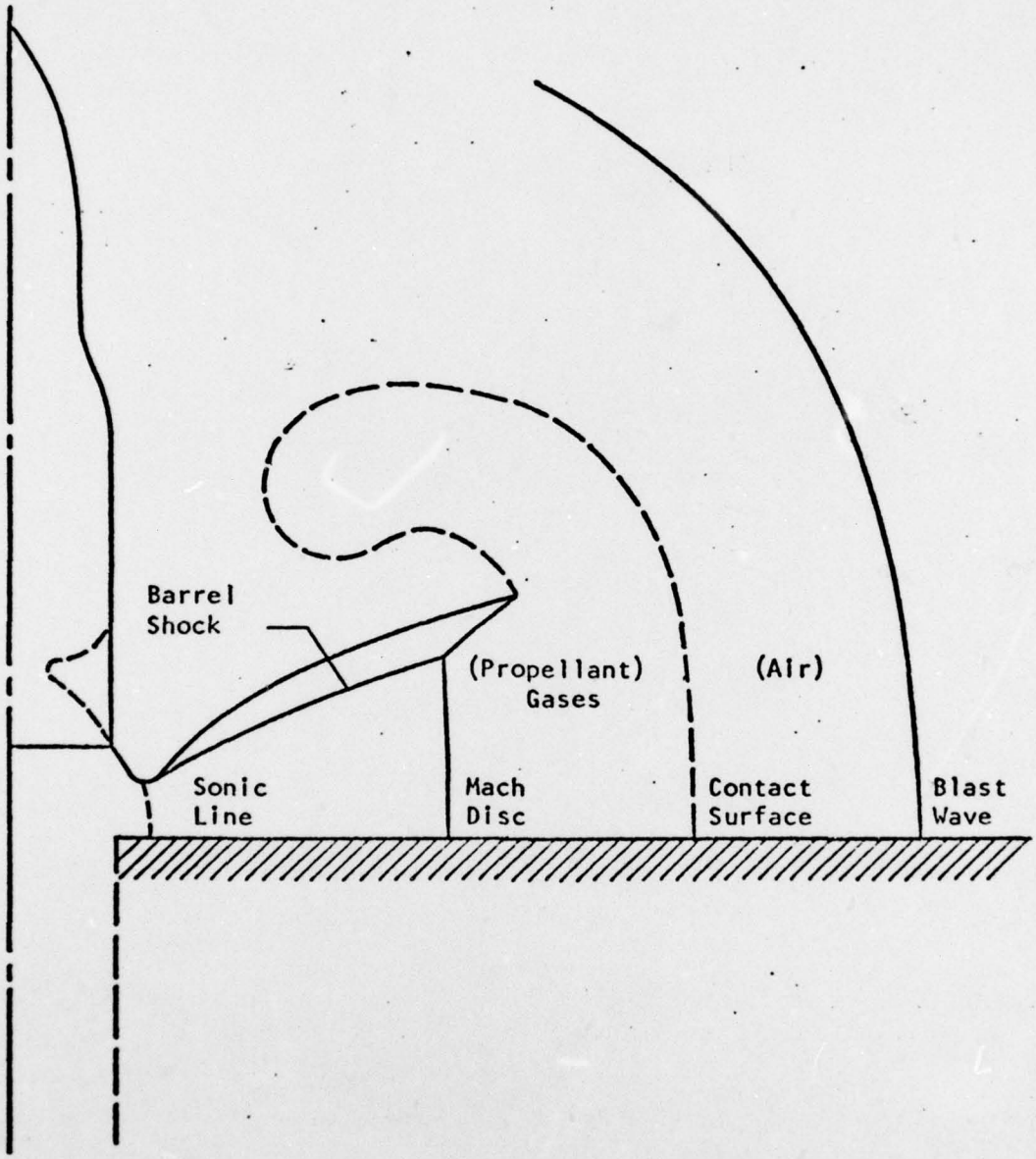

FIGURE 1. STRUCTURE OF IGNITION PHASE BLAST FIELD

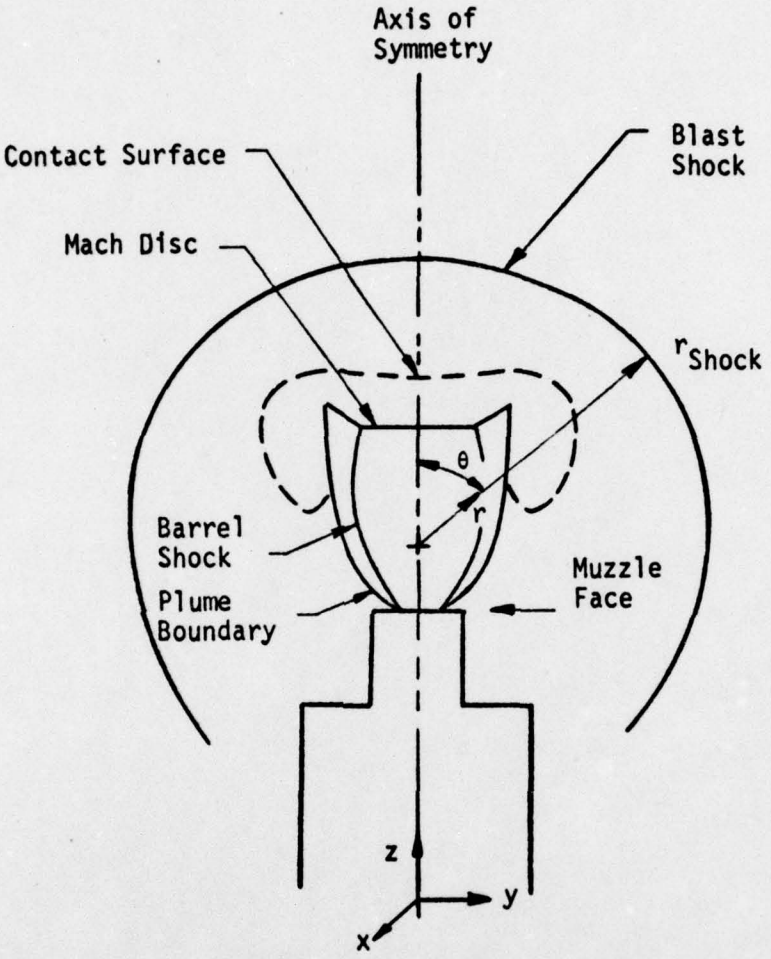

FIGURE 2. STRUCTURE OF BLAST FIELD OF A SMALL CALIBER (5.56MM) RIFLE

gas cloud is eventually dispersed by prevailing winds and buoyant forces. During the interim period, however, the unsteady plume will produce a blast field and flash analogous to (although perhaps less intensely than) the well-known muzzle blast and flash of a gun. The strength of the blast field, as measured in terms of overpressure, will depend on factors like the ignition time, vehicle acceleration, etc. The flash intensity will depend on these factors plus afterburning of unburnt propellant and/or combustion products, opacity of the surrounding layers, etc.

1.3 Present Approach - Obviously, the subject problem is very complex to describe in complete detail. However, it can be reduced to an assembly of component problems for which approximate solutions are tractable, which yield physical insights to the overall problem, and from which limited scaling laws suitable for certain applications can be derived. The present report summarizes the results of study of the various component problems and attempts to bring them together into a unified, although approximate, description of the main features of the unsteady plume and blast field generated by a missile launch.

The present approach to the subject problem derives in a large part from previous work on muzzle blast field analyses for guns[1,2]. These, in turn, initially viewed the muzzle blast as a spherical explosion, with a constant rate of energy addition[3]. This approach successfully described the trajectory of the leading shock wave at early times, and thus lent credibility to further exploitation of the assumption of spherical symmetry. The asymptotic shock motion was subsequently[2] described by Whitham's theory[4]. This approach also clearly identified the rate and duration of energy addition as primary parameters controlling the blast field. Accordingly, the rate and duration of energy deposition at the ground surface from an accelerating rocket is derived in Section III. The asymptotic inviscid structure of the plume and blast field is reviewed in Section IV. Description of the actual thermochemical properties in the unsteady inviscid shock layer requires numerical solution of the governing equations; the methodology and sample solutions are presented in Section V. A simple model of the unsteady turbulent mixing layer that develops along the interface between the exhaust gases and the air has been developed and is discussed in Section VI.

Finally, in Section VII an overview of the problem is presented in terms of the model derived herein, and conclusions are discussed.

II. DESCRIPTION OF THE PRESENT MODEL

2.1 Time Scales - A rocket motor begins to transfer thermal and kinetic energy to atmosphere upon emergence of the leading pressure wave from nozzle. After a series of reflections of pressure waves within the combustion chamber, an approximately constant chamber pressure and burning rate is achieved, if the combustion process is stable, producing correspondingly constant thrust and energy flux rate in the exhaust. The ignition transient period (for a solid propellant)* is of the order[5]:

$$t_i/c_r/L^* = 10 \text{ to } 20 \qquad (1)$$

For example, using $L^* = 10$ feet and $c_r = 3000$ ft/sec as representative values, give ignition times of about 30 to 60 milliseconds.

As the vehicle lifts off, the rate of energy deposition in the atmosphere at the launch site varies due to a combination of relative motion between the vehicle and the ground surface, and turbulent mixing of the exhaust gases and the surrounding air. For the present purposes, lift-off is considered complete when the rate of energy deposition at the launch site drops to zero. The lift-off period, t_ℓ, is thus defined as the time from ignition to completion of lift-off. It will be shown subsequently that this period ranges from about 5 seconds for a high acceleration (100 g) launch to about 12 seconds for a low acceleration (1.2 g) launch. In the high acceleration case, $t_\ell \sim a^{-1}$; thus even a five-fold increase in acceleration (500 g) will still result in $t_\ell > 10t_i$. Therefore, for a very wide range of conditions of interest, ignition is virtually instanteous on the time scale of lift-off, and the two proecesses may be considered independently.

2.2 Flow Pattern - In view of the different time scales for ignition and lift-off, the interaction of the rocket plume and the ground plane can be regarded as the impingement of an established, steady plume on a moving, planar

*Liquid propellant ignition transient periods have not been examined, but should be of a comparable order, i.e., the time for about 10 to 20 wave reflections in the combustion chamber.

surface, as indicated schematically in Figure (3). The flow is turned from vertical to horizontal through a shock (Mach disc) and subsonic stagnation point type flow pattern. The flow then expands radially outward along the ground surface. The flow can either continue to decelerate, thus remaining subsonic, or can re-expand becoming supersonic very quickly; the former case leads to a continuously increasing pressure which in general cannot match the prevailing atmospheric pressure, whereas the latter gives rise to a cylindrically symmetric supersonic plume pattern (as indicated in Figure 1) in which the flow shocks up to the prevailing back pressure, through a Mach disc, as in the case of a muzzle blast field[1]. Thus the supersonic plume pattern is assumed to prevail, in general. This pattern has also been observed experimentally in this case steady, underexpanded, sonic jet impinging on a wall[6].

Since the ignition time is short relative to the lift-off time, the flowfield can be considered to begin impulsively. Accordingly, a leading pressure wave is driven ahead of the expanding propellant gases into the ambient atmosphere. Under suitable conditions, this wave can be represented by a semi-spherical blast wave, which asymptotically deteriorates to a sound wave, having it origin at the point of impingement of the exhaust gases on the ground surface. As in the muzzle blast case , the effective origin may actually be a ring within the cylindrically symmetric supersonic plume which forms along the surface, leading to a distortion of the assumed semi-spherical shock shape, but, like the muzzle blast, the distortion is probably most pronounced at very early times and asymptotically negligible.

As in a muzzle blast, the flowfield is quickly engulfed by turbulence, and the inviscid structure shown in Figure (3) at time t_1 is covered by a turbulent cloud as indicated at time t_2. In the present problem, the exhaust plume shear layers present one evident source of turbulence due to velocity jumps in the inviscid flow. However, as in the muzzle blast, the extreme temperature jump across the radially expanding front between the propellant gases and air (termed the contact surface in Figure 1) presents another source of turbulence. Although the effects of turbulent mixing are important, the inviscid structure of the flowfield must be determined first. The turbulent mixing processes can then be

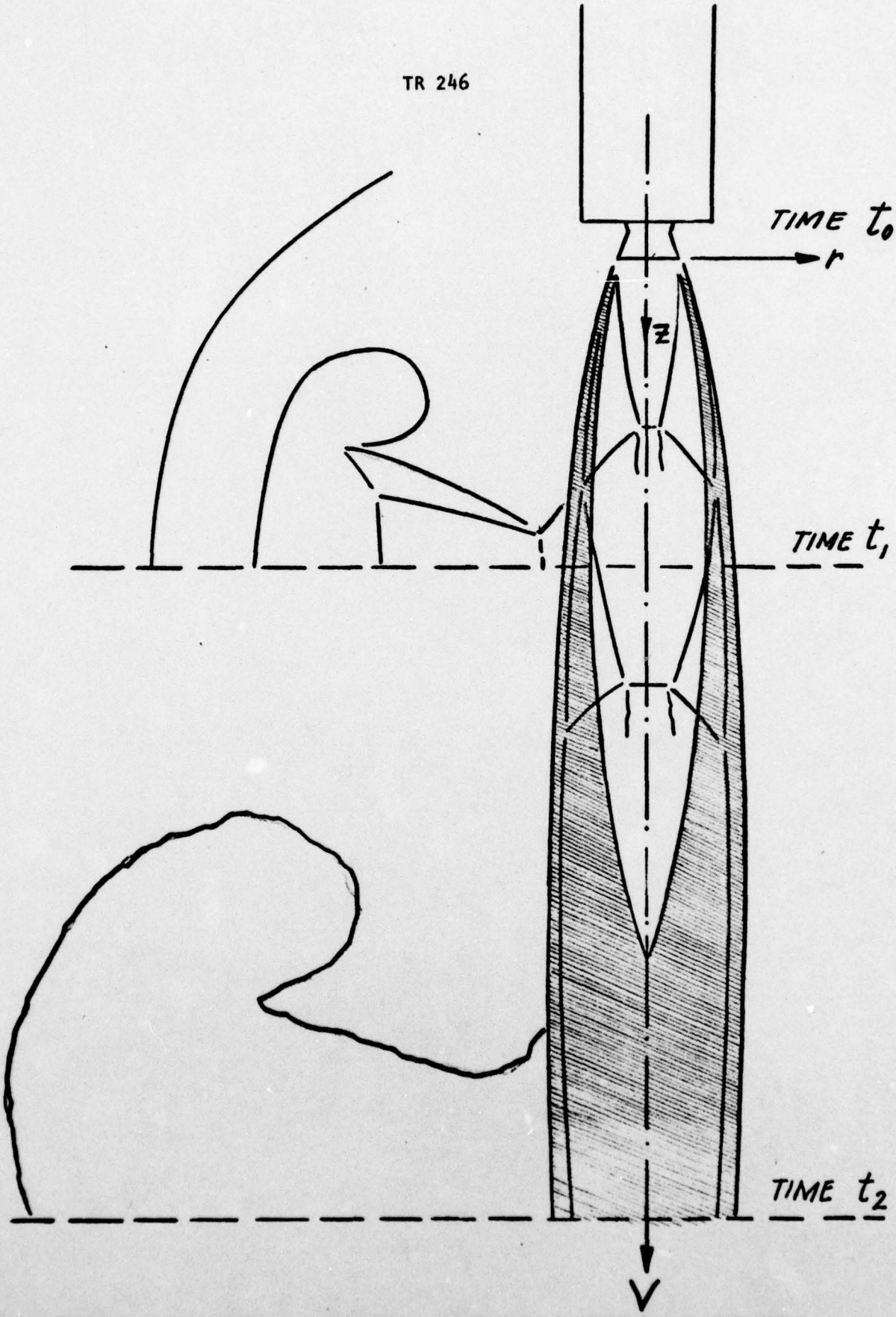

FIGURE 3. SCHEMATIC OF INTERACTION OF STEADY EXHAUST PLUME WITH THE GROUND SURFACE

superimposed on the inviscid solution, in the usual vein of boundary layer theory, as a first approximation.

III. ENERGY DEPOSITION

3.1 General Remarks - In an earth-fixed frame of reference, the rocket motor can be regarded simply as a source of high temperature, high pressure gases released into the atmosphere in an confined stream which impinges on the ground. The point of impingement can, in turn, be viewed as an effective source of energetic gases which spread over the ground as an unsteady plume and blast field. This source is fed by the exhaust stream of the rocket motor. Since, as noted, the ignition transient time is short relative to the lift-off time, the process can be considered to begin impulsively.

In this source-flow approximation, the similitude solutions of blast wave theory apply, and the boundary conditions can be stated in terms of one-dimensional flow representations of the rocket exhaust gases. The boundary conditions controlling the supersonic plume can be approximated from the same one-dimensional model. However, the blast wave solutions can be stated in terms of the rate of energy depositon, whereas the plume additionally requires the knowledge of the mass flow rate, since the plume is two-dimensional while the blast solution is one-dimensional.

3.2 Inviscid Scaling - A brief review of the essential elements of the theory of variable energy blast waves[3] is informative with respect to the subject problem. In particular, the energy released at the source of the blast wave must conform to the power-law;

$$E(t) = Wt^{\beta} \tag{2}$$

where W and β are constants. The shock wave trajectory is then given by:

$$r_s = B^{-1} t^n \tag{3}$$

where

$$W = B^{-(j+3)} p_\infty n^2 J_o^2/c_\infty^2 \tag{4}$$

$$n = (\beta+2)/(j+3) \tag{5}$$

$$J_o\ (n,j,\gamma) = \text{constant}, \quad \text{and } B = \text{constant} \tag{6}$$

The index j is 2 for spherical symmetry (as in the present case), 1 for cylindrical symmetry and 0 for planar symmetry. Thus, with j = 2 and β = 0 the classical point explosion solution, n = 2/5, is recovered, whereas with β = 1 the solution for a constant rate of energy addition, n = 3/5, is obtained.

Few actual processes of interest conform to a power law variation, although a combination of different power laws for different periods can provide a reasonable approximation to the total energy release rate. In the present problem the combination of $\beta \simeq 1$ for $0 < t \leq t_1$, $\beta < 1$ for $t_1 < t \leq t_2$ and $\beta \simeq 0$ for $t > t_2$ will prove to be appropriate. However, the validity of blast wave theory, or of scaling based on blast theory variables, may be questioned if $\beta \neq$ constant. Dabora[3] suggested use of a length scale R_o based on the total amount of energy released as $t \to \infty$. In the present case this length scale is

$$R_o = (2E(t_2)/P_\infty)^{1/3} \tag{7}$$

where $dE/dt = 0$ for $t > t_2$, and the factor of 2 has been inserted to account for symmetry with respect to the ground plane. Finite difference solutions for variable β and widely differing values of R_o were examined in Reference (2); the trajectories of the blast wave, and the contact surface were found to correlate according to:

$$r_s/R_o = f_1\ (t\ c_\infty/R_o) \tag{8}$$

$$r_c/R_o = f_2\ (t\ c_\infty/R_o) \tag{9}$$

for $t < t_2$. Examples are shown in Figures (4) and (5), where the data points are taken from the numerical solutions of Reference (2) for various size and type high muzzle velocity weapons. The Mach disc position was also found to be correlated by:

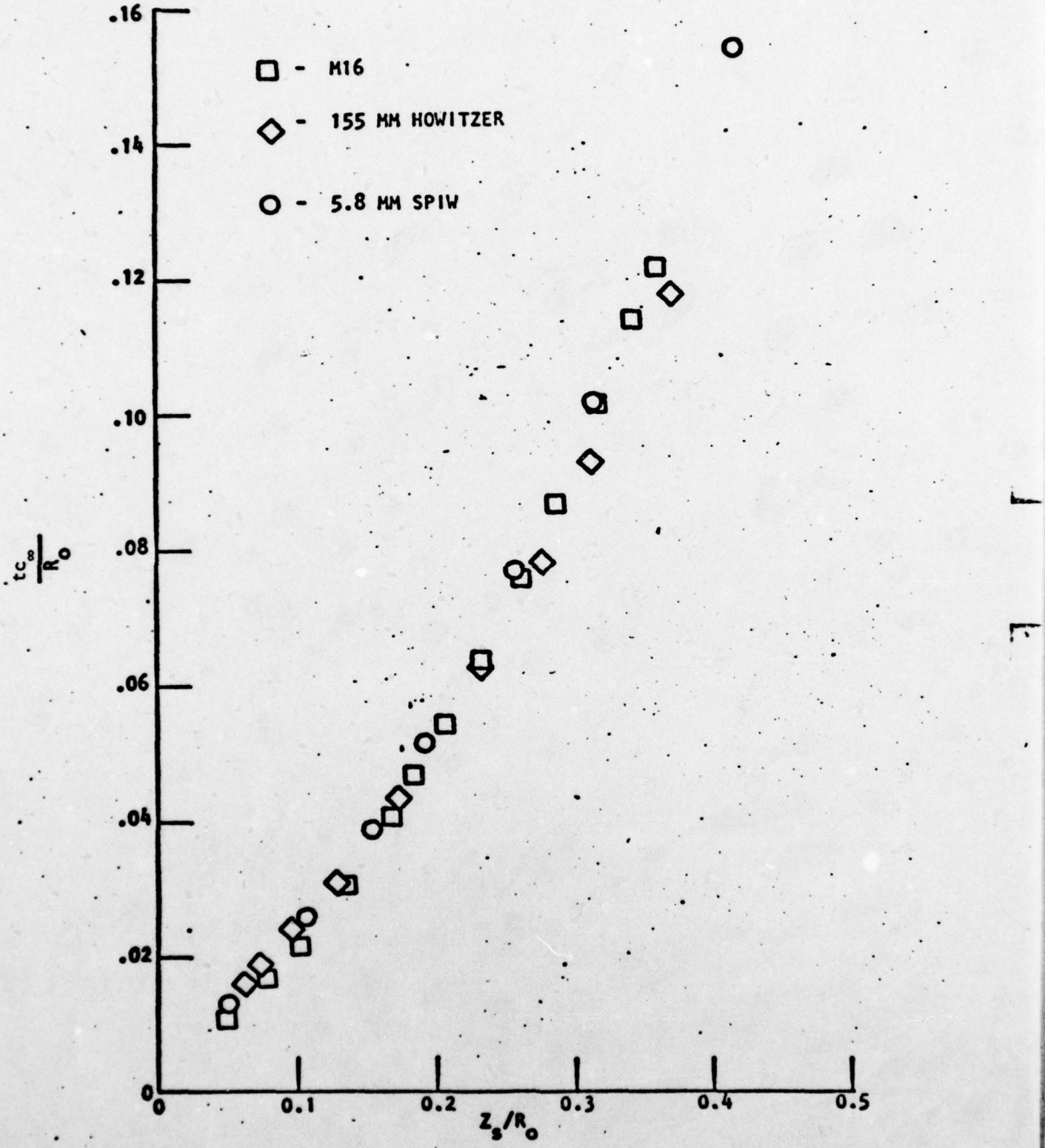

FIGURE 4. CORRELATION OF BLAST WAVE TRAJECTORIES IN THE NEAR FIELD

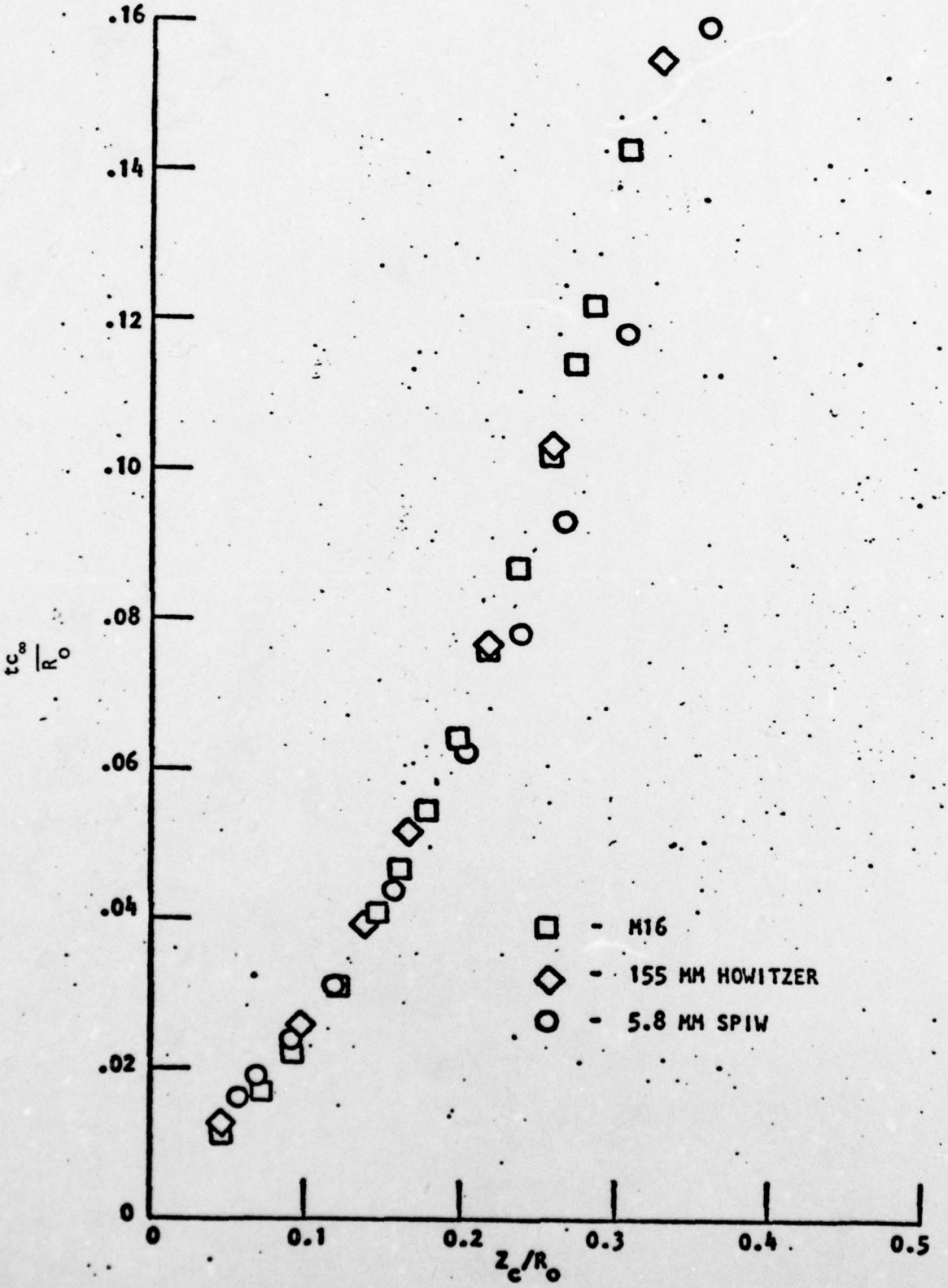

FIGURE 5. CORRELATION OF CONTACT SURFACE TRAJECTORIES IN THE NEAR FIELD

$$r_m/R_o = f_3\ (t\ c_\infty/R_o) \tag{10}$$

for $t << t_2$. The behavior of the Mach disc for $t \to t_2$ will be discussed later.

For values of $t >> t_2$ the shock trajectory decays to the weak shock solution of Whitham[4]:

$$r_s = c_\infty t + R_o \log^{\frac{1}{2}} (r_s/R_o) \simeq c_\infty t \tag{11}$$

while the contact surface tends toward a constant of order R_o. However, the Mach disc collapses back to origin as $t \to t_2$. It is pointed out parenthethically, that as this limit is approached, the pressure becomes atmospheric everywhere except immediately adjacent to the shock, and the (frozen) temperature of the propellant gases approaches

$$T \simeq T_\infty \exp\ (\Delta S/C_v) \tag{12}$$

where ΔS refers to the entropy increment in the propellant gases produced by the combination of combustion and shock heating. Thus a substantial temperature increment across the contact surface will persist (in the absence of mixing) as $t \to \infty$.

Therefore, determination of the rate of energy deposition is essential to specification of the boundary conditions on the subject problem and of the length scale for the inviscid structure of the flowfield.

3.3 Mass Flow Rate - The energy flow rate in the rocket exhaust is given by the product of the total specific energy and the mass flow rate. For this reason, and another to be discussed, it is of interest to consider first the rate of mass flow impinging on the ground surface:

$$\dot{m} = 2\pi \int_0^{r_e} \rho\ (u-V) r dr \tag{13}$$

where r_e is the plume radius, u the gas velocity in vehicle-fixed coordinates, and V the vehicle velocity, or equivalently the velocity at which the ground surface recedes from the vehicle. In the absence of mixing, the mass flow rate in vehicle-fixed coordinates is constant:

$$\langle \dot{m} \rangle = 2\pi \int_0^{r_e} \rho u r dr = \rho_e u_e A_e \tag{14}$$

or

$$\rho_e A_e = 2\pi \int_0^{r_e} \rho r dr \tag{15}$$

$$u_e(z) = \frac{\langle \dot{m} \rangle}{\rho_e A_e} \tag{16}$$

Thus

$$\dot{m} = \langle \dot{m} \rangle (1 - V/u_e) \tag{17}$$

The vehicle velocity is easily obtained, assuming a vertical launch:

$$V = g\, Isp \left[\log \left(1 + \left(\frac{Th}{m_o g}\right) \frac{t}{Isp} \right) - \frac{t}{Isp} \right] \tag{18}$$

$$\simeq gt \left[\left(\frac{Th}{m_o g}\right) - 1 \right], \text{ for } \frac{t}{Isp} \ll \left(\frac{Th}{m_o g}\right)^{-1} \tag{19}$$

Using

$$u_e \simeq g\, Isp \tag{20}$$

and

$$\langle \dot{m} \rangle = Th/g\ Isp \tag{21}$$

the inviscid approximation to the mass flow rate is:

$$\dot{m} = \frac{Th}{g\ Isp}\left[1 + \frac{t}{Isp} - \log\left(1 + \left(\frac{Th}{m_o g}\right)\ \frac{t}{Isp}\right)\right] \tag{22}$$

$$\simeq \frac{Th}{g\ Isp}\left[1 - \frac{t}{Isp}\ \left(\frac{Th}{m_o g} - 1\right)\right], \quad \text{for} \quad \frac{t}{Isp} << \left(\frac{Th}{m_o g}\right)^{-1} \tag{23}$$

This expression yields $\dot{m} \simeq Th/gIsp$ = constant when $t/Isp << (Th/m_o g - 1)^{-1}$, and $\dot{m} \to 0$ as $[\log(1 + (\frac{Th}{m_o g})\ \frac{t}{Isp}) - \frac{t}{Isp}] \to 1$; i.e., a very slow rate of decrease in the mass flow rate at the ground surface. Returning to Equation (17), it is obvious that in this inviscid approximation, $\dot{m} \to 0$ only as the vehicle velocity approaches the exhaust gas velocity.

Mixing can be expected to have two important but opposing effects on the inviscid result expressed by Equation (17) or (22). First, the mass flow rate in the plume $\langle \dot{m} \rangle$ will increase due to entrainment of additional mass from the atmosphere, and second, the (mass-averaged) exhaust gas velocity $u_e(z)$ will decrease due to momentum transfer with the atmosphere. These effects have been examined by using actual mixing calculations[7] for a full-scale, single nozzle, rocket motor producing approximately 2×10^6 N thrust at sea level, with an effective exhaust velocity of $u_e \simeq 2800$ m/s and a nozzle exit radius of about 0.9m. The conversion from vehicle-fixed (axial distance,z) to ground-fixed (time,t) coordinates was made using Equation (18), i.e.:

$$z = \int_o^t V dt = g\ Isp\ t \left\{ \frac{1 + (\frac{Th}{m_o g})\ \frac{t}{Isp}}{(\frac{Th}{m_o g})\ \frac{t}{Isp}} \log\left[1 + \left(\frac{Th}{m_o g}\right)\ \frac{t}{Isp}\right] - 1 - \frac{t}{2Isp} \right\} \tag{24}$$

$$\simeq g \frac{t^2}{2} \left(\frac{Th}{m_o g} - 1\right), \quad \text{for } \frac{t}{Isp} << \left(\frac{Th}{m_o g}\right)^{-1} \tag{25}$$

Representative curves of non-dimensional mass flow rate, i. e., $\dot{m}/\langle\dot{m}\rangle$, are shown in Figure (6), using Isp = 250 s and $Th/m_o g$ = 1.17, 1.25, 1.50 and 2.00. It is evident that mixing first produces a marked increase in the mass flow rate relative to the inviscid value, up to nearly a factor of 10 in the lowest acceleration case, but then an abrupt cut-off occurs as u_e is decreased and approaches V. As the acceleration rate increases, the entrainment of additional mass decreases, but the cut-off occurs earlier and more abruptly. It is also evident that the viscous solution at $Th/m_o g$ = 2.0 bears no resemblence to the corresponding inviscid solution. The range of validity of the inviscid solution will be explored further in the following discussion; the point here is to emphasize the effects on the mass flow rate produced by mixing.

3.4 Energy Deposition Rate - The energy flux at the ground surface is given by:

$$\dot{E}(t) = \left\{ 2\pi \int_o^{r_e} \rho(u-V) \left[\Sigma\alpha_i \left(\int_o^T C_{v_i}\, dT + \Delta e_o \right) + \frac{1}{2} q^2 \right] r\, dr \right\}_{z=\int V dt} \tag{26}$$

where the contributions of thermal, chemical and kinetic energy have been included. The corresponding energy flux in the steady exhaust plume, in vehicle-fixed coordinates, is given by:

$$\langle\dot{E}(z)\rangle = 2\pi \int_o^{r_e} \rho u \left[\Sigma\alpha_i \left(\int_o^T C_{v_i}\, dT + \Delta e_o \right) + \frac{1}{2} q^2 \right] r\, dr \tag{27}$$

Again assuming inviscid flow, $q \simeq u \simeq gIsp$, and $e \simeq h << \frac{1}{2}q^2$, gives:

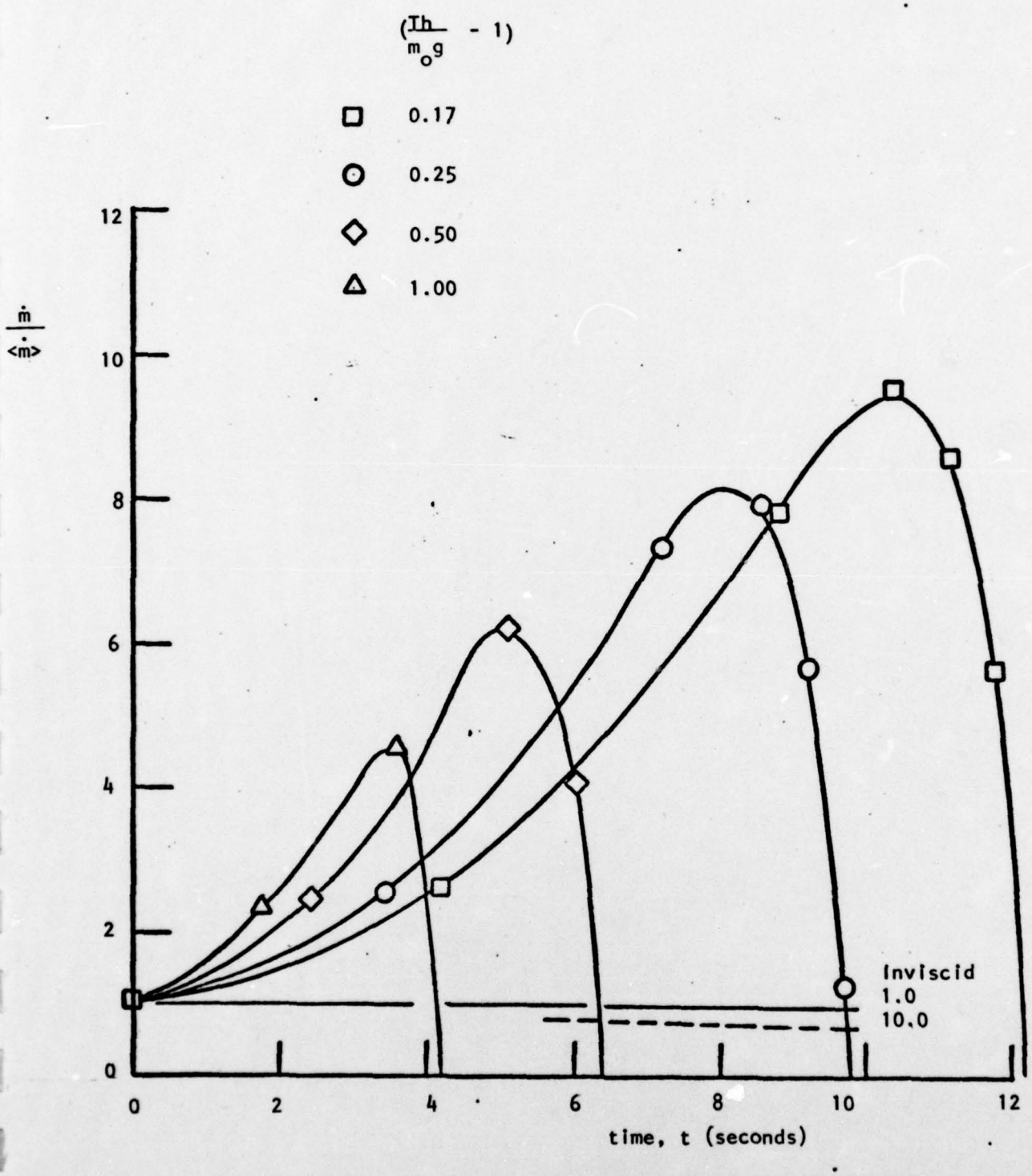

FIGURE 6. MASS FLUX INTO THE UNSTEADY PLUME AT GROUND LEVEL

$$\langle \dot{E}(z) \rangle \simeq \langle \dot{E}_o \rangle = g\, Isp \left(\frac{p_e A_e}{\gamma - 1} + \frac{1}{2} Th \right) \tag{28}$$

Thus:

$$\dot{E}(t) \simeq \langle \dot{E}_o \rangle \left(1 - V/g\, Isp\right) \tag{29}$$

and

$$E(t) = \int_o^t \dot{E}\, dt \simeq \langle \dot{E}_o \rangle\, t \left\{ 2 + \frac{t}{2Isp} - \frac{1 + \left(\frac{Th}{m_o g}\right) \frac{t}{Isp}}{\left(\frac{Th}{m_o g}\right) \frac{t}{Isp}} \log \left(1 + \left(\frac{Th}{m_o g}\right) \frac{t}{Isp}\right) \right\} \tag{30}$$

In accord with the notation adopted earlier, $dE/dt \to 0$ for $t > t_2$, and $E(t_2)$ denotes the total amount of energy deposited at the launch site. Then, from Equation (30), $E(t) = E(t_2)$ for

$$\log \left(1 + \left(\frac{Th}{m_o g}\right) \frac{t_2}{Isp}\right) - \frac{t_2}{Isp} = 1 \tag{31}$$

If $t_2/Isp \ll 1$ and $Th/m_o g \gg 1$ (i.e., a high acceleration launch), then:

$$t_2 \simeq (e - 1)\, Isp\, (Th/m_o g)^{-1} \simeq 1.718\, Isp\, (Th/m_o g)^{-1} \tag{32}$$

and

$$E(t_2)/\langle \dot{E}_o \rangle \simeq Isp\, (Th/m_o g)^{-1} \left\{ 5.905 \left(\frac{Th}{m_o g}\right)^{-1} + 0.718 \right\} \tag{33}$$

or

$$E(t_2) \simeq g\, Isp^2 \; \frac{\left(\frac{p_e A_e}{\gamma - 1} + \frac{1}{2} Th\right)}{\left(\frac{Th}{m_o g}\right)} \left\{ 5.905 \left(\frac{Th}{m_o g}\right)^{-1} + 0.718 \right\} \tag{34}$$

$$\simeq 0.36\, m_o\, (g\, Isp)^2 \quad \text{for} \quad \left\{ \begin{array}{l} \frac{\gamma-1}{2} \; \frac{Th}{p_e A_e} >> 1 \\ \\ \frac{Th}{m_o g} >> 1 \end{array} \right\} \tag{35}$$

Equations (32) and (35) provide very simple formulas for the time required to complete the deposition of energy at the launch site, i.e., the lift-off time, and the total amount of energy deposited, which may be compared to the "exact" inviscid solution given by Equation (30). Solutions to Equation (30) for a range of values of $Th/m_o g$ are presented in Figure (7). The values of t_2 and $E(t_2)$ given by Equations (32) and (35) are also shown in Figure (7) as data points for values of $(Th/m_o g - 1) = 100$, 50, 20 and 20. It can be seen that Equations (32) and (35) predict t_2 and $E(t_2)$ very well for $(Th/m_o g - 1) = 100$, but the prediction of $E(t_2)$ becomes less accurate for lower acceleration rates, and is over-estimated by a factor of 2 at $(Th/m_o g - 1) = 10$. However, the lift-off time t_2 remains quite accurate over the considered range. It is also apparent from this figure that the (inviscid) energy release given by Equation (30) can be represented by a power law, i.e., Equation (2), with $\beta = 1$ up to a time t_1 such that $(Th/m_o g)\,(t_1/Isp) << 1$. A reasonable approximation is

$$\beta = \left\{ \begin{array}{ll} 1 & t \leq t_1 = 0.1\, Isp/(Th/m_o g) \\ \\ (t_2 - t)/(t_2 - t_1) & t_1 < t < t_2 \\ \\ 0 & t \geq t_2 = 1.72\, Isp/(Th/m_o g) \end{array} \right\} \tag{36}$$

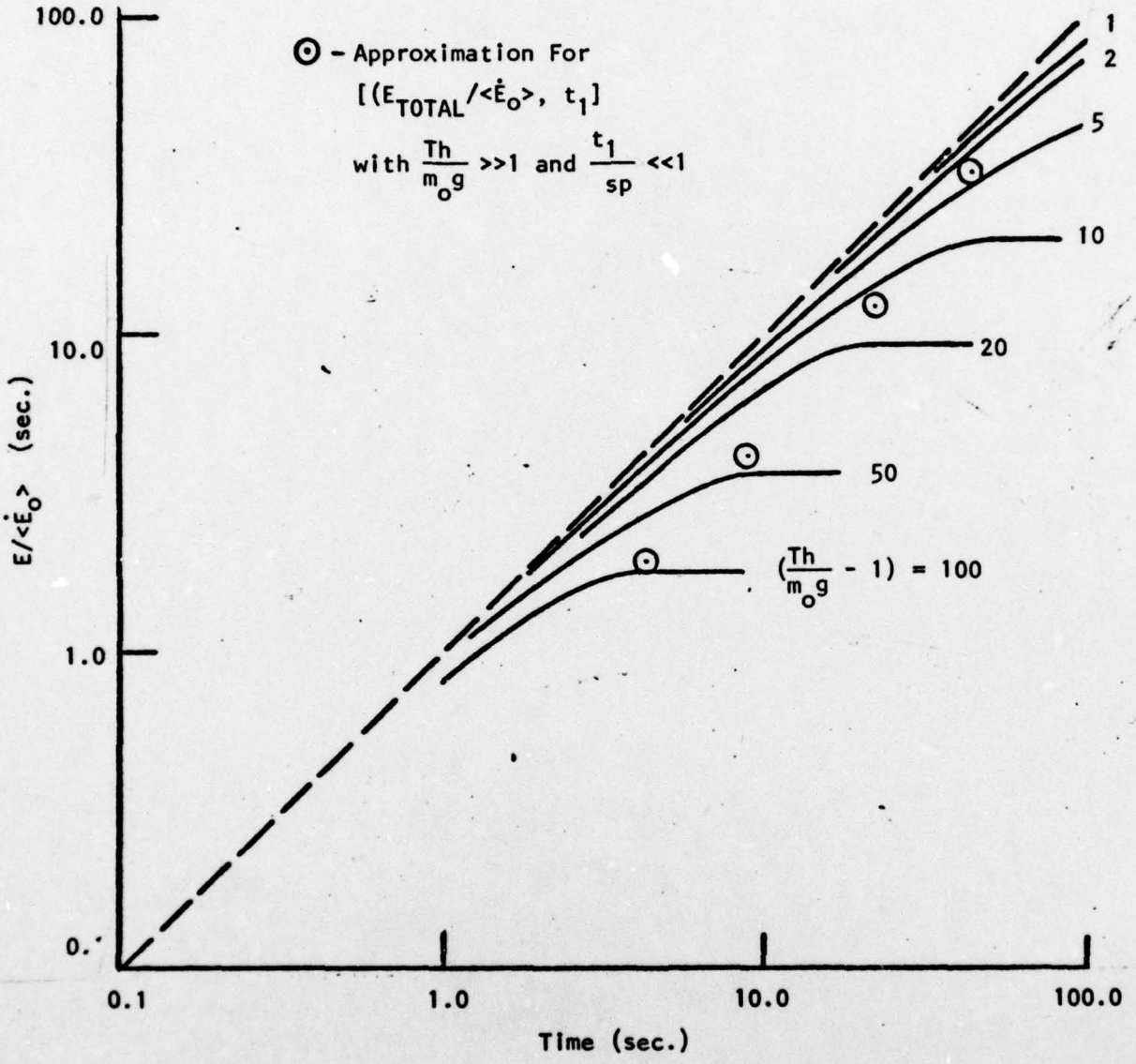

FIGURE 7. INVISCID APPROXIMATION FOR ENERGY DEPOSITED INTO THE UNSTEADY PLUME AT GROUND LEVEL

However, these results must now be qualified by examining the effect of viscosity, which has been shown to predominate the mass flow results. Equation (26) has been evaluated using the previously cited steady plume solution with turbulent mixing[7] to produce the curves displayed in Figure (8). Comparison of Figures (8) and (6) indicates that the initial growth of energy flux, $\dot{E}$, and its subsequent rapid cut-off are largely the result of the corresponding growth and cut-off of the mass flow rate. These curves have been integrated to obtain the total energy released E(t), corresponding to Equation (30). The viscous and inviscid results are compared in Figure (9). It is clear that mixing reduces dramatically both the total amount of energy deposited at the launch site, $E(t_2)$, and the lift-off time, t_2, as well as increasing the rate of energy deposition; $\beta > 1$ for $t < t_2$.

The viscous calculations were not carried to higher accelerations, i.e., $Th/m_o g \gg 2$, because the nozzle exit plane would be closer to the ground at time t_2 than the first axial station of the steady plume solution[7] selected for integration. The first axial station selected was that at which the turbulent mixing layer just reached the plume axis; thus viscous effects would diminish significantly at stations closer to the nozzle exit plane. Therefore, it is clear that the inviscid solutions must represent the actual behavior for sufficiently high acceleration rates, e.g., $Th/m_o g > 20$. The dependence of $\dot{E}/\langle \dot{E}_o \rangle$ on $Th/m_o g$ will therefore be controlled by turbulent mixing for low acceleration rates, $Th/m_o g < 2$, but will be essentially inviscid at high acceleration rates, $Th/m_o g > 20$. A minimum in the ratio $\dot{E}/\langle \dot{E}_o \rangle$ may be expected, as suggested in Figure (10), for acceleration rates in the intermediate range $2 < Th/m_o g < 20$. However, the transition curve from the viscous to inviscid solution shown in this figure is conjectured.

3.5 Representative Values of R_o and t_2 - To demonstrate some representative values, consider a specific impulse Isp=250s and a thrust $Th = 2\times10^6$ N. As a very low acceleration lift-off example, take $Th/m_o g = 1.17$, for which the viscous solution clearly applies. Assume $p_e A_e \approx Th/10$ and $\gamma = 1.20$, giving an initial (nozzle exit plane) energy flux $\dot{E}_o = 4.9\times10^9$ N·m/s and a total energy deposition at the ground surface $E = 2\times10^{11}$ N·m. Thus $R_o \approx 157$m and $t_2 \approx 12$s in

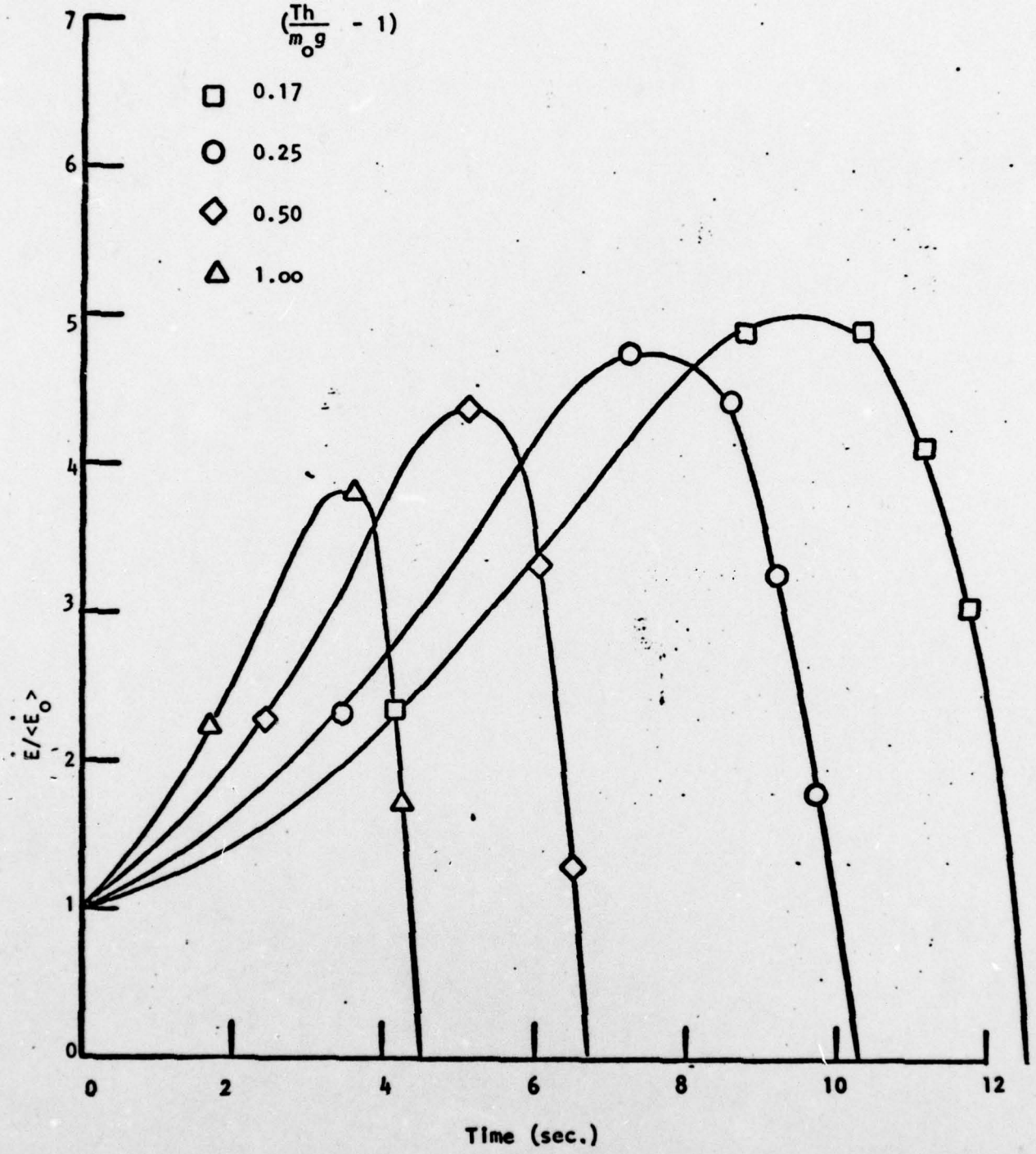

FIGURE 8. ENERGY DEPOSITION RATE INTO THE UNSTEADY PLUME AT GROUND LEVEL (INCLUDING TURBULENT MIXING).

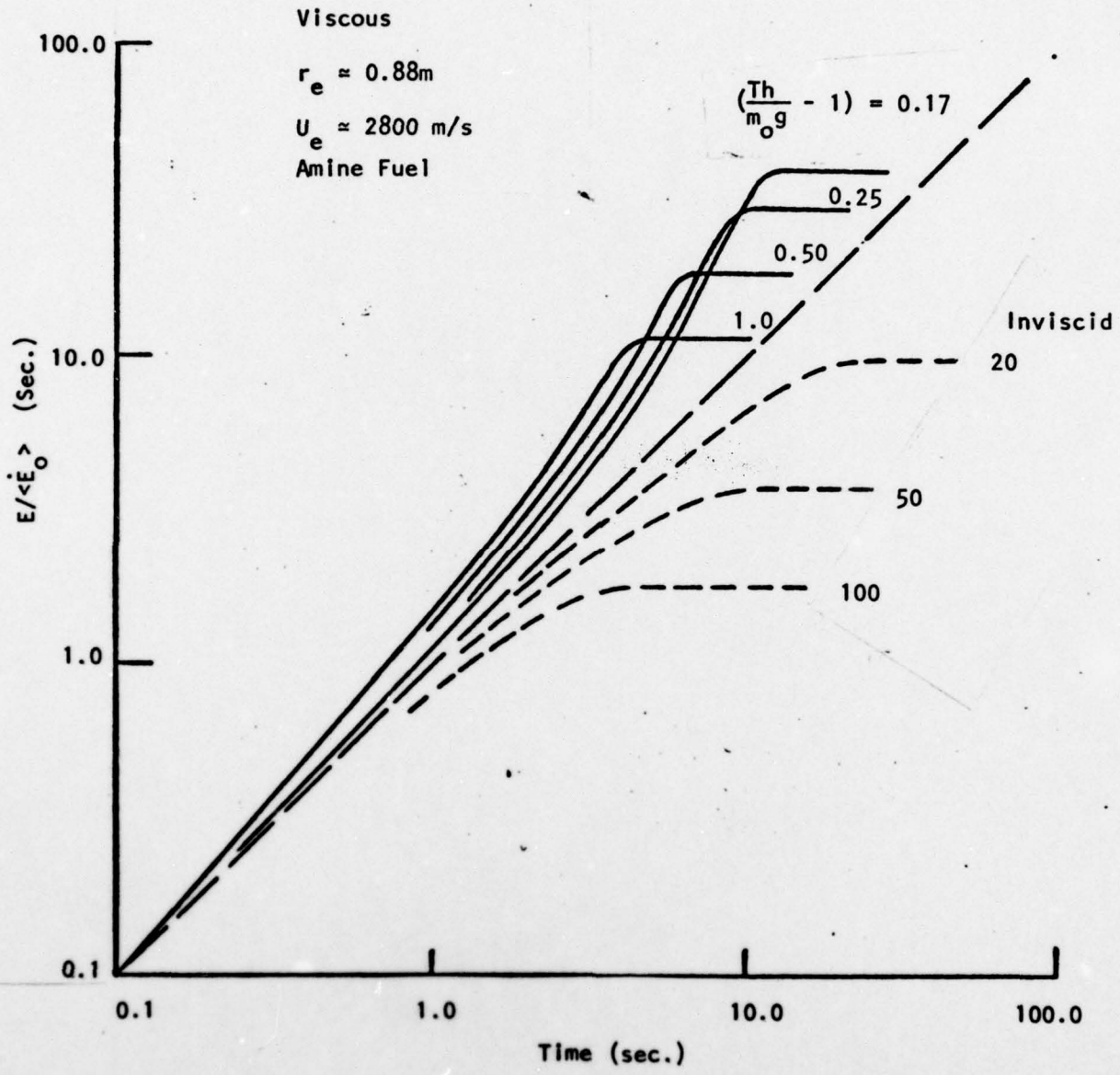

FIGURE 9. COMPARISON OF VISCOUS AND INVISCID SOLUTIONS FOR ENERGY DEPOSITION AT GROUND LEVEL

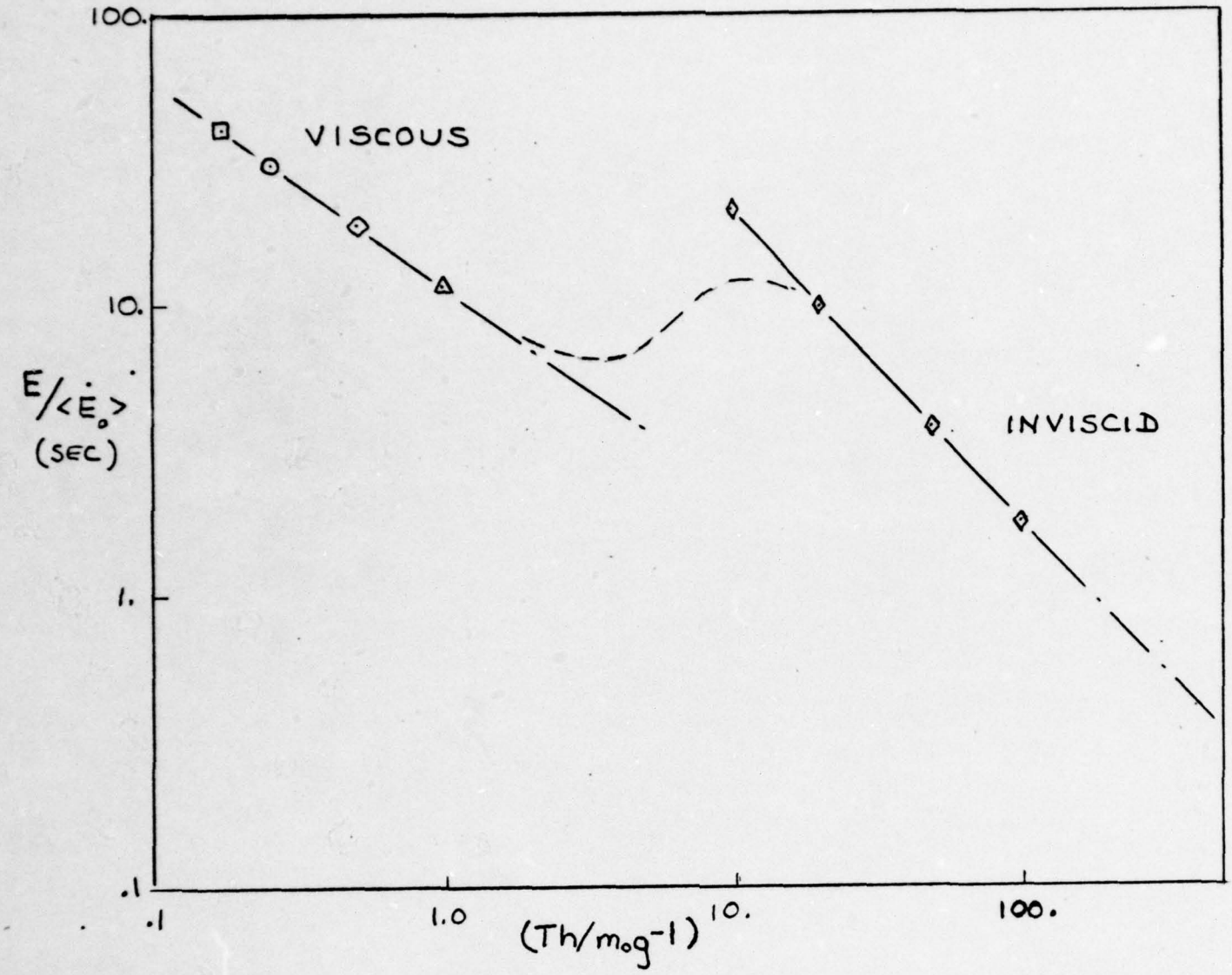

FIGURE 10. RATIO OF TOTAL ENERGY DEPOSITION TO INITIAL ENERGY FLUX AS A FUNCTION OF ROCKET ACCELERATION

this case. On the otherhand, as a very high acceleration lift-off example, take $Th/m_o g = 100$, for which the inviscid solution should apply. Again assume $p_e A_e \simeq Th/10$ and $\gamma = 1.20$, giving $\langle \dot{E} \rangle = 4.9 \times 10^9$ N·m/s as in the previous case. However, $E = 8.8 \times 10^9$ N·m, $R_o \simeq 56$ m and $t_2 \simeq 5$s in this case.

IV. ASYMPTOTIC INVISCID STRUCTURE

4.1 Unsteady Mach Disc and Plume Collapse - As noted by Erdos and Del Guidice[1], the supersonic plume is quasi-steady from the sonic line to the Mach disc in the sense that it can be accurately described at any instant by a steady solution subject to the boundary conditions prevailing at the sonic line. However, the motion of the Mach disc is controlled by the instantaneous pressure imposed on its downstream side; thus its position is determined by the interaction of the quasi-steady plume with the unsteady blast field. This interaction in general requires numerical solution of the unsteady shock layer contained between the Mach disc and blast wave[1]. However, considerable insight regarding the role of the unsteady shock layer can be gained without reverting to the numerical solution itself. For example, as pointed out by Schmidt and Shear[8], at late times, when the blast wave weakens and the pressure acting on the Mach disc decays to atmospheric, the plume and blast fields uncouple. Thus, during the collapse of the plume, the instantaneous Mach disc position can be approximated closely by the steady state correlation formula[8]:

$$z_m/d = 0.70\ (\gamma p_e/p_\infty)^{\frac{1}{2}}\ M_e \tag{37}$$

where d is the diameter of the gun barrel, $p_e(t)$ is the muzzle exit pressure and $M_e(t)$ is the muzzle exit Mach number (usually unity). This behavior is demonstrated[2] in Figure (11).

In the case of a rocket launch this formula can be rewritten as:

$$r_m = 1.40\ \left(\frac{\gamma \dot{E}}{\pi\, p_\infty c^*}\right)^{\frac{1}{2}} \tag{38}$$

where c^* is the exhaust sound speed at the sonic line and $\dot{E}$ is given by Equation (26). This form clearly shows the dependence of the Mach disc position, during the time of plume collapse, on the rate of energy desposition, rather than the amount.

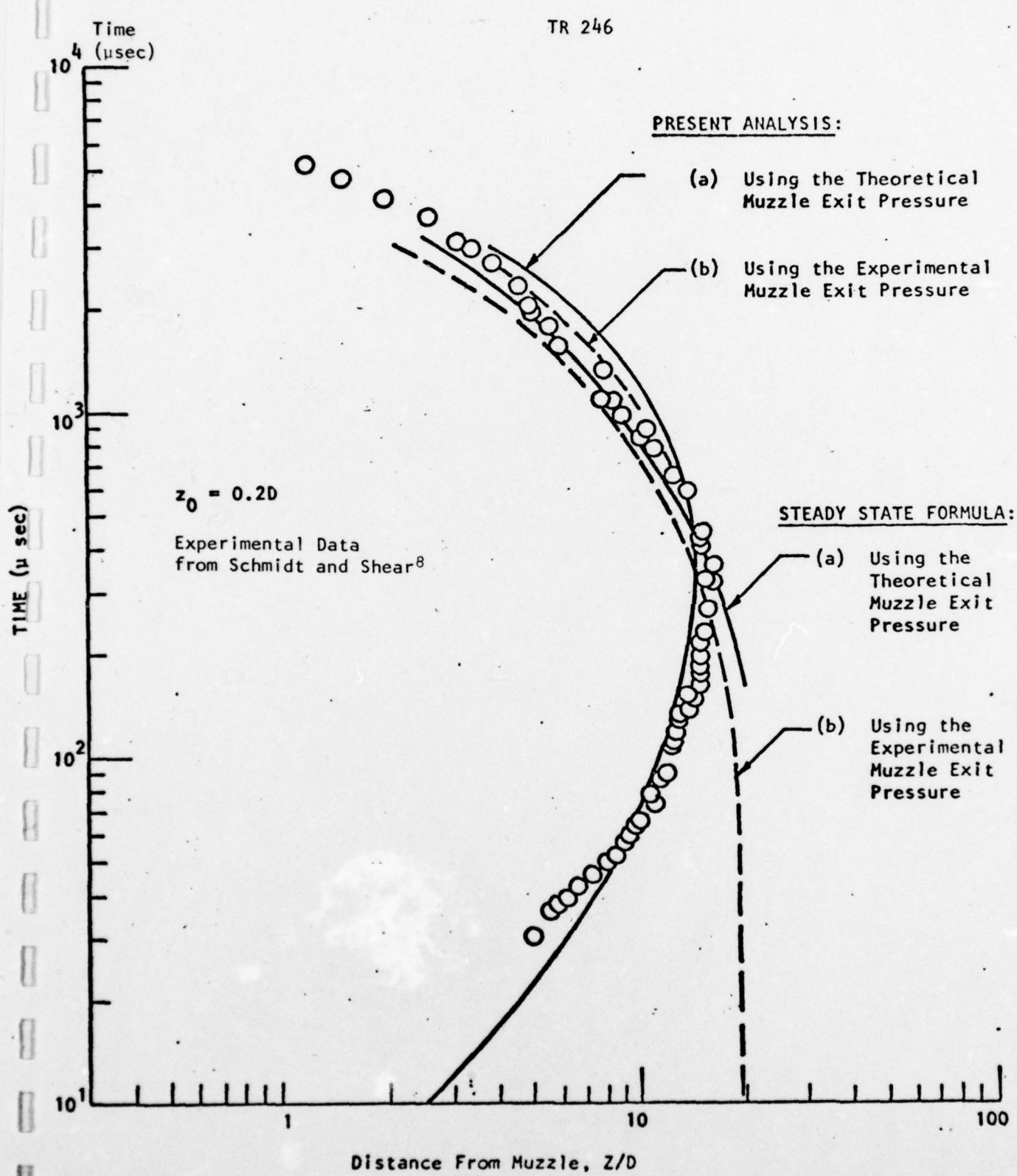

FIGURE 11. COMPARISON OF MACH DISC TRAJECTORY FOR THE M16 OBTAINED WITH THEORETICAL EXIT PROPERTIES AND EXPERIMENTAL EXIT PROPERTIES

On the other hand, during the early period when the plume is growing, rather than collapsing, the pressure imposed on the Mach disc is essentially that produced by the blast wave. Thus, a correlation formula of the form given by Equation (10) may be expected to apply; this is confirmed[2] by the numerical examples shown in Figure (12). However, it should be noted that the range of applicability of Equation (10) must be limited to the duration of strong coupling between the blast field and plume. Interestingly, as indicated in Figure (12), the correlation appears to begin to deteriorate when the forward motion of the Mach disc drops below Mach 2 (based on atmospheric sound speed).

Therefore, the behavior of the Mach disc over the entire duration of existence of the unsteady plume can be approximated by application of the correlation formulas, or scaling laws, represented by Figure (12) and Equation (37) or (38), in their appropriate range of validity, i.e., $t \ll t_2$ and $t \to t_2$, respectively.

4.2 Asymptotic Blast Field - The contact surface and blast wave trajectories at early times, i.e., $t < t_2$, have been shown[2] in Figures (4) and (5) to correlate in the form of Equations (8) and (9). During this time the unsteady shock layer flowfield has been described numerically[1]. No attempt to correlate the radial distribution of flow properties was made[2] because of the ease and speed with which the numerical solution could be carried out. However, as the distance between the shock and contact grows, and the strength of the blast wave diminishes, the accuracy of the numerical solution deteriorates, and recourse to an asymptotic formulation becomes desirable[1]. Note that for $t > t_2$, the plume has collapsed, and the exhaust gases remaining at the launch site are contained in a constant (atmospheric) pressure volume bounded by the inviscid contact surface. However, the blast wave continues to travel outward producing a local perturbation in pressure, temperature, and velocity in the atmosphere. The asymptotic solution for the flowfield produced by such a spherical shock wave has been derived by Whitham[4]. Ranlet and Erdos[2] have correlated their numerical solutions for a particular weapon, the M16 rifle, at late times when the blast shock Mach number is between 1.10 and 1.04, in terms of the variables from Whitham's

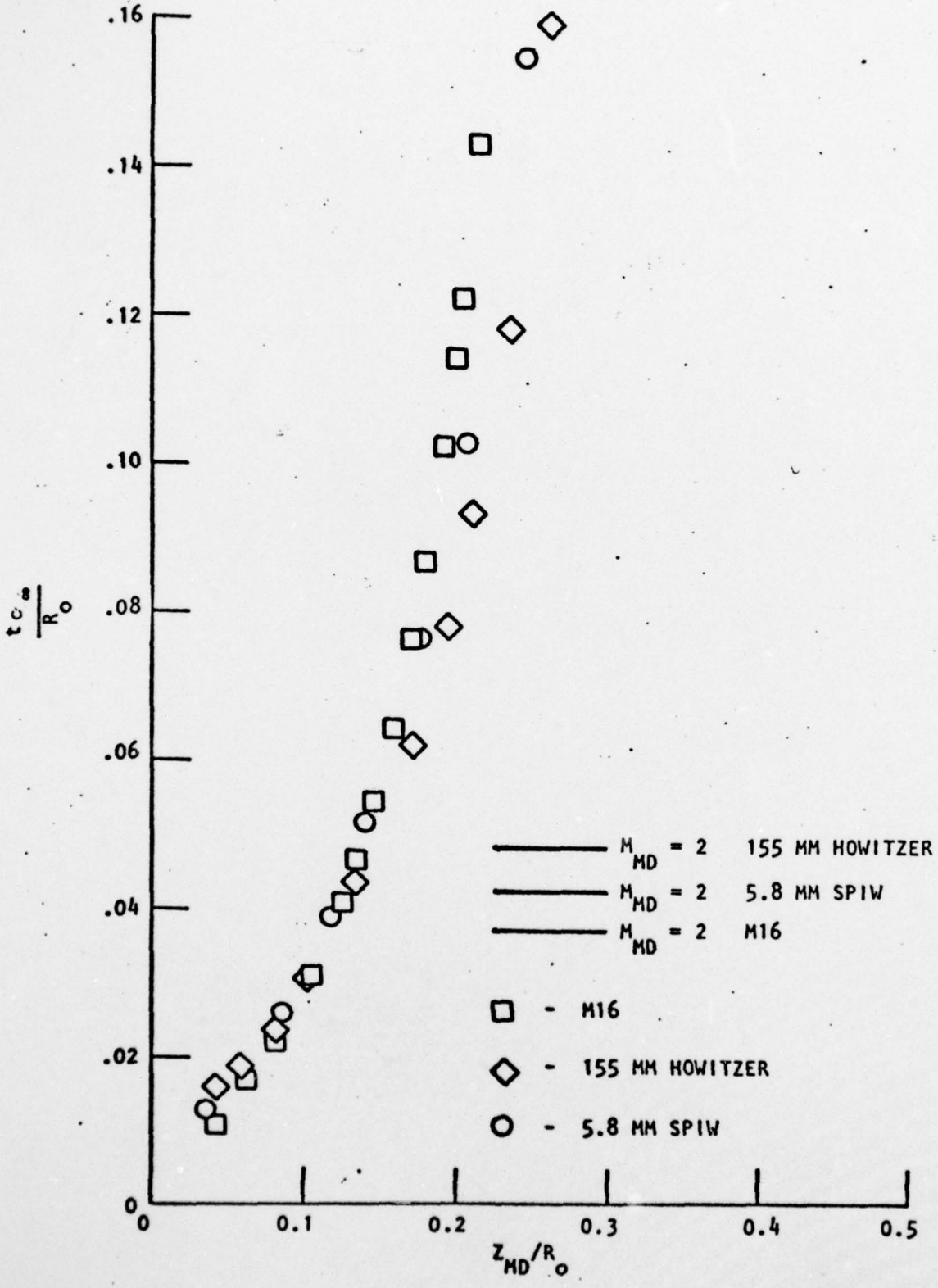

FIGURE 12. MACH DISC TRAJECTORIES IN THE NEAR FIELD

asymptotic solution, namely:

$$\frac{r}{d}\left(\frac{p}{p_\infty} - 1\right) = f_1(\eta) \tag{39}$$

$$\frac{r}{d}\left(\frac{\rho}{\rho_\infty} - 1\right) = \frac{1}{\gamma} f_1(\eta) \tag{40}$$

$$\left(\frac{r}{d}\right)^2 \left(\frac{\rho}{\rho_\infty} - 1 - \frac{u}{c_\infty}\right) = f_2(\eta) \tag{41}$$

where

$$\eta = \frac{r - a_\infty t}{d \ln (r/d)} \tag{42}$$

which applies to $M_s \to 1$ *and* $r_s \to \infty$, [as opposed to the strong blast theory used previously (Equations 2 - 10), which is limited to $M_s >> 1$.] The asymptotic shock solution was stated earlier, Equation (11). (Note that the gun bore diameter, d, was used by Ranlet and Erdos[2] as the length scale, rather than R_o. However, this simply introduces a constant factor which is irrelevant to the following discussion). It should be pointed out that Whitham[4] finds the asymptotic flowfield to be an N wave, i.e., a dual shock system with the functions f_1 and f_2 linear and quadratic, respectively, between the two shocks.

The pressure distribution across the shock layer, from contact to blast wave, obtained[2] from the numerical solution for an M16 rifle, is plotted in Figure (13) in the form given by Equation (39). It is evident that the numerical results are well correlated in terms of the variable η, although a true N wave is not obtained. The corresponding density distributions are shown in Figure (14). In this figure the presence of an entropy layer adjacent to the contact surface can be clearly seen; however, outside the entropy layer the density distributions are also well correlated. The entropy layer consists

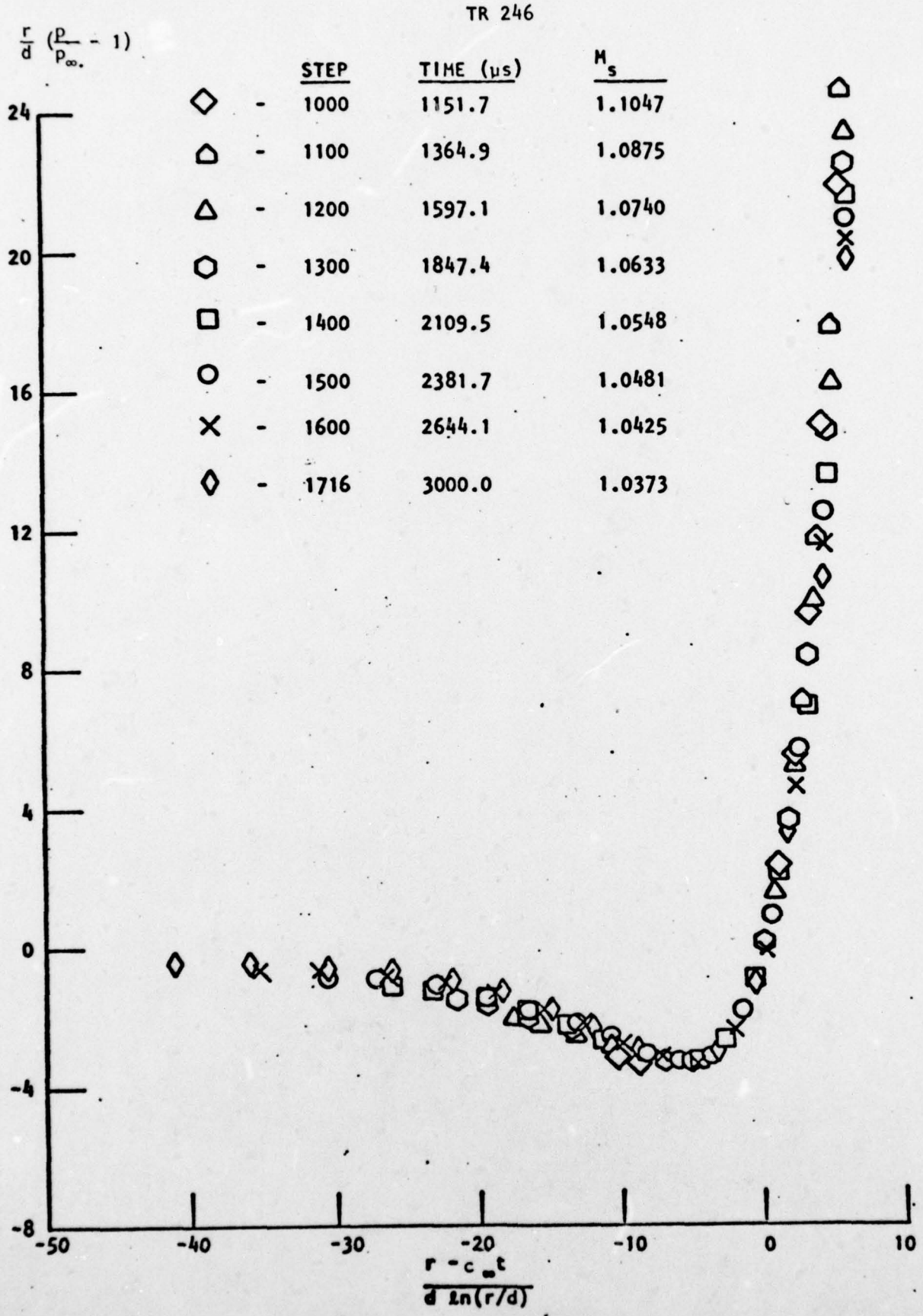

FIGURE 13. SHOCK LAYER PRESSURE DISTRIBUTION FOR AN M16 RIFLE (5.56 MM)

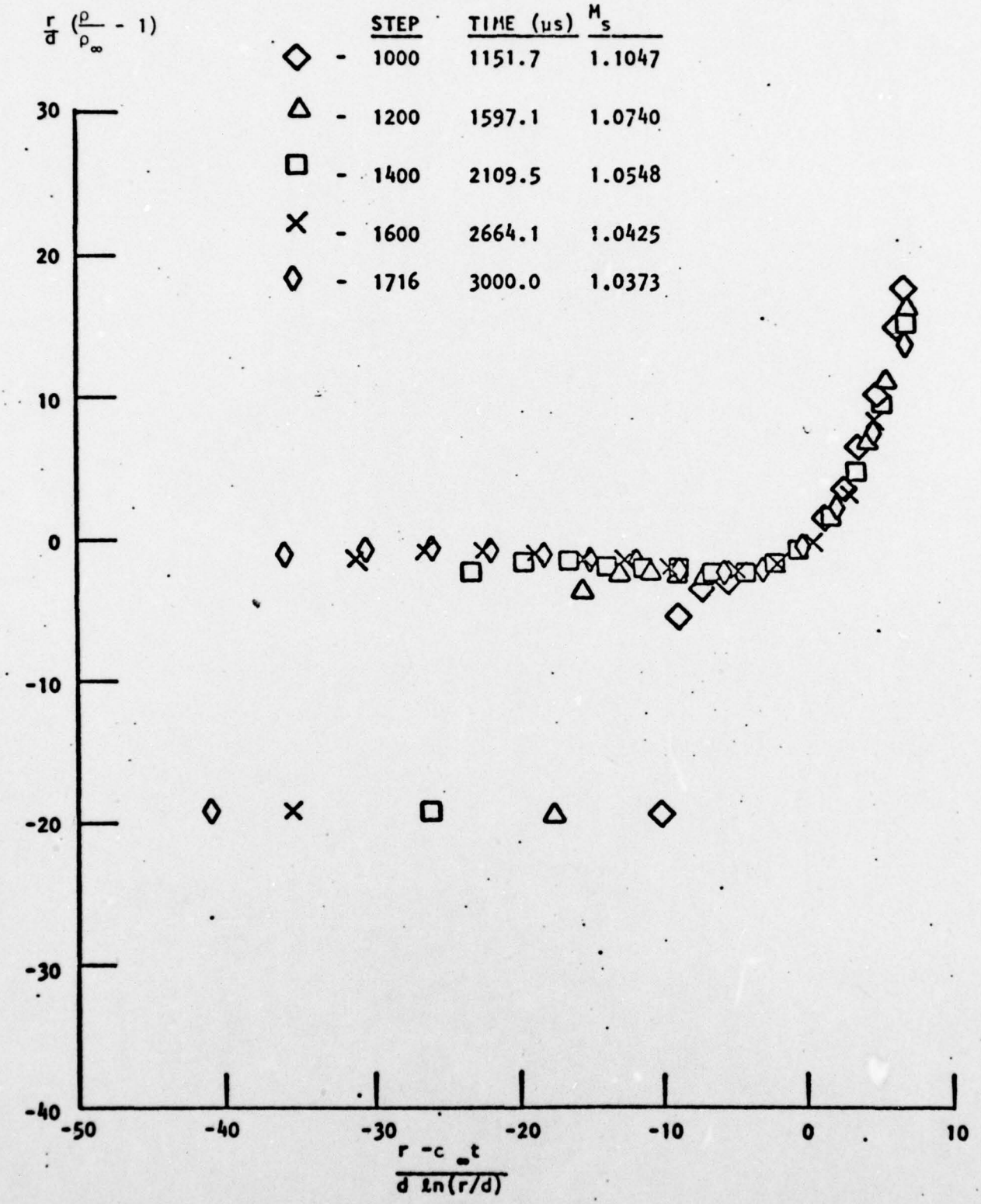

FIGURE 14. SHOCK LAYER DENSITY DISTRIBUTION FOR AN M16 RIFLE (5.56 MM)

of shock-heated air generated at early times, when $M_s >> 1$. The existence of such an entropy layer is, of course, not included in Whitham's asymptotic theory. The difference between the density and velocity in the form given by Equation (4) is shown in Figure (15). In this figure the effect of the entropy layer appears even more pronounced; however, note that the considered velocity-density parameter is a higher order quantity than either the pressure increment or density increment. It should also be noted from Figures (14) and (15) as well as Figure (13), that the solutions near the blast wave correlate at the earliest times considered and the correlated region subsequently expands inward.

Since the asymptotic behavior of the blast field is independent of the initiating mechanism, the numerical solutions for muzzle blasts of widely varying guns should also correlate (asymptotically) in terms of the parameters given by Equations (39) - (42). This has been verified by a comparison[2] of numerical solutions for the M16 rifle (5.56 mm bore), a special purpose infantry weapon, SPIW (a 5.8 mm rifle with a non-standard round) and a howitzer (155 mm bore). As can be seen in Figures (16) and (17) the pressure and density distributions for these three weapons are again well correlated. However, the parameter representing the difference between the density and velocity (Equation 41) retains a dependence on the initiating mechanism which does not appear to vanish aymptotically. However, as shown in Figure (18), scaling of this parameter to a reference value chosen as the value at $r = a_\infty t$, minimizes the dependence on the initiating mechanism and produces a satisfactory correlation for the three weapons.

Although these correlations were originally developed to demonstrate that the numerical computation did, in fact, retain a satisfactory degree of accuracy as $M_s \to 1$ and $r_s \to \infty$, provided adequate grid control was used[2], they furnish additional valuable insight regarding the asymptotic behavior of far field. This is particularly useful in consideration of the boundary conditions on the turbulent mixing field which develops in the presence of the entropy layers bounding both sides of the inviscid contact surface.

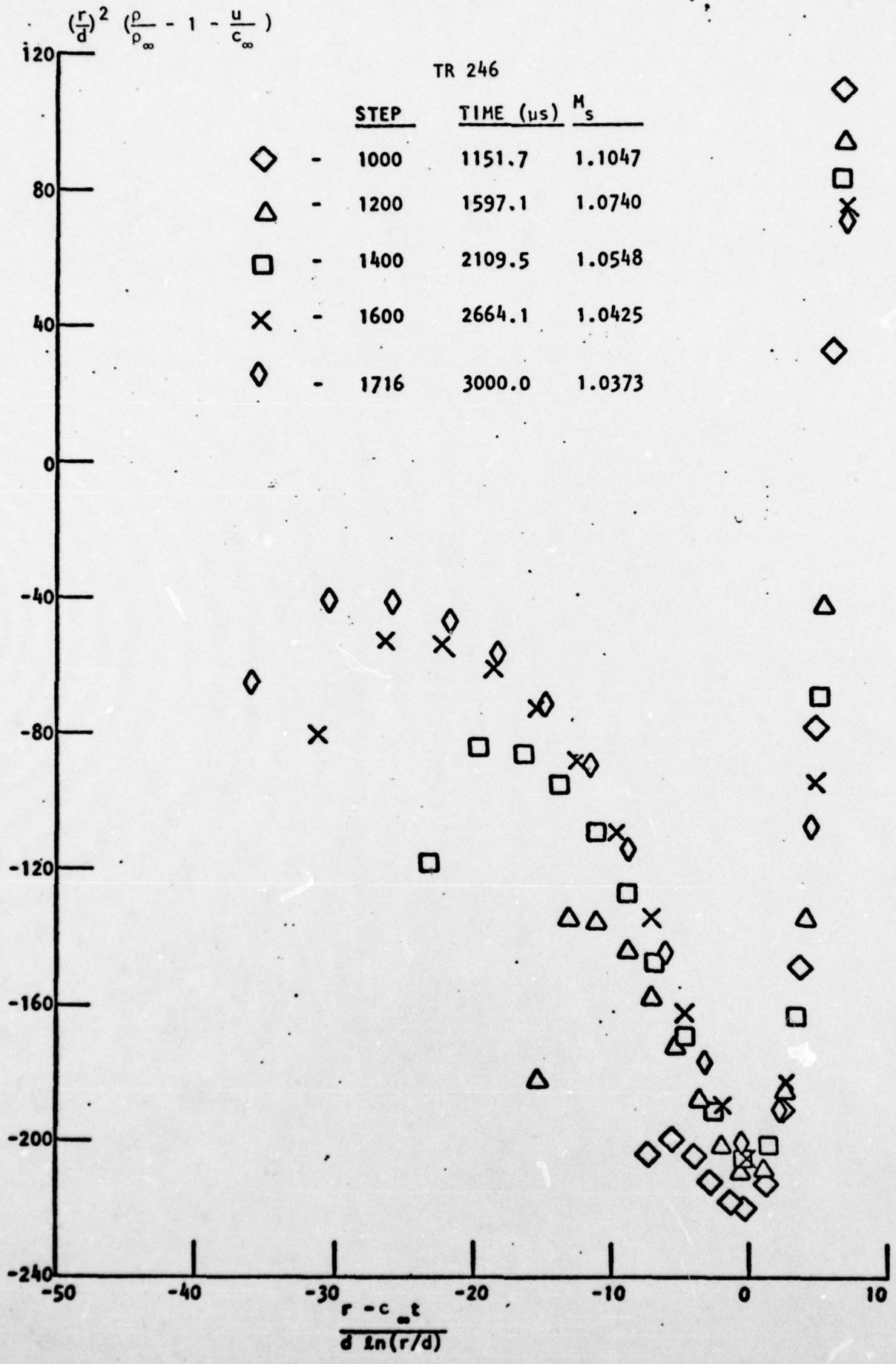

FIGURE 15. SHOCK LAYER VELOCITY-DENSITY PARAMETER DISTRIBUTION FOR AN M16 RIFLE (5.56 MM)

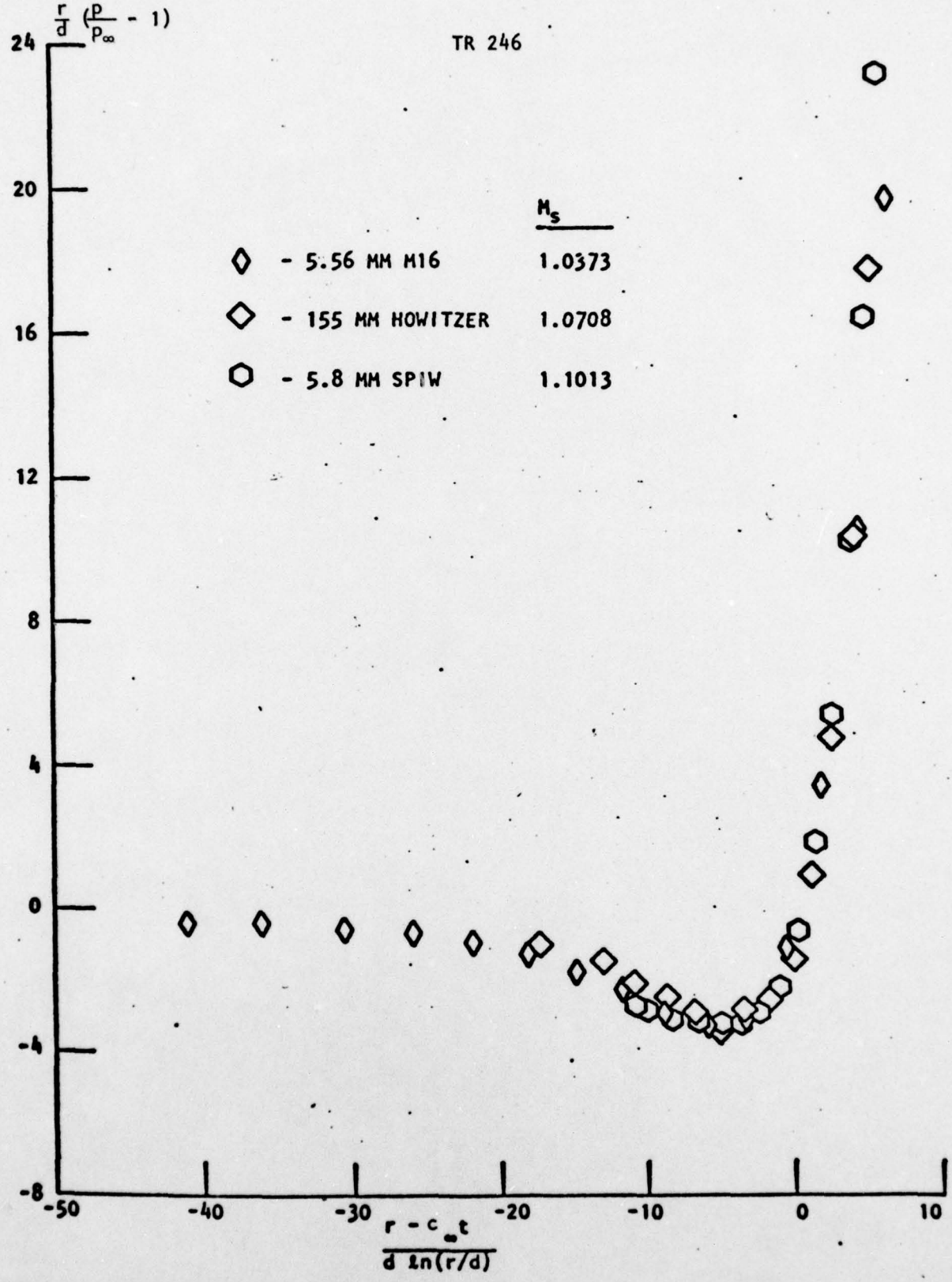

FIGURE 16. SHOCK LAYER PRESSURE DISTRIBUTION FOR VARIOUS WEAPONS

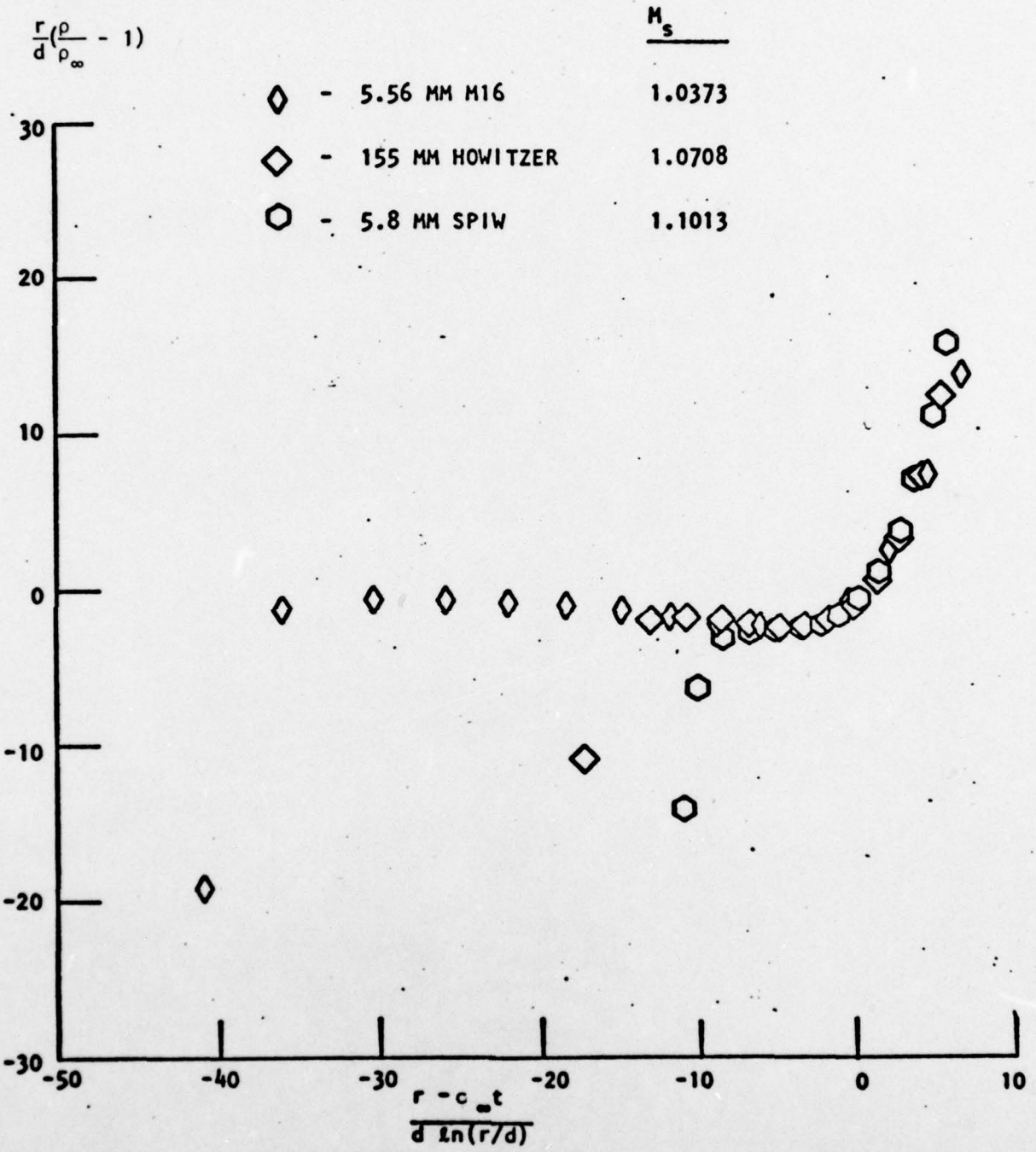

FIGURE 17. SHOCK LAYER DENSITY DISTRIBUTION FOR VARIOUS WEAPONS

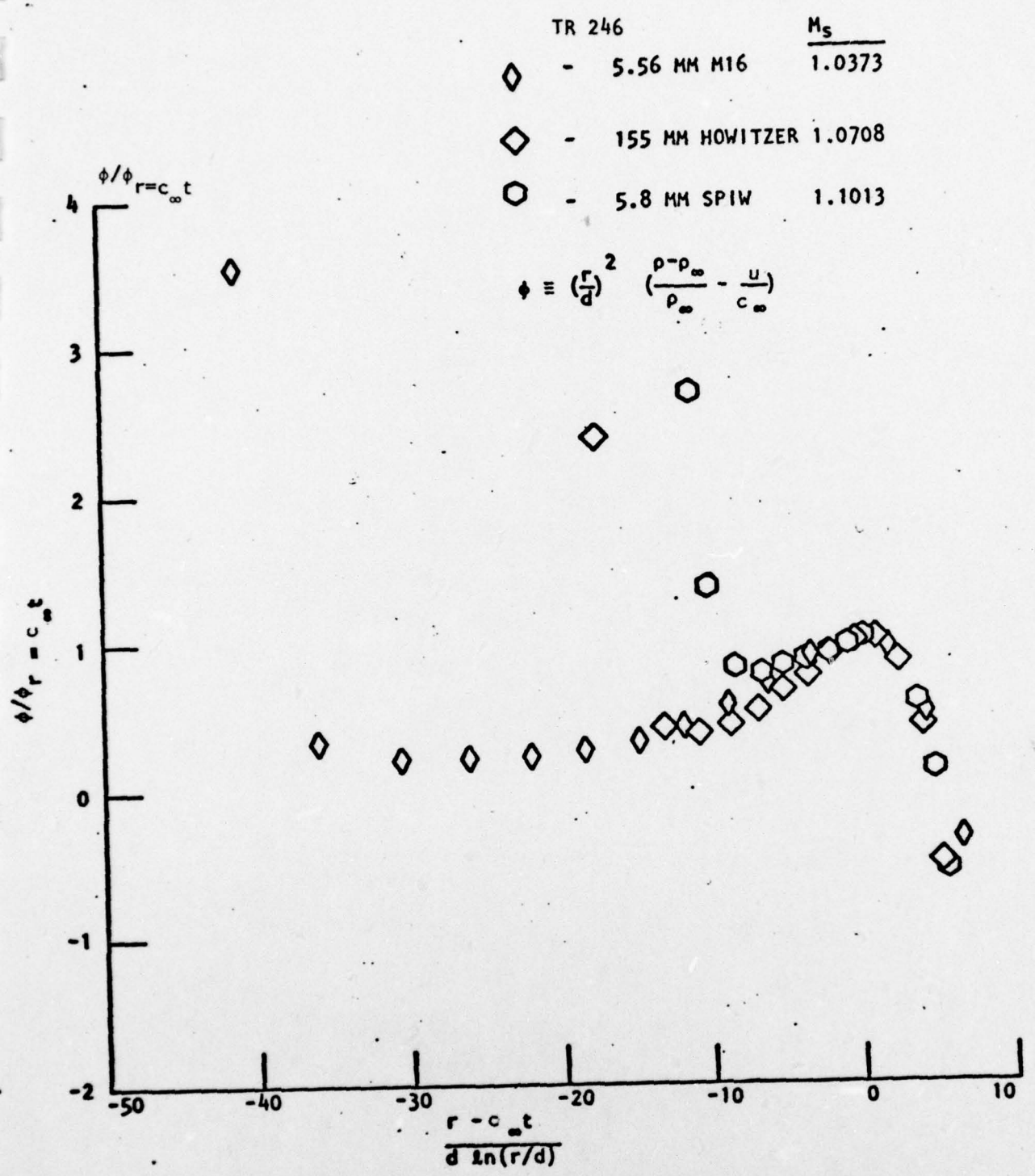

FIGURE 18. NORMALIZED SHOCK LAYER VELOCITY-DENSITY PARAMETER DISTRIBUTION FOR VARIOUS WEAPONS

V. NONEQUILIBRIUM UNSTEADY SHOCK LAYER

5.1 Introductory Remarks - The unsteady shock layer is defined as the region between the plume Mach disc and the blast wave. It contains propellant gases at temperatures on the order of combustion chamber temperature, located between the Mach disc and the contact surface, and shock-heated air, located between the contact surface and blast wave (but mainly adjacent to the contact surface). Turbulent mixing of the propellant gases and air along the contact surface will be considered in a following section; for the present they will be assumed to be separated by the contact surface, an impermeable membrane in the context of an inviscid solution.

Chemical reactions occurring in the combustion chamber typically freeze during the rapid expansion in the exhaust nozzle, and remain frozen in the supersonic portion of the plume within which a continued expansion of the flow occurs. Chemical reactions may be expected to reinitiate in the stagnation region where the exhaust flow impinges on the ground surface and turns radially outward. However, a second freeze-out is likely in the supersonic plume which forms along the ground, Figure (2). For the purposes of the present exploratory study, the impingement region has been neglected, and all chemical reactions have been assumed to freeze in the exhaust nozzle and remain frozen until the unsteady shock layer is entered. (However, this assumption will be subsequently reexamined in the light of computational results.)

Supersonic expansion of the propellant gases produces the well-known underexpanded plume configuration shown in Figure (1), including the barrel shock needed to match the continuously decreasing pressure within the core of the plume to the ambient field prevailing along its lateral boundaries. Consequently, the supersonic expansion is not a true source flow, and the differences, even along an axis of symmetry, can produce an appreciable shift in the Mach disc location, as demonstrated in References (1) and (2). Nevertheless, the supersonic source flow model is extremely useful in an exploratory study since the solution is provided by well-known isentropic flow relations rather than by a cumbersome numerical solution. However, its limitations in

accuracy and its lack of dependence on the ambient pressure should be recognized.

The flow pattern indicated in Figure (1) may begin at earliest times with roughly cylindrical symmetry (relative to the launch axis); however, a more nearly spherical symmetry should be expected near the blast wave after a short time (during which the vehicle does not move appreciably). The success with which the gun blast can be modelled as a spherically symmetric shock layer [1,2] suggests the same approximation should be equally useful in this case. Therefore, the supersonic plume is represented by a spherical, quasi-steady source flow. The unsteady subsonic flow between the Mach disc and the blast is described by a finite-difference solution of the one-dimensional time-dependent, inviscid equations of motion (with spherical symmetry), in the same manner as employed in Reference (1) and (2). The resulting solution should be most accurate along the ground (or sea) surface, and least accurate along the launch axis (where the blast is considerably less intense). In addition, the existence of turbulent mixing of the propellant gas and air along their interface and of buoyant forces is pointed out; however, neither is included in the present inviscid model. The turbulent mixing problem will be addressed in the following section.

5.2 Governing Equations and Solution Algorithm - The system of governing equations (for a perfect gas) and the solution algorithm have been described in Reference (1) and (2), therefore, they will be only briefly reviewed here. The principal modifications relate to the non-equilibrium chemical kinetics, which will be described in depth. The system of governing equations is stated as:

Continuity:
$$\frac{\partial \rho}{\partial t} + \frac{\partial}{\partial r}(\rho u) = - k \frac{\rho u}{r} \tag{43}$$

Momentum:
$$\frac{\partial \rho u}{\partial t} + \frac{\partial}{\partial r}(\rho u^2 + p) = - k \frac{\rho u^2}{r} \tag{44}$$

Energy:
$$\frac{De}{Dt} + p \frac{D\rho^{-1}}{Dt} = 0 \quad , \qquad \text{on } \frac{dr}{dt} = u \tag{45}$$

Species:* $$\frac{D\alpha_i}{Dt} = \frac{\dot{\omega}_i}{\rho} \quad (i=1,2,3\ldots), \quad \text{on} \quad \frac{dr}{dt} = u \tag{46}$$

State: $$p = \rho R_o T \Sigma \alpha_i/M_i \tag{47}$$

$$e = h - \frac{p}{\rho} = \Sigma \alpha_i h_i - R_o T \Sigma \alpha_i/M_i \tag{48}$$

$$h_i = a_i + b_i T + c_i T^2 \tag{49}$$

where k is an integer which is 0 for plane symmetry, 1 for cylindrical symmetry and 2 for spherical symmetry. Only k = 2 is used in the present study. The region between the Mach disc and the blast wave is divided into two layers; the first extends from the Mach disc to the contact surface, which as previously mentioned, is an impermeable interface between the propellant gases and air, and the second extends from the contact surface to the blast wave. These three boundaries are treated as moving surfaces of discontinuity across which certain gas-dynamic jumps occur. Denoting their instantaneous positions as r_1, r_2 and r_3, respectively, a stretched coordinate ξ_i for each layer is defined by:

$$\xi_i = (r-r_i)/(r_{i+1}-r_i) \tag{50}$$

where i = 1 refers to the first layer (from Mach disc to contact) and i = 2 to the second (from contact to blast wave). The above system of equations is transfromed from (r,t) to (ξ_i,t) coordinates by:

$$\frac{\partial}{\partial r} = \frac{1}{\Delta r_i} \frac{\partial}{\partial \xi_i} \tag{51}$$

*Note that the use of Equation (46) for all species together with Equation (43) produces a redundant system. The redundancy is used to obtain an independent check on error accumulation. The error defined as

$$\left|1 - \sum_{i=1}^{I} \alpha_i\right|$$

is less than 10^{-5} in all results obtained thus far.

$$\frac{\partial}{\partial t} = \frac{\partial}{\partial t} - \frac{(1-\xi_i)\, u_i + \xi_i\, u_{i+1}}{\Delta r_i} \quad \frac{\partial}{\partial \xi_i} \tag{52}$$

where

$$\Delta r_i = r_{i+1} - r_i \tag{53}$$

$$u_i = \frac{dr_i}{dt} \tag{54}$$

The two domains are each divided into a series of equally spaced intervals of size $\Delta\xi_i$. The magnitude of $\Delta\xi_1$ and $\Delta\xi_2$ are independently controlled such that the magnitude of the grid size ($\Delta r_i\ \Delta\xi_i$) remains within a preselected range. This is accomplished by adding or subtracting a single grid point when the size falls out of the range, shifting the other points, and linearly interpolating the data at the new grid point locations. Since the resulting shift in grid location is of the order $\Delta\xi_i^2$, no loss of accuracy is incurred by the linear interpolation.

Equations (43), (44) and (46) are expressed in finite difference form and solved at each of the interior grid points by the MacCormack algorithm[9]. Equation (45) is solved by a Lagrangian method, i.e., the streampath dr/dt = u is traced from a grid pont back to its intersection with the previous time plane. Recall that in the case of a perfect gas Equation (45) reduces to:

$$\frac{DS}{Dt} = 0, \quad \text{or} \quad S = \text{constant}, \quad \text{on} \quad \frac{dr}{dt} = u \tag{55}$$

Thus, interpolation of the value of the entropy, S, from the point of intersection of the streampath with the previous time plane provides the "exact" solution in this case, and accordingly any numerical diffusion of an entropy gradient is minimized. To maintain a consistent degree of accuracy in the solution of energy equation with chemical reactions, Equation (45) was solved in the same fashion as Equation (55).

$$e + \bar{p}/\rho = \text{constant} \quad \text{on} \quad \frac{dr}{dt} = u \tag{56}$$

where $\bar{p}$ is the average pressure along the considered streampath segment.

Solution of Equations (43) and (44) by the MacCormack algorithm is stable (without any additional numerical damping) if the standard CFL criterion is observed[9]. In simple terms, the maximum permissible time step is limited by the time for a wave to reach an adjacent grid point. However, addition of Equation (46) to the system introduces a second time scale, namely that for chemical relaxation. By analogy with the results obtained by Cheng[10] for combined wave and diffusion processes, the time step criterion for the present system is postulated as:

$$\Delta t = \min \left[\Delta t^{-1}_{\substack{\text{wave} \\ \text{speed}}} + \Delta t^{-1}_{\substack{\text{chemical} \\ \text{relaxation}}} \right]^{-1} \tag{57}$$

where the characteristic time scales are:

$$\Delta t^{-1}_{\substack{\text{wave} \\ \text{speed}}} = (u + c_f)/\Delta r \tag{58}$$

$$\Delta t^{-1}_{\substack{\text{chemical} \\ \text{relaxation}}} = \max \left[\frac{\partial}{\partial \alpha_i} \left(\frac{\dot{\omega}_i}{\rho} \right) \right]_{\rho,T} \tag{59}$$

and the frozen sound speed c_f is defined by

$$c_f^2 \equiv \left(\frac{\partial p}{\partial \rho} \right)_{S,\alpha_i} = - \left(\frac{\partial h}{\partial \rho} \right) / \left(\frac{\partial h}{\partial p} - \frac{1}{\rho} \right) \tag{60}$$

which can be analytically evaluated using the state relations provided by Equations (47), (48) and (49).

It should be pointed out that only in the case where Δt_{wave} and $\Delta t_{chemical}$ are of distinctly different orders of magnitude does Equation (57) correspond to using the minimum of the two time scales. On the other hand, if they are approximately equal, Equation (57) yields:

$$\Delta t = \frac{1}{2} \Delta t_{\substack{chemical \\ relaxation}} \quad , \text{ or } \quad \Delta t = \frac{1}{2} \Delta t_{\substack{wave \\ speed}} \tag{61}$$

This behavior may account for the empirical proportionality constant which Anderson[11] found to be necessary when using the minimum of the two time scales. The case in which the time scales are of the same order of magnitude corresponds to a true non-equilibrium situation; the cases in which they are distinctly different correspond to frozen and equilibrium limits.

At the bounding surfaces of discontinuity, namely; the blast wave, contact surface and Mach disc, the method-of-characteristics procedure[1] for determinating the motion of these surfaces and flow properties thereon has been retained using a locally defined frozen sound speed and isentropic exponent. The effects of chemical reaction are, therefore, neglected within narrow zones of thickness $(u \pm c_f)\ \Delta t$ adjacent to each of these surfaces. The isentropic exponent, γ , is evaluated locally from:

$$\gamma = c_f^2 \ \rho/p \tag{62}$$

As indicated in the introductory remarks, the flowfield upstream of the Mach disc is approximated by a supersonic spherical source. In effect, the sonic line (surface) is located at a radius r*, and the Mach number at any radius $r > r^*$ is obtained from the isentropic flow relationship.

$$(r^*/r)^2 = \left[\frac{\gamma+1}{2}\right]^{\frac{\gamma+1}{2(\gamma-1)}} \cdot M \left[1 + \frac{\gamma-1}{2} M^2\right]^{-\frac{\gamma+1}{2(\gamma-1)}} \tag{63}$$

The instantaneous conditions on the upstream side of the Mach disc are obtained from the above equation with $r = r_1(t)$ and with the entropy, total enthalpy and species concentrations on a streampath traced from the sonic

line to a position $r_1(t)$. The latter procedure introduces a time lag between the variation of sonic line conditions and the resulting variation of conditions at the Mach disc which is only appreciable when $r_1 >> r^*$.

Ambient atmospheric conditions are assumed to prevail upstream of the blast wave (i.e., any effects of precursor waves due to ejection from a silo, for example, are neglected). The instantaneous velocities of the Mach disc and blast wave, u_1 and u_3, are determined by matching the solution of the Rankine-Hugoniot shock jump relations to the characteristic compatibility equation along the wave impinging each shock from the interior (i.e., an upstream running wave at the Mach disc and a downstream running wave at the blast wave). The velocity of the contact surface, u_2, is determined by equating the pressures and (normal component of) velocities at the contact given by the compatibility equations on the pair of waves impinging on the contact (one from the propellant side and one from the air side). Due to the assumption of spherical symmetry, no tangential component of velocity exists. Therefore, only the entropy or related thermodynamic properties, and the species concentrations are discontinuous across the contact surface.

5.3 Gas Dynamic Properties - As a prelude to analysis of the chemical kinetics of the propellant gases in the blast field, it is instructive to study the gas dynamics of the problem with a view toward characterizing the time scales, as well as temperature, pressure and velocities. This preliminary assessment can be conveniently carried out on the basis of a binary perfect gas model; one gas represents air (γ = 1.4 and R = 1716 $ft^2/sec^2/^oR$) and the other represents the propellant gas (γ = 1.25 and R = 2140 $ft^2/sec^2/^oR$). In this case Equation (55) is used in place of Equation (56), $\dot{\omega}_i = 0$, etc.

As pointed out earlier, the energy deposition process can be veiwed as beginning impulsively, $t_i << t_\ell$, and the mass and energy flux into the blast field can be approximated by integrating flow properties radially across a steady exhaust plume at various stations behind the nozzle exit plane. It is assumed that a quasi-steady supersonic exhaust flow and plume will be established behind the leading (double) shock system expelled from the nozzle as the chamber pressure rises; thus the time to establish a quasi-steady plume

should be even less than t_i. (Shadowgraphs[8] of the muzzle blast of the M16 rifle when the projectile is still within one bore diameter of the muzzle corroborate this assumption.) A quantitative assessment of the effect of the relative magnitude of t_i on the blast field processes of present interest has been carried out by comparing the solution for an "instantaneous" ignition ($t_i = 0$) with solutions for a finite ignition time. The ignition process has been represented by a chamber pressure rise time curve taken from Reference (5). Using the engine and propellant parameters selected for Case 1 in Reference (5), e.g., axial engine length of 10 ft., nozzle area ratio of 4.0, etc., the steady chamber pressure is reached in about 25 milliseconds. The pressure at the sonic line was assumed to respond instantaneously to the chamber pressure history. The sonic line pressure-time curve is reproduced here as Figure (19). An intermediate case in which t_i = 2.5 milliseconds has also been carried out, using the same form of the pressure rise curve.

The gas temperatures on each side of the Mach disc and at the blast wave are shown in Figure (20) as a function of time. The temperatures on each side of the contact surface are shown in Figure (21). It is evident that substantial differences in the shock layer temperature field from the Mach disc to the contact occur during the ignition transient, i.e., $t < t_i$, but for $t > t_i$ the solutions tend to converge. This results becomes obvious as the time for energy deposition becomes small compared to the observation time. Thus the effect of finite ignition time need be considered only in (extreme) cases where it is comparable to the time scale of interest.

Radial distributions of temperature at various instants are displayed in Figure (22). It is clear that the bulk of the propellant gas is at a temperature characterized by that behind the Mach disc, which in this perfect gas example is close to 8000°R. The blast wave produces a very minor heating of the air, although the volume of air processed by the blast wave grows quite rapidly. The temperature ratio across the contact surface is of the order of 6 to 1, and, as will be discussed later, may produce a thermally-driven turbulent mixing along this interface. A steep temperature gradient is also observed on the propellant side of the contact, which may be expected to further

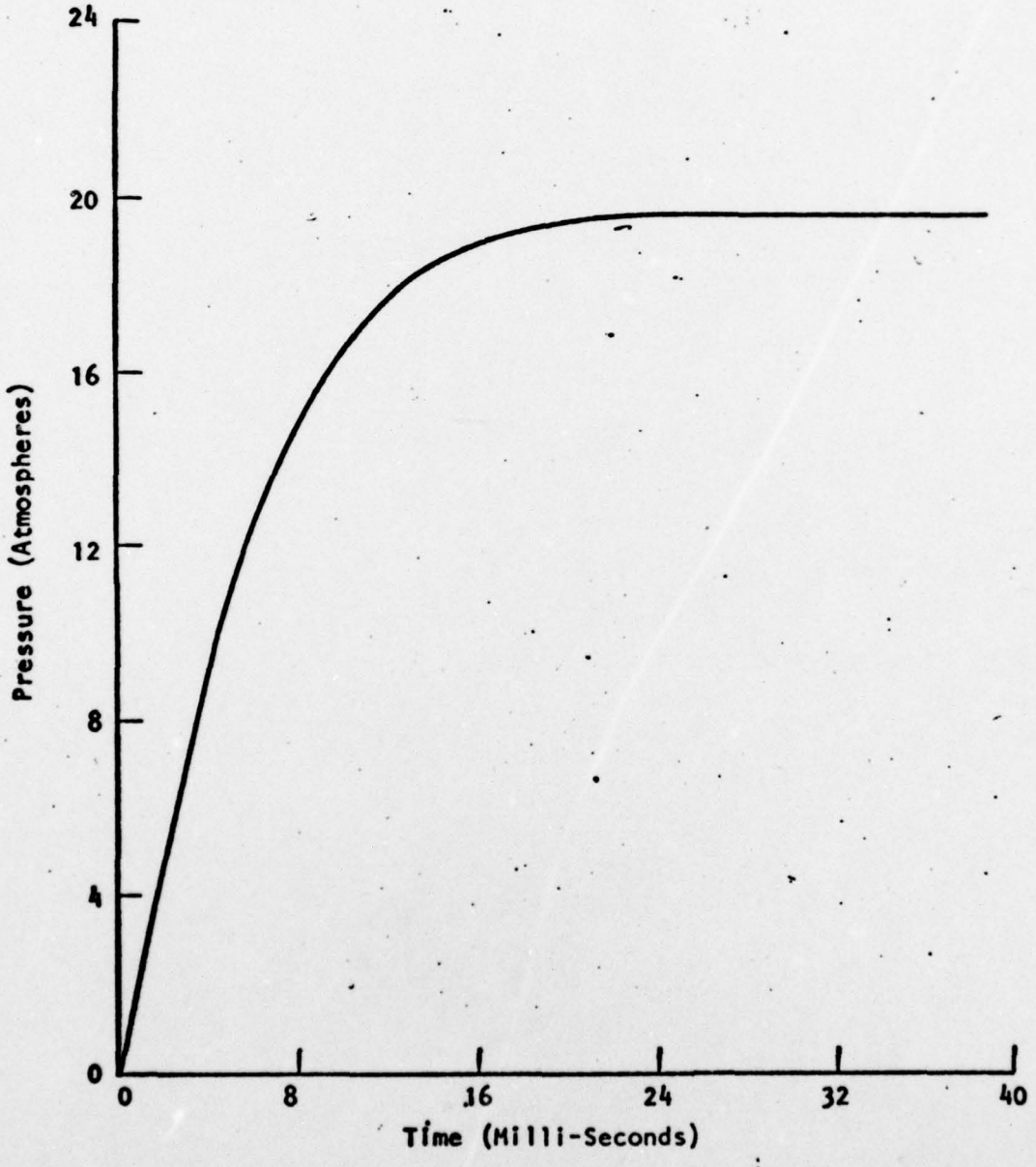

FIGURE 19. THE PRESSURE AT THE SONIC LINE AS A FUNCTION OF TIME

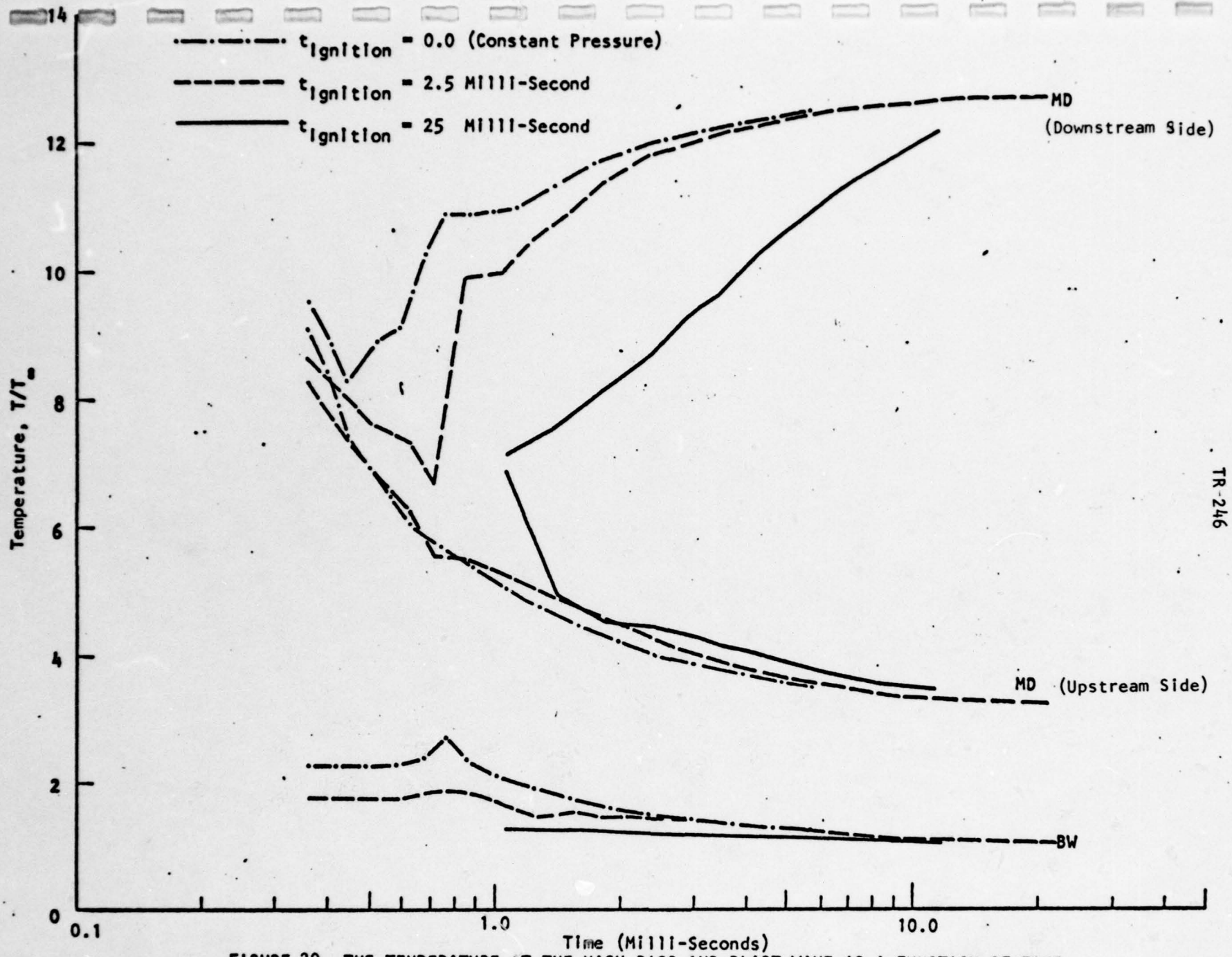

FIGURE 20. THE TEMPERATURE AT THE MACH DISC AND BLAST WAVE AS A FUNCTION OF TIME

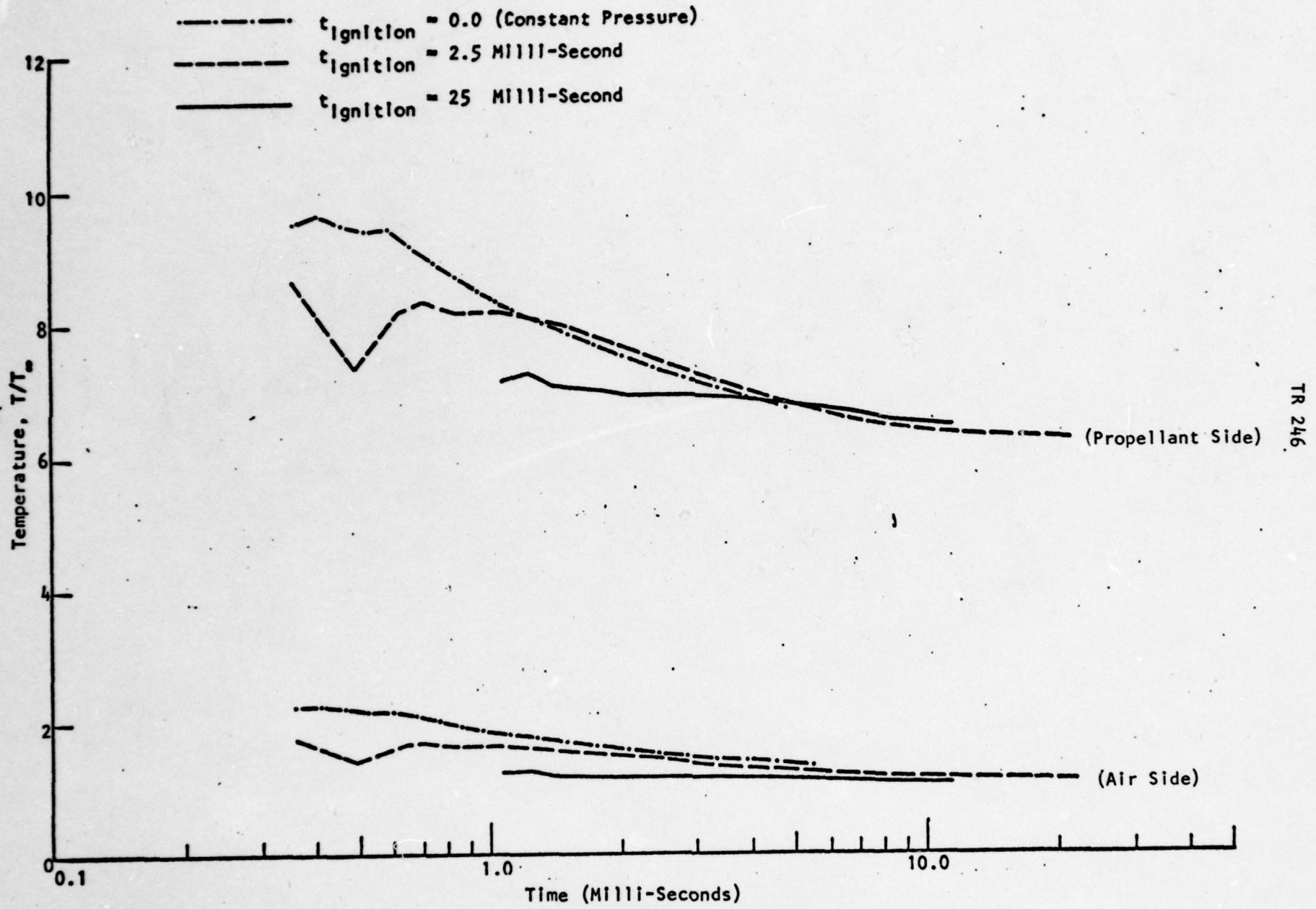

FIGURE 21. THE TEMPERATURE AT THE CONTACT SURFACE AS A FUNCTION OF TIME

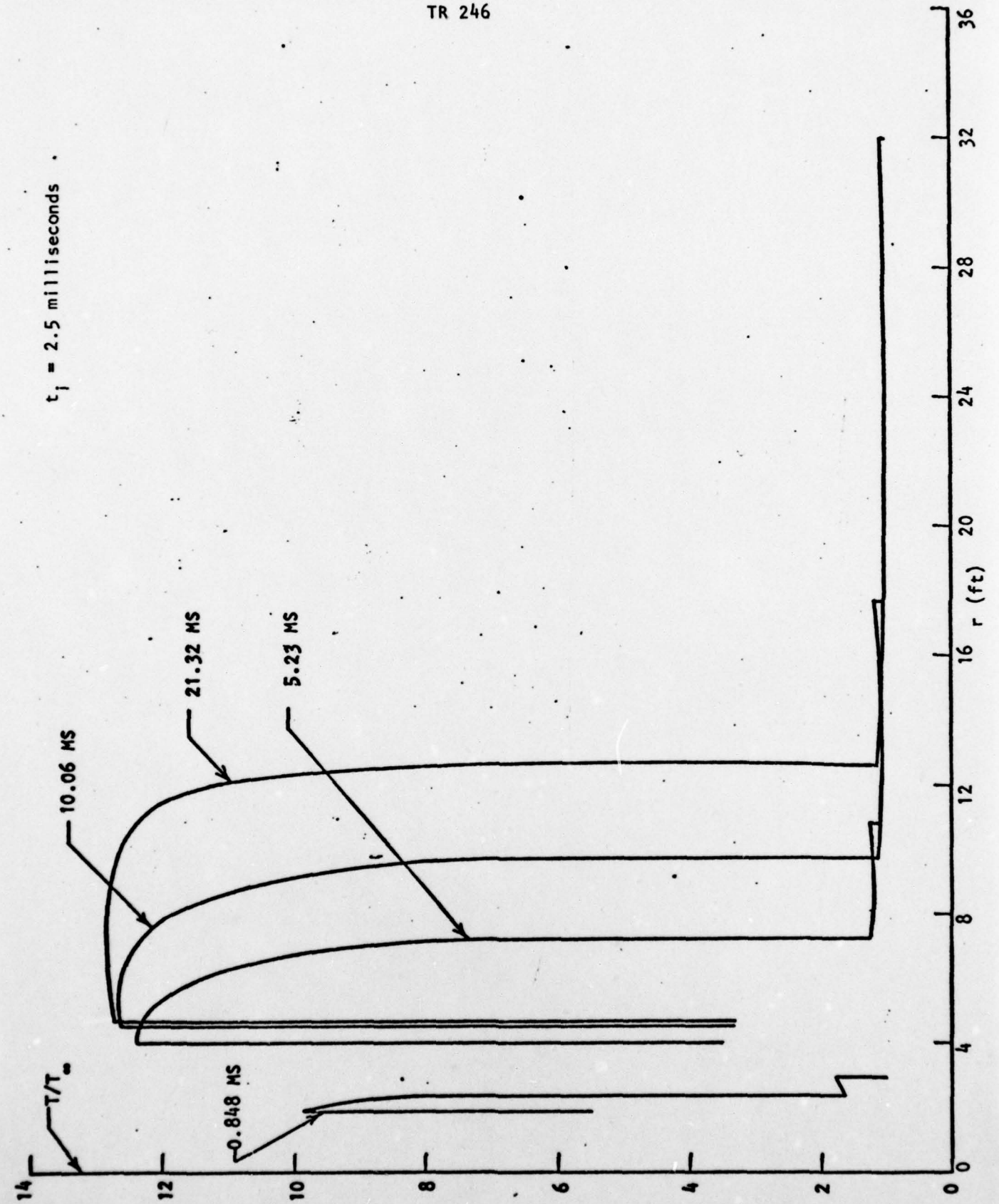

FIGURE 22. SHOCK LAYER RADIAL TEMPERATURE DISTRIBUTIONS AT SELECTED TIMES.

contribute to the turbulent mixing of hot propellant gases and air.

Radial distribution of gas pressure, temperature and velocity at a much later time are shown in Figures (23), (24) and (25). The assumption of a chemical freeze in the rocket nozzle and supersonic exhaust plume are justified heuristically on the basis of the rapid pressure and temperature drop and increasing gas velocity which characterize the exhaust nozzle and supersonic plume, cf. Figures (23), (24) and (25). These considerations pertain to the quasi-steady flow which exists upstream of the Mach disc. However, the present unsteady analysis is initiated when the Mach disc first forms, which is at a position close to the sonic line (as shown in Figure 1). At this early time, the assumption of a chemical freeze upstream of the Mach disc is less tenable and the initial conditions may more closely correspond to the local equilibrium, as will be seen below.

The nearly constant pressure plateau between the Mach disc and contact surface exhibited in Figure (23) extends well into the region between the contact and blast wave at later time; cf. Figures (13) and (16). Thus, the velocity field, shown in Figure (25), is correspondingly constant. The fact that no velocity jump* exists across the contact surface is reemphasized, in contrast to the temperature jump, seen in Figure (24), which persists forever in the absence of turbulent motion. Therefore, the asymptotic behavior of the propellant gas cloud must clearly be dominated by thermal rather than inertial or pressure gradients.

5.4 Thermo-chemical Properties - The following chemical reaction system was selected as a representative mechanism for afterburning of a hypothetical hydrocarbon fuel which produces a combination of H_2O, H_2, CO_2 and CO and N_2 as principal exhaust products.

---

*The assumption of spherical symmetry precludes the existence of a finite velocity component parallel to the contact surface, which could have a jump.

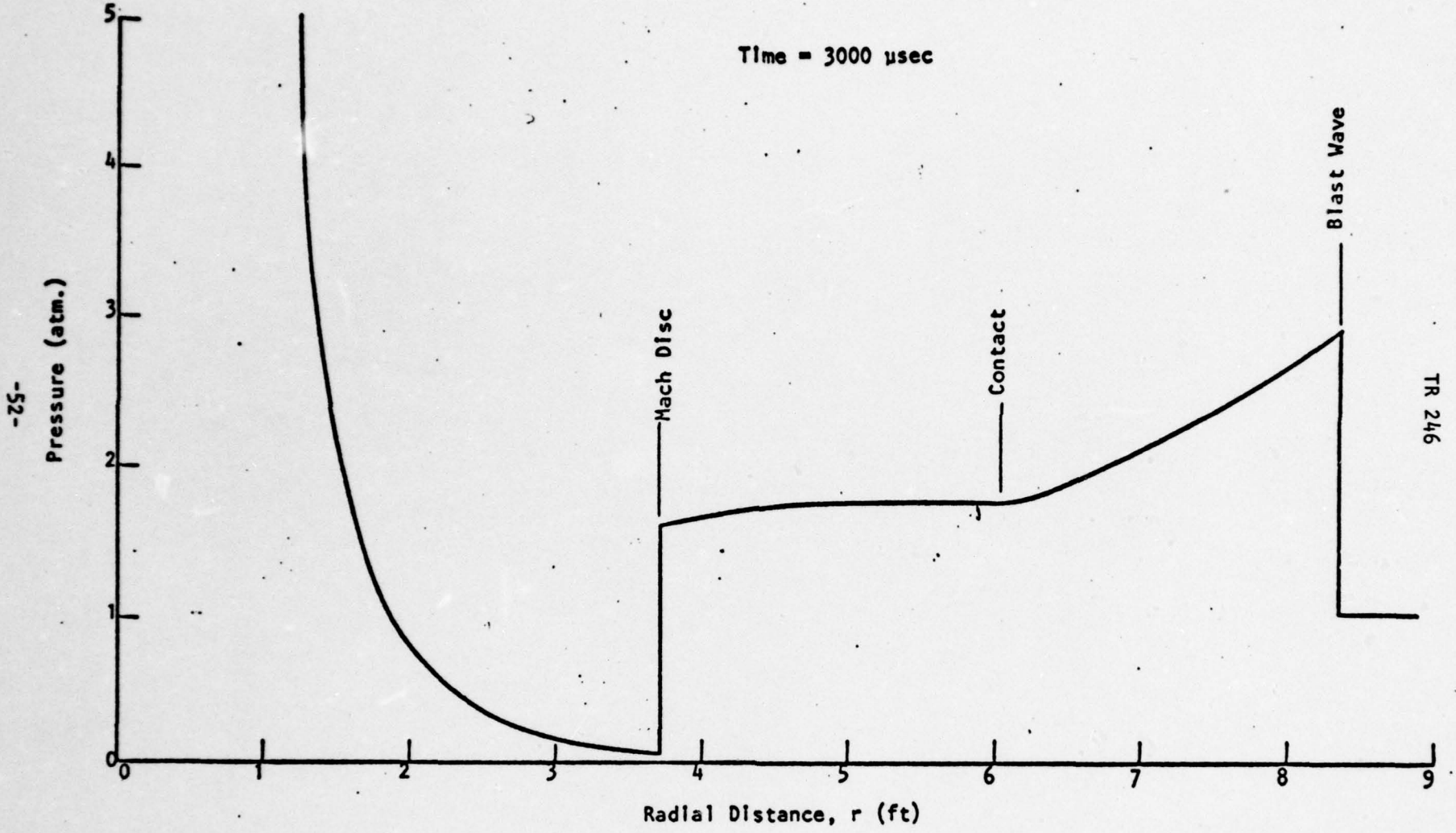

FIGURE 23. PRESSURE DISTRIBUTION IN SPHERICAL BLAST FIELD

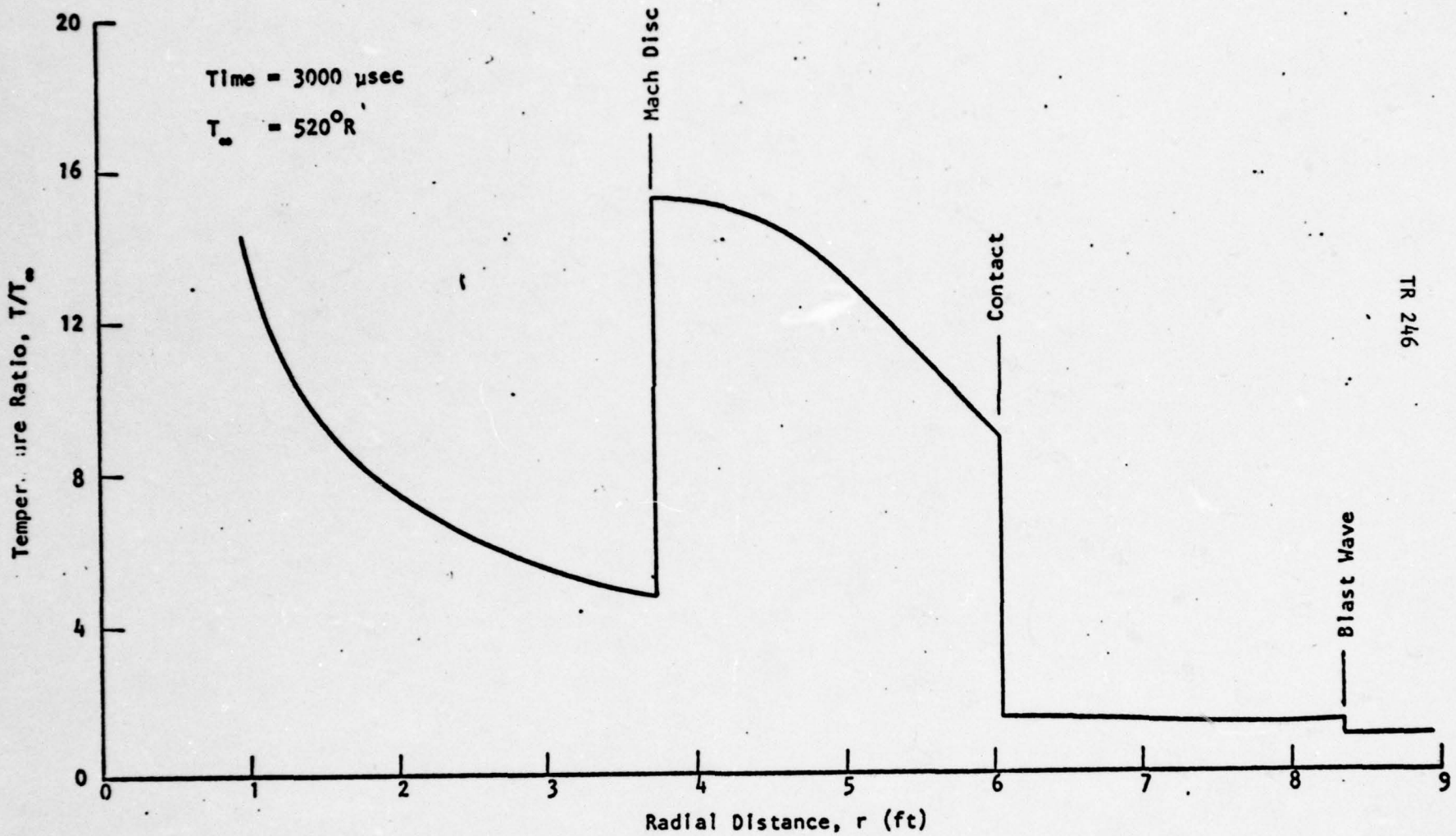

FIGURE 24. TEMPERATURE DISTRIBUTION ON SPHERICAL BLAST FIELD (FROZEN GASES)

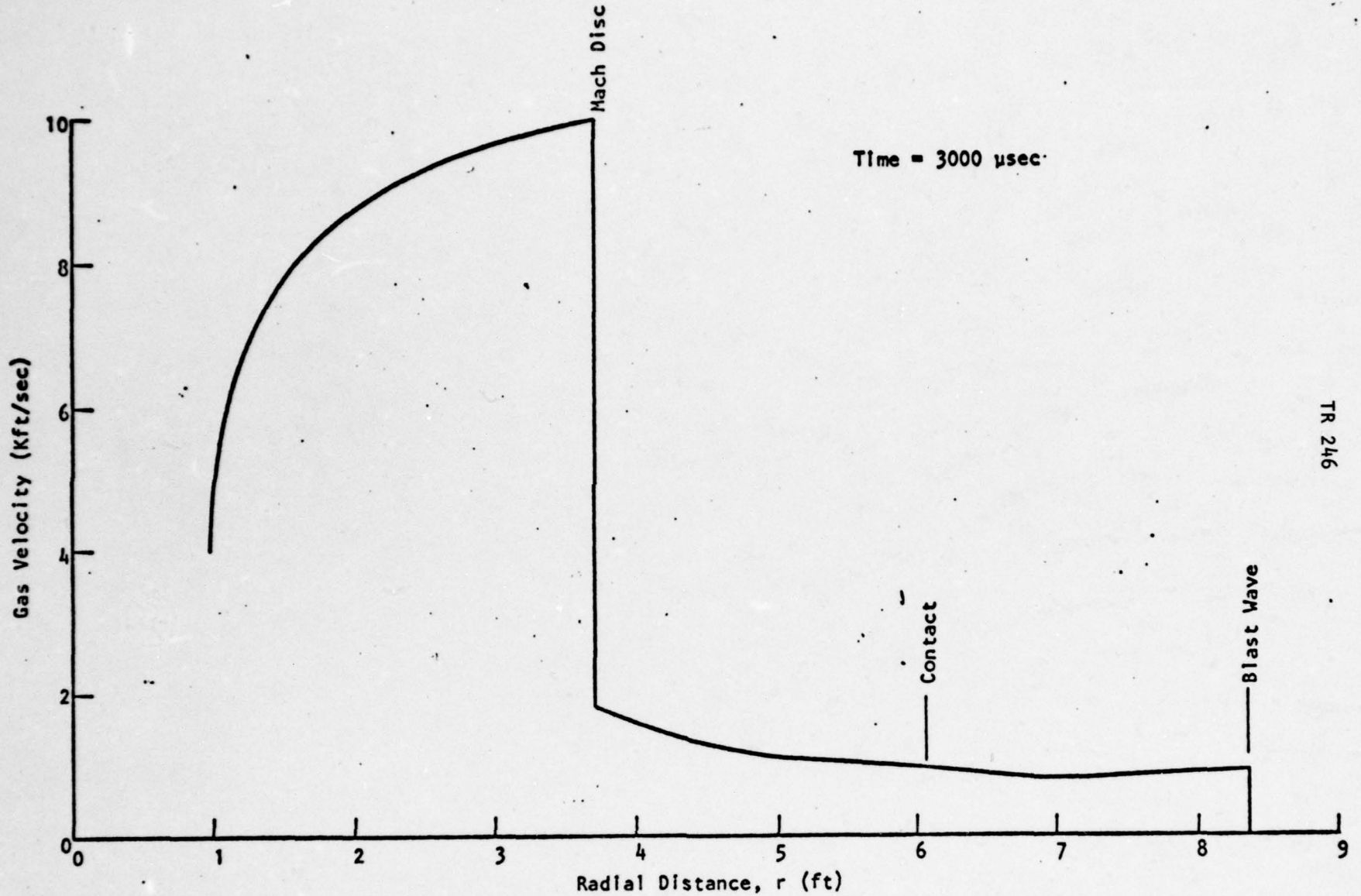

FIGURE 25. GAS VELOCITY DISTRIBUTION IN SPHERICAL BLAST FIELD

$$H_2O + N_2 = H + OH + N_2 \quad (64a)$$

$$OH + OH = H_2O + O \quad (64b)$$

$$O + OH = H + O_2 \quad (64c)$$

$$H + OH = O + H_2 \quad (64d)$$

$$CO + OH = CO_2 + H \quad (64e)$$

$$O_2 + N_2 = 2O + N_2 \quad (64f)$$

$$N_2 + O = NO + N \quad (64g)$$

$$NO + O = O_2 + N \quad (64h)$$

Rates for the collisional dissociation of H_2O and O_2 by N_2 impact were taken from Reference (12); the remaining rates were taken from Reference (13). The thermodynamic data for the constituent species was taken from Reference (14) and Reference (15).

For illustrative purposes, the chemical composition of the exhaust stream at the nozzle exit plane was taken from the study by Woodroffe[16]. Two cases were considered, designated as fuel rich and fuel lean; the mole fractions are listed in Table I. As mentioned earlier, the composition was assumed to be frozen from the nozzle exit plane to the Mach disc of the ground surface plume.

TABLE I

Assumed Chemical Composition of Nozzle Exhaust Stream By Mole Fraction (From Woodroffe, Reference (16)

Species	Fuel Lean	Fuel Rich
H_2O	.30	.10
H_2	.05	.25
CO_2	.30	.10
CO	.05	.25
N_2	.30	.30

The species mass fractions at the propellant side of the contact surface are shown as a function of time in Figures (26) and (27). The rapid variation during the first 10 μsec, together with the fact that $\Delta t_{chem}^{-1} >> \Delta t_{wave}^{-1}$, indicate that a near-equilibrium condition prevails initially and the anticipated freeze-out will develop later. Therefore, non-equilibrium chemistry should be included in the rocket nozzle and supersonic plume solutions. In addition, it may be more appropriate to initialize the shock layer with equilibrium, rather than frozen, species concentrations.

The variation of species concentration across the layer from the Mach disc to the contact surface at t = 254 μsec (for the fuel lean case) is shown in Figure (28). The corresponding temperature distribution is depicted in Figure (29). It is apparent that the reaction zone is just downstream of the Mach disc, with the flow equilibribrating as it approaches the contact surface. On the other hand, examining the complete temperature distribution across the shock layer, in Figure (30), it also is apparent that the contact surface is artificially separating the equilibrated propellant species from a surrounding "bath" of shock-heated air. Therefore, additional afterburning must be anticipated along the contact at a rate limited only by turbulent dilution of the mixture. The mixing problem is addressed in the following section. The present non-equilibrium chemical kinetic model is also an idealization in the sense that (a) the propellant exhaust products are assumed to consist of a mixture of relatively simple molecules such as water, hydrogen, carbon dioxide, carbon monoxide and nitrogen, and (b) the reaction scheme only includes collisional dissociation of water vapor and oxygen molecules by molecular nitrogen, a few representative hydroxyl radical reactions, and the Zeldovich reactions for atomic nitrogen production. Future effort should focus on expansion of the present basic reaction scheme to include all well-established reactions haveing a potentially measurable impact on the temperature and concentration of optically significant species, with a view toward quantifying the intensity and duration of the optical flash.

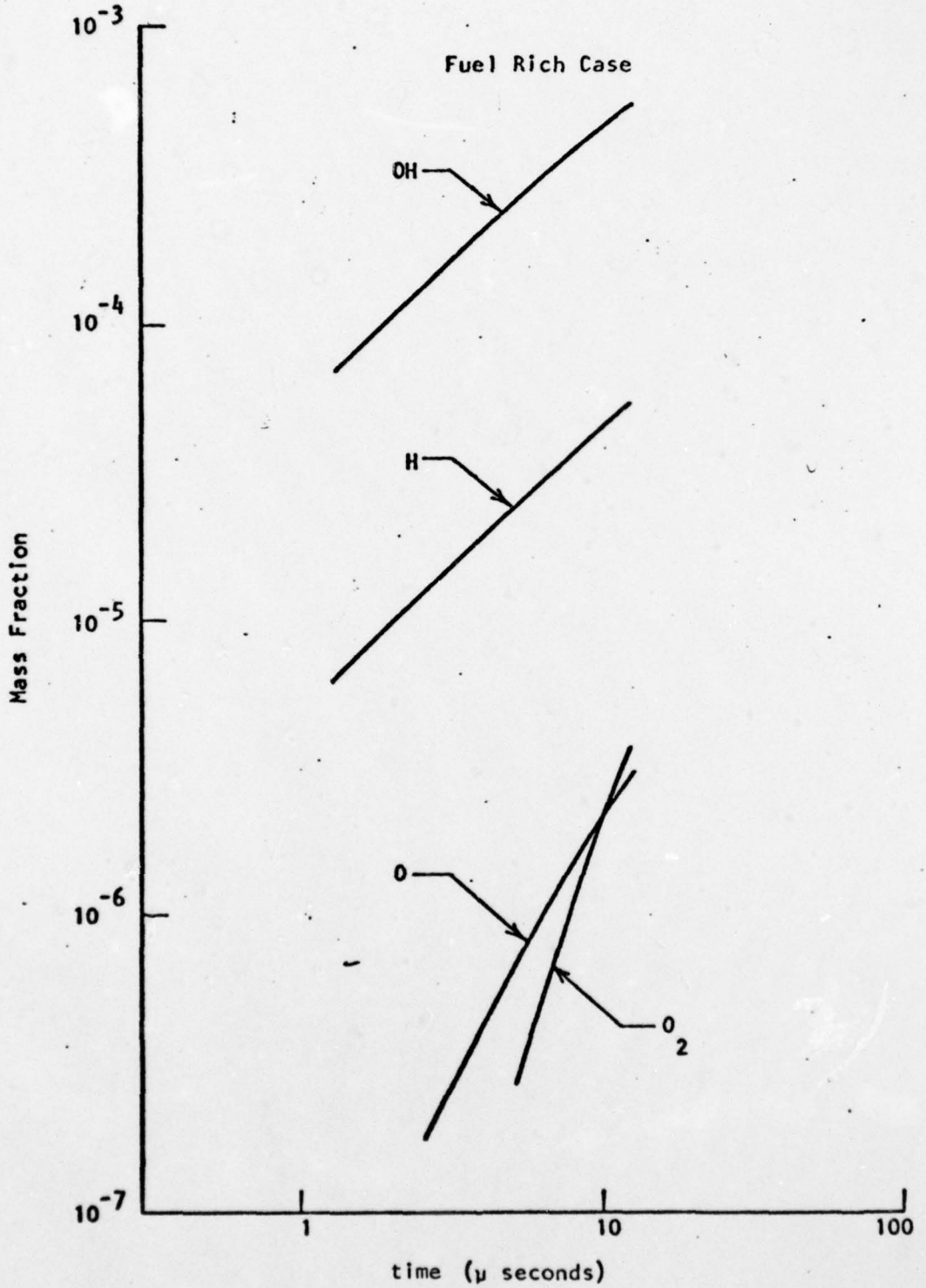

FIGURE 26. SPECIES MASS FRACTIONS AT THE PROPELLANT SIDE OF THE CONTACT AS A FUNCTION OF TIME (FUEL RICH CASE)

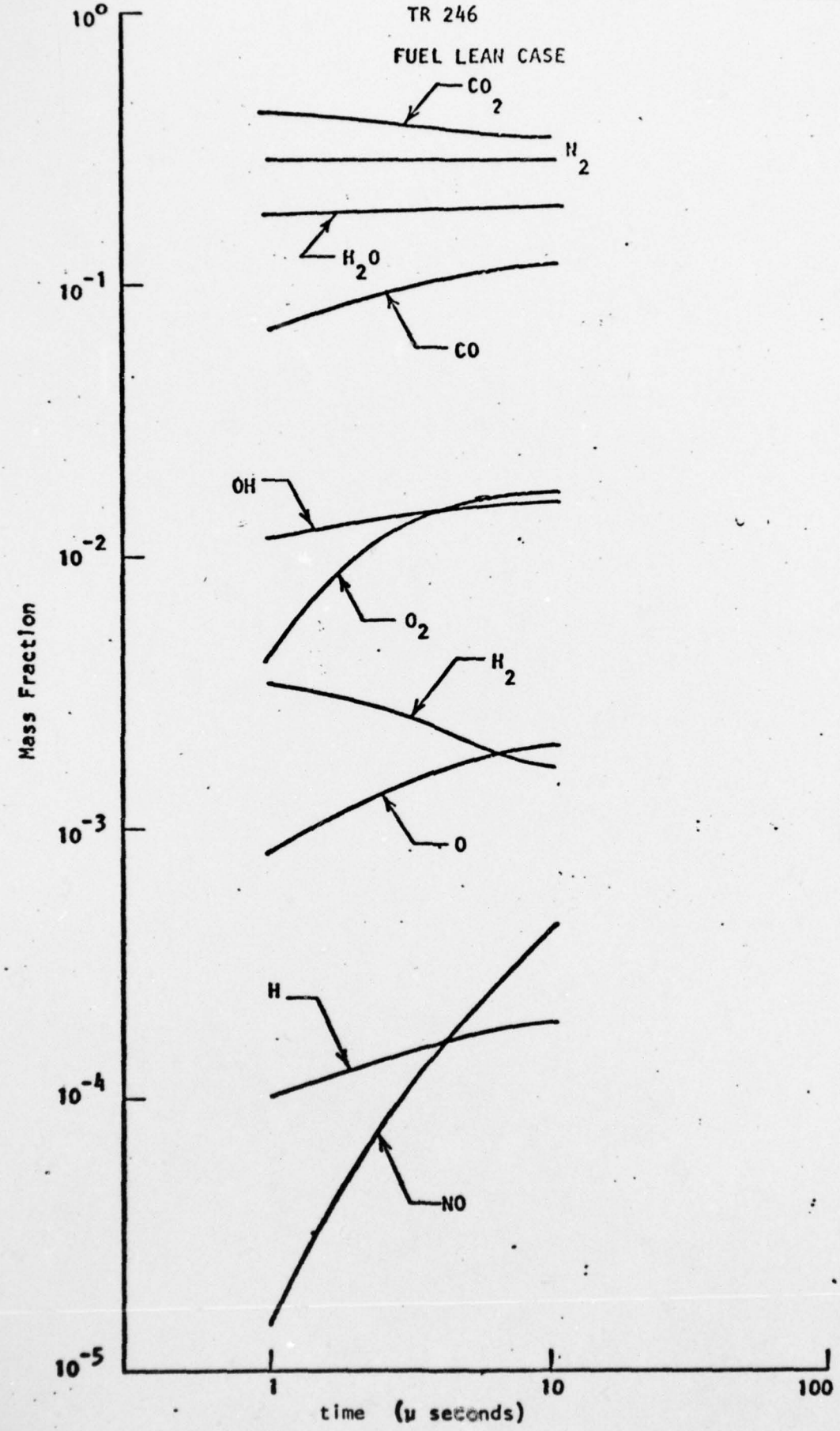

FIGURE 27. SPECIES MASS FRACTIONS AT THE PROPELLANT SIDE OF THE CONTACT AS A FUNCTION OF TIME (FUEL LEAN CASE)

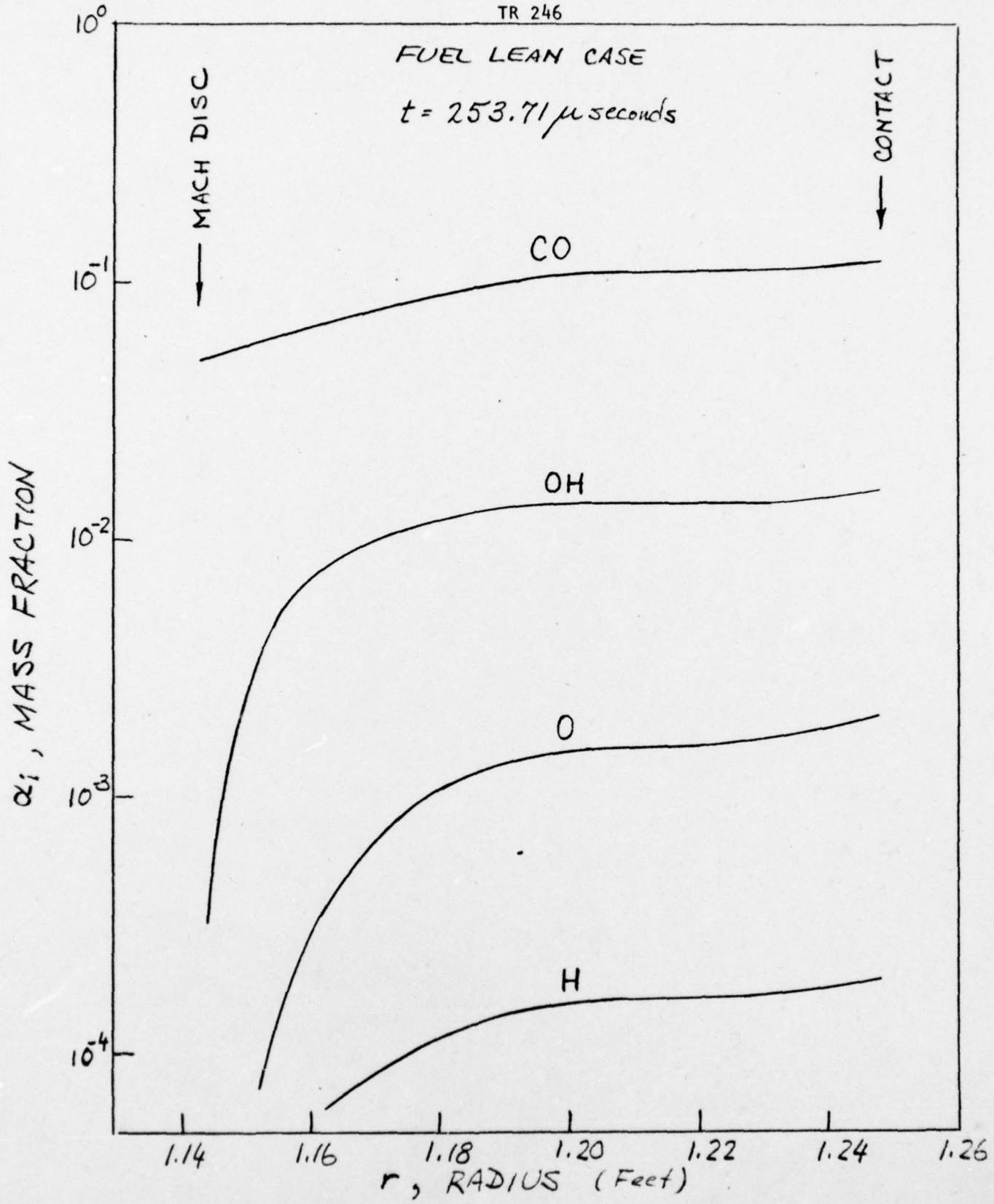

FIGURE 28. DISTRIBUTION OF SPECIES ACROSS THE PROPELLANT SIDE OF THE UNSTEADY SHOCK LAYER

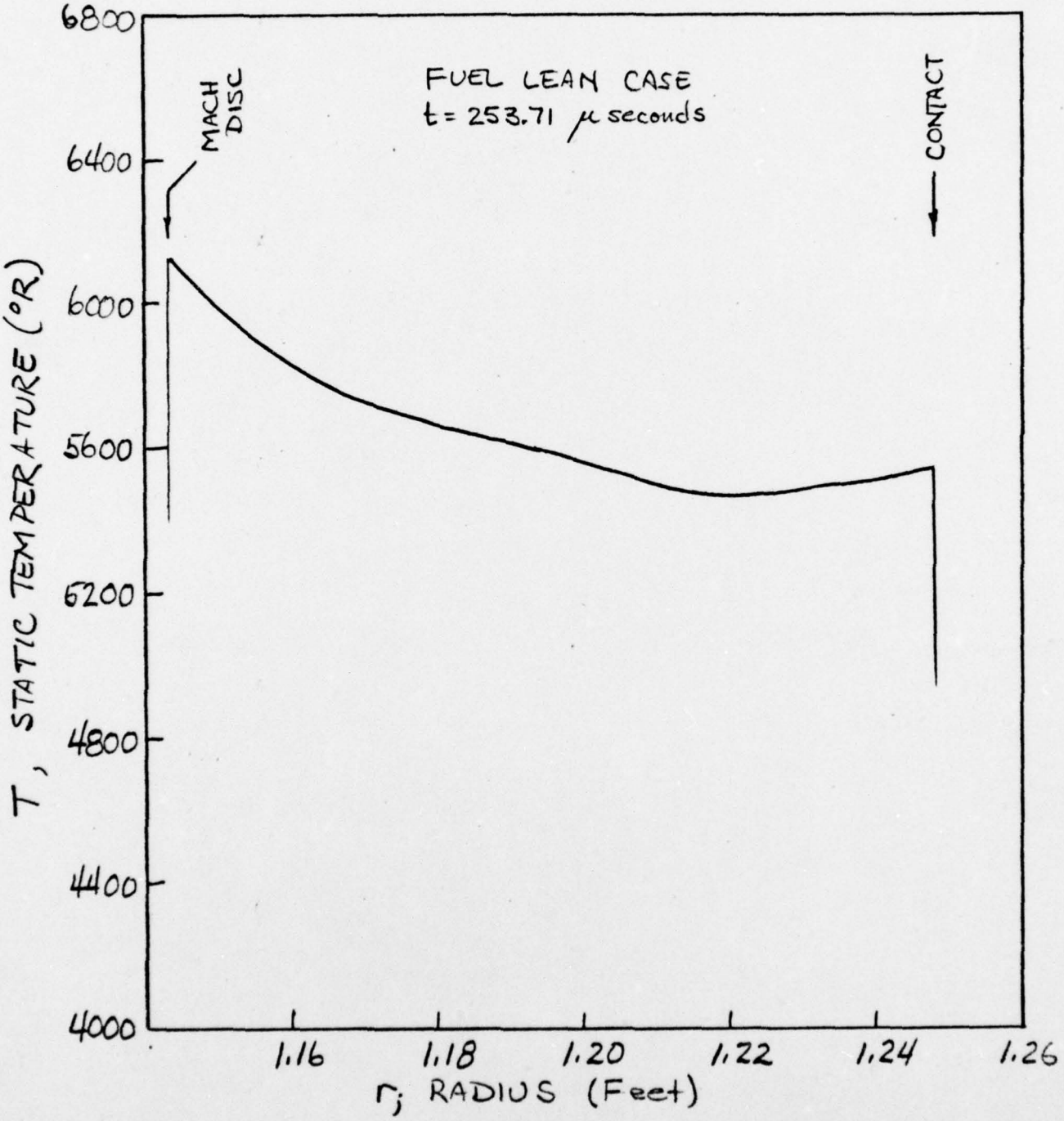

FIGURE 29. TEMPERATURE DISTRIBUTION ACROSS THE PROPELLANT SIDE OF THE UNSTEADY SHOCK LAYER

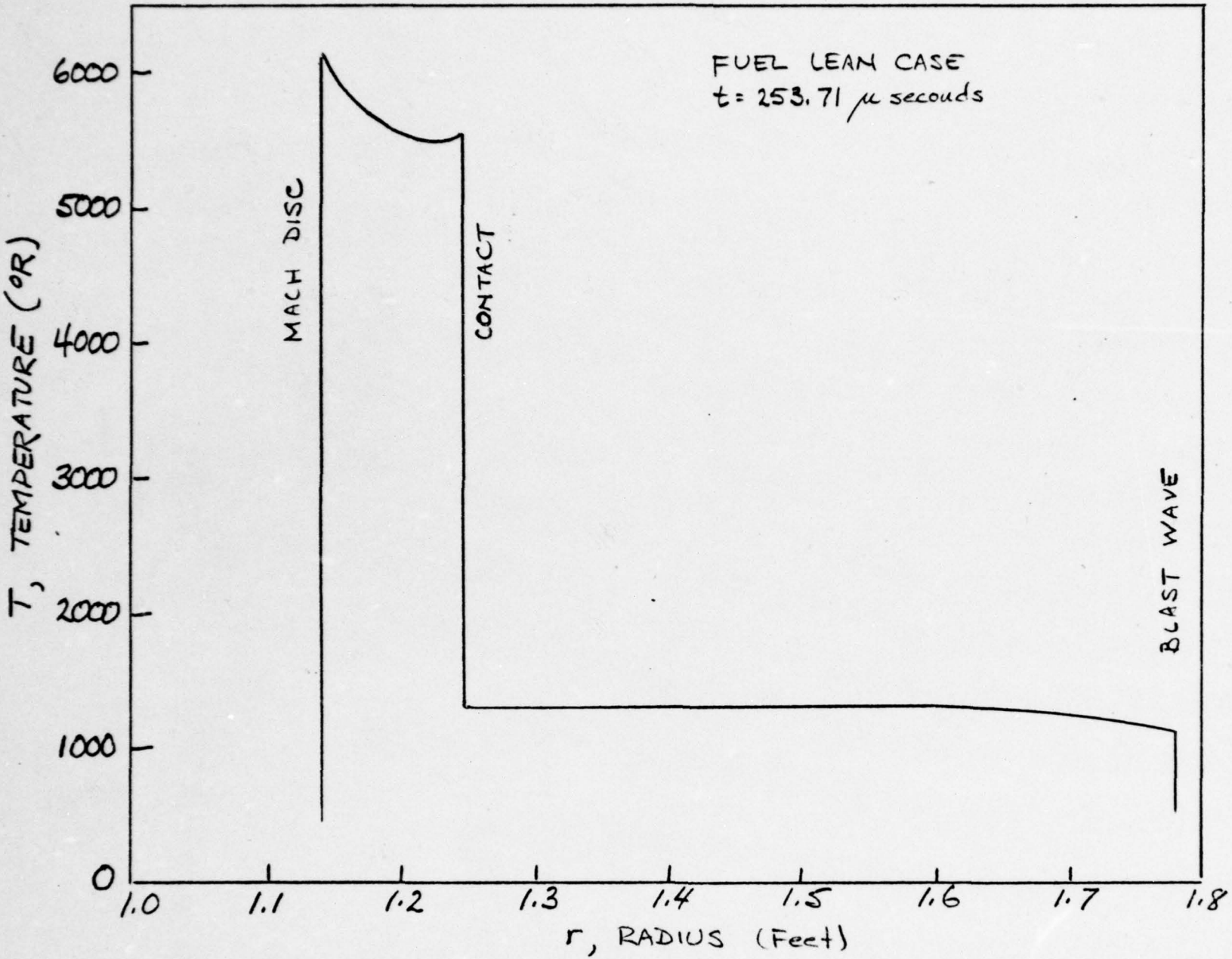

FIGURE 30. TEMPERATURE DISTRIBUTION ACROSS THE ENTIRE UNSTEADY SHOCK LAYER

VI. UNSTEADY TURBULENT MIXING LAYER

6.1 General Approach - Observations[8] of muzzle blasts show the presence of intense turbulence at very early stages of development of the flowfield, which eventually engulfs the entire propellant cloud. Press photographs of unclassified missile launches also exhibit the same sort of turbulent propellant cloud. (In retrospect, it could have been very interesting to examine movies of rocket launches to study the details at very early times following ignition.) However, the source of the turbulence is not identifiable from these observations. Among the possible sources are high frequency pressure oscillations originating in the combustion chamber, shear-induced turbulence along the lateral boundaries of the exhaust plume and/or ground surface plume, and Taylor instability[17] of the contact surface. The last mechanism is produced by acceleration of a light gas toward a heavy gas[17]. Thus, a spherical volume of hot, light gas (propellant gases) expanding into a heavier gas (air) should experience Taylor instability along its front (the contact surface). As previously noted, no velocity jump exists across the contact, but an extreme temperature jump is present. Therefore, the somewhat unconventional notion of thermally-driven turbulence production along the contact surface is suggested. If the ideas of similitude between heat and mass transfer, and of a turbulent Prandtl number, representing the ratio of eddy viscosity to eddy conductivity, near unity, are acceptable, then the idea of a similitude between an eddy viscosity produced by velocity gradients and an eddy conductivity produced by temperature gradients should be palatable. Although temperature fluctuations are conventionally regarded as the product of velocity fluctuations, it is suggested herein that the opposite may occur in the absence of shear forces as a driving mechanism for the production of velocity fluctuations.

The development of turbulence models and closure statements for steady boundary layer and wake (free mixing) type flows has been the subject of considerable research, cf., the review by Mellor and Herring (Reference 18). While extension of these models to unsteady flows is not conceptually difficult the experimental data base is considerably more meager. Unfortunately, most attention in the study of unsteady boundary layers has focussed on definition

and prediction of unsteady separation. In this regard, the subject problem provides an attractive framework for the study of free turbulent mixing since it is (at least approximately) two-dimensional (i.e., time and radius) and free of such complexities as laminar sublayers and separation. Furthermore, as shown in the preceding section, self-similar inviscid solutions describe the outer inviscid layer at early time (strong blast theory) and at late time (Whitham's asymptotic theory), which may be combined using the method of matched asymptotic expansions. The inner inviscid layer (between the Mach disc and contact) still appears to require numerical solution, although á posteriori examination of the available solutions suggests certain simplifying approximations may provide an adequate representation. Thus, the boundary conditions on the mixing layer along the contact surface are well defined both in terms of the present numerical solution and asymptotic theories.

Based on the observations of Baronti and Miller (Reference 19) for steady boundary layers and of Telionis (Reference 20) for unsteady boundary layers, integral methods continue to provide as good renditions of turbulent flows as do the more numerically detailed finite difference solutions. Therefore, a two layer (i.e., two-strip) integral method analysis of the subject free mixing problem is strongly suggested by both physical and pragmatic computational considerations. The physical interpretation of the proposed two layer model is indicated in Figure (31). The first layer δ_1 grows radially outward from the contact surface while the second layer δ_2 grows radially inward. The variations of elemental fractions of "propellant" (i.e., the sum of all propellant species) and of "air" (i.e., the sum of N_2 and O_2 from the air) are indicated in this sketch. The temperature distribution should follow roughly the curve shown for the "propellant" mass fraction. It is emphasized that the mixing layer model is formulated in a coordinate system fixed at the moving contact surface; thus the mean velocity is zero everywhere.

As mentioned above, the available data base for mixing layers of this type is rather meager. However, comparison shown in Figure (32) of the experimental observations by Schmidt and Shear[8] of the growth of the turbulent front along the axis of a muzzle blast, with the inviscid contact surface prediction by Erdos and Del Guidice[1] provides one set of data which can be interpretted as the

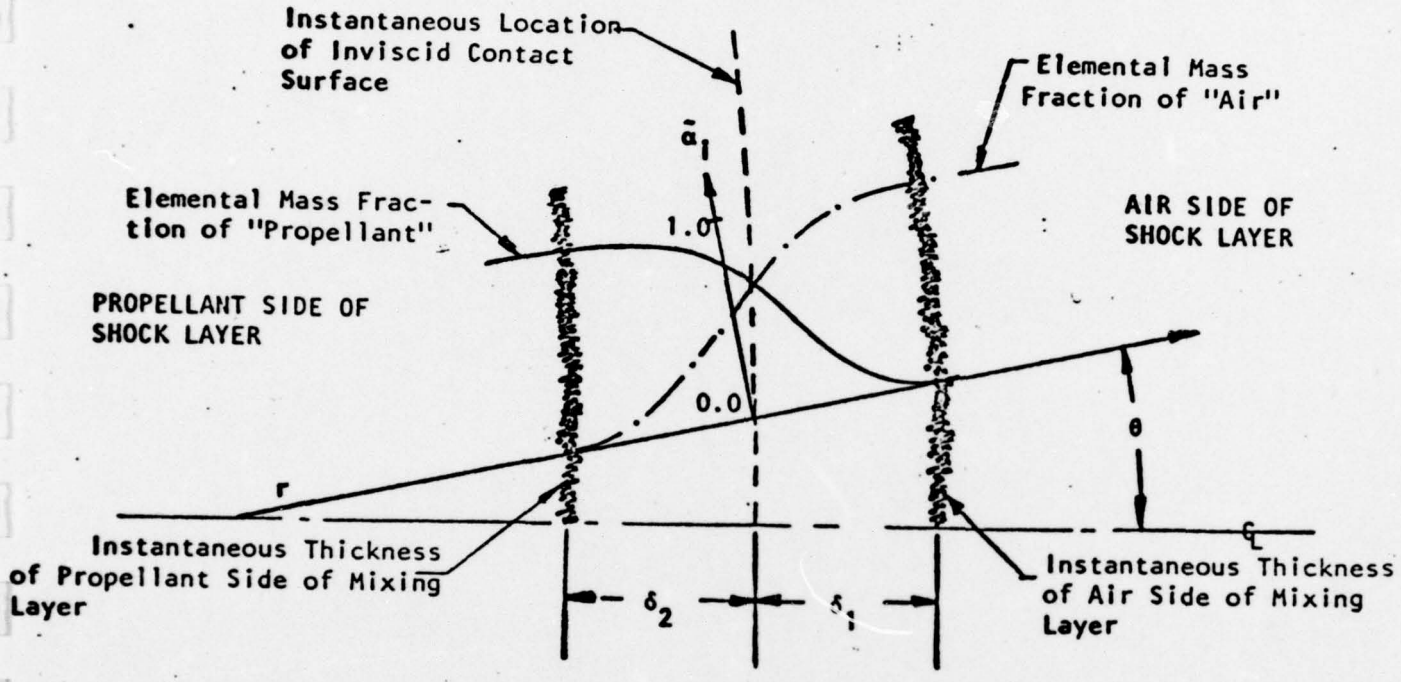

FIGURE 31. SCHEMATIC OF TWO-LAYER MODEL OF BLAST FIELD MIXING LAYER

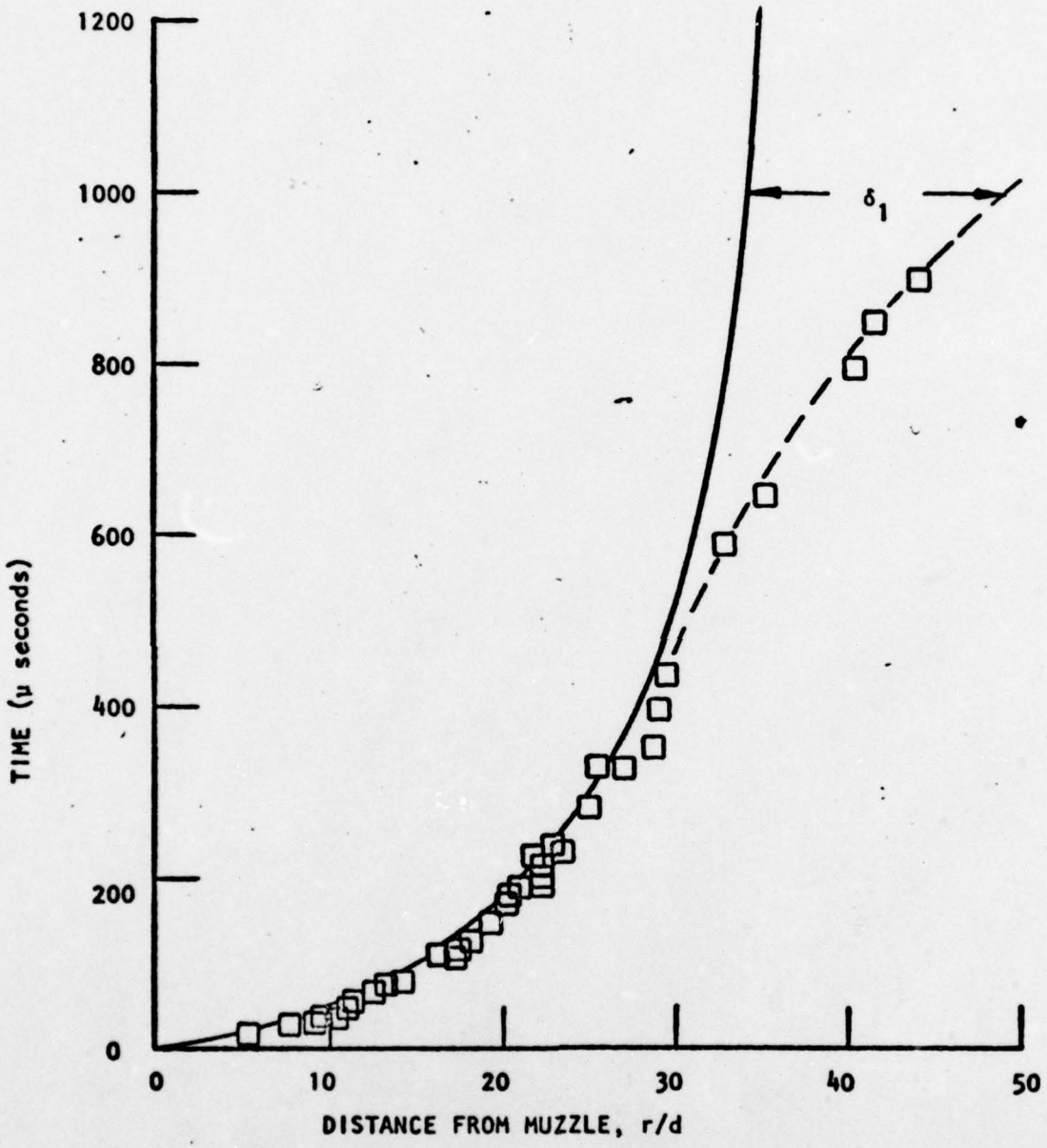

FIGURE 32. COMPARISON OF CALCULATED CONTACT SURFACE TRAJECTORY AND OBSERVED TURBULENT FRONT FOR 5.56 MM RIFLE MUZZLE BLAST

growth of δ_1. A corresponding observation of δ_2 is, however, totally obscured by the propellant cloud.

6.2 Formulation of a Turbulence Model - The turbulent kinetic energy (TKE) equation forms the basis of most of the widely accepted higher-order closure models now in use. The well-known term-by-term interpretation of this equation is included below:

$$\underset{\text{(convection)}}{\rho \frac{D\bar{k}}{Dt}} + \underset{\text{(production)}}{\rho\overline{u'v'}\frac{\partial U}{\partial y}} + \underset{\text{(diffusion)}}{\frac{\partial}{\partial y}\left(\rho\overline{v'k} + \overline{p'v'}\right)} + \underset{\text{(dissipation)}}{\mu\left(\frac{\partial u'}{\partial y}\right)^2} = 0 \tag{65}$$

where: $$\bar{k} = \frac{1}{2}\left(\overline{u'^2} + \overline{v'^2}\right) \tag{66}$$

(The need for a mean velocity gradient $\partial U/\partial y$ to drive the production of turbulent kinetic energy is clearly seen.)

Spaulding's[21] two-equation model of the TKE equation is one of the more widely employed closures:

$$\rho \frac{D\bar{k}}{Dt} - \mu_T \left(\frac{\partial U}{\partial y}\right)^2 - \frac{\partial}{\partial y}\left(\mu_T \frac{\partial \bar{k}}{\partial y}\right) + \rho\varepsilon = 0 \tag{67}$$

$$\rho \frac{D\varepsilon}{Dt} - C_1 \frac{\mu_T \varepsilon}{\bar{k}} \left(\frac{\partial U}{\partial y}\right)^2 - C_2 \frac{\partial U}{\partial y}\left(\mu_T \frac{\partial \varepsilon}{\partial y}\right) + C_3 \frac{\rho\varepsilon^2}{\bar{k}} = 0 \tag{68}$$

where $$\mu_T = C_o \rho \bar{k}^2/\varepsilon \tag{69}$$

The 4 constants C_0, C_1, C_2 and C_3 have been selected by Spaulding[21] to provide the best agreement with the data base for steady turbulent boundary layers (mainly incompressible):

$$C_0 = .09 \qquad C_2 = 1.43$$
$$C_1 = .77 \qquad C_3 = 1.92 \tag{70}$$

Obviously, since $\partial U/\partial y = 0$ in the present problem, the necessary production mechanism is absent in the TKE equation, and therefore also in the Spaulding closure model. However, application to the thermal energy (or heat balance) equation of procedures analogous to those used to derive the TKE equation yields[22,23] a turbulent thermal energy (TTE) equation, having a similar term-by-term interpretation:

$$\underset{\text{(convection)}}{\frac{D\overline{\theta^2}}{Dt}} + \underset{\text{(production)}}{2\rho\,\overline{v'\theta}\,\frac{\partial \bar{T}}{\partial y}} + \underset{\text{(diffusion)}}{\frac{\partial}{\partial y}\left(\overline{\rho v'\theta^2}\right)}$$

$$+ \underset{\text{(molecular transport and smearing)}}{\frac{\mu}{Pr}\left(\overline{\frac{\partial^2\theta^2}{\partial y^2}} + 2\,\overline{\left(\frac{\partial\theta}{\partial y}\right)^2}\right)} = 0 \tag{71}$$

where: $$\overline{\theta^2} = \overline{(\bar{T} - T)^2} \tag{72}$$

A two-equation closure model can be defined by analogy with the above TKE closure model:

$$\rho\,\frac{D\overline{\theta^2}}{Dt} - k_T\left(\frac{\partial T}{\partial y}\right)^2 - \frac{\partial}{\partial y}\left(k_T\,\frac{\partial\overline{\theta^2}}{\partial y}\right) + \rho\phi = 0 \tag{73}$$

$$\rho\,\frac{D\phi}{Dt} - C_1\,\frac{k_T\phi}{\overline{\theta^2}}\left(\frac{\partial T}{\partial y}\right)^2 - C_2\,\frac{\partial}{\partial y}\left(k_T\,\frac{\partial\phi}{\partial y}\right) + C_3\rho\,\frac{\phi^2}{\overline{\theta^2}} = 0 \tag{74}$$

where: $$k_T = C_0\,\rho\,C_p\,\left(\overline{\theta^2}\right)^{3/2}\cdot/\phi \tag{75}$$

Since no data base is available with which to calibrate the constants C_0, C_1, C_2 and C_3, Spalding's[21] values, given by Equation (70), for the TKE closure have been adopted. If the assumed analogy between turbulent transport of heat

and mass exists, these values should be at least approximately correct.

6.3 Method of Solution - The system of equations consists of the statements of conservation of mass, energy and species, the two-equation TTE model, and an equation of state. For the present discussion, the species equation can be dropped and a single-component perfect gas assumed for illustrative purposes. The system can then be stated consisely by:

$$L(f) = B \tag{76}$$

where

$$L = \frac{\partial}{\partial t} + v\frac{\partial}{\partial y} - A\frac{\partial}{\partial y}\left(k_T \frac{\partial}{\partial y}\right) \tag{77}$$

$$f = [\rho, T, \overline{\theta^2}, \phi] \tag{78}$$

$$A = [0, \rho^{-1}, \rho^{-1}, C_2\rho^{-1}] \tag{79}$$

$$B = \left[-\rho\frac{\partial v}{\partial y}, \frac{1}{\rho C_p}\frac{\partial p}{\partial t}, \left(\frac{k_T}{\rho}\left(\frac{\partial T}{\partial y}\right)^2 - \phi\right), \left(C_1\frac{k_T\phi}{\rho\overline{\theta^2}}\left(\frac{\partial T}{\partial y}\right)^2 - C_3\phi^2/\overline{\theta^2}\right)\right] \tag{80}$$

(Note that y is measured outward from the contact surface and v is the mean velocity component in the y direction produced by the turbulent heat conduction. Since spherical symmetry has been assumed there are no gradients along the contact surface or velocity component parallel to it.)

Following standard procedures, the first two components of the system represented by Equations (76) through (80), namely the continuity and energy equation, can be integrated from y = 0 to y = δ_1 (t) and from y = 0 to δ_2 (t), yielding:

$$v_i = \frac{d\delta_i}{dt} - \frac{1}{\rho_i}\frac{d}{dt}\int_0^{\delta_i}\rho\, dy \tag{81}$$

and $$\rho_i T_i \frac{d\delta_i}{dt} + \frac{\delta_i}{C_p}\frac{dp}{dt} = \rho_i v_i T_i + \frac{d}{dt}\int_o^{\delta_i} \rho T\, dy + \left(k_T \frac{\partial T}{\partial y}_o\right) \tag{82}$$

where $(\ )_o$ denotes $y = 0$ (i.e., at the contact surface), $i = 1$ and 2 denotes values at $y = \delta_1$ and $y = \delta_2$ respectively, and $(\partial/\partial y)_1 = (\partial/\partial y)_2 = 0$ is assumed, in accord with standard practice for first order boundary layer theory. Substituting Equations (81) into (82) gives:

$$\frac{d}{dt}\int_o^{\delta_i} \rho T\, dy = T_i \frac{d}{dt}\int_o^{\delta_i} \rho dy = \frac{\delta_i}{C_p}\frac{dp}{dt} - \left(k_T \frac{\partial T}{\partial y}\right)_o \tag{83}$$

Utilizing the perfect gas equation of state the first term in Equation (83) becomes:

$$\frac{d}{dt}\int_o^{\delta_i} \rho T\, dy = \left(p \frac{d\delta_i}{dt} + \delta_i \frac{dp}{dt}\right)\Big/ R \tag{84}$$

Assume:

$$\frac{\rho - \rho_1}{\rho_2 - \rho_1} = \frac{1}{2}(1 + \cos \pi\eta) \tag{85}$$

where

$$\eta = (y - \delta_2)/(\delta_1 - \delta_2) \tag{86}$$

Then:

$$\left(p \frac{d\delta_i}{dt} + \delta_i \frac{dp}{dt}\right)\Big/ R - T_i \frac{d}{dt}\left(\frac{\rho_1 + \rho_2}{2}\right)\delta_i - T_1 \frac{d}{dt}\left(\frac{\rho_1 - \rho_2}{2}\right)\left(\frac{\delta_1 - \delta_2}{\pi}\right) = \frac{\delta_i}{C_p}\frac{dp}{dt} - \left(k_T \frac{\partial T}{\partial y}\right)_o \tag{87}$$

If p, ρ_1 and ρ_2 are prescribed functions of time, from the inviscid solution, then Equation (87) provides two equations (i = 1 and 2) for two unknowns, δ_1 and δ_2, in terms of the turbulent heat conduction rate across the contact surface, $(k_T\ \partial T/\partial y)_o$. Thus, it is only necessary to evaluate k_T at y = 0, using the last two components of the system represented by Equations (76) through (80). However, it is necessary to assume distribution functions for $\overline{\theta^2}$ and ϕ; the following have been selected.

$$\overline{\theta^2} = \overline{\theta_o^2}\ (1 - \cos 2\pi\ \eta)/2 \tag{88}$$

$$\phi = \phi_o\ (1 - \cos 2\pi\ \eta)/2 \tag{89}$$

Therefore, the two-equation TTE model becomes:

$$\frac{d\overline{\theta_o^2}}{dt} = -\frac{k_{T_o}}{\rho_o}\ \frac{2\pi^2\ \overline{\theta_o^2}}{(\delta_1-\delta_2)^2} + \frac{k_{T_o}}{\rho_o}\ \left(\frac{\partial T}{\partial y}\right)_o^2 - \phi_o \tag{90}$$

$$\frac{d\phi_o}{dt} = -C_1\ \frac{k_{T_o}}{\rho_o}\ \frac{2\pi^2\ \overline{\phi_o^2}}{(\delta_1-\delta_2)^2} + C_2\ \frac{k_{T_o}}{\rho_o}\ \frac{\phi_o}{\overline{\theta_o^2}}\ \left(\frac{\partial T}{\partial y}\right)_o^2 - C_3\ \phi_o^2/\overline{\theta_o^2} \tag{91}$$

where

$$\left(\frac{\partial T}{\partial y}\right)_o = \frac{p}{R\rho_o^2}\ \left(\frac{\rho_2-\rho_1}{2}\right)\ \frac{\pi}{(\delta_1-\delta_2)} \tag{92}$$

Thus, Equations (87), (90) and (91) represent 4 ordinary differential equations in 4 unknowns, δ_1, δ_2, $\overline{\theta_o^2}$ and ϕ_o. However, due to the present assumption of a single component perfect gas, $\delta_2 = -\delta_1$ necessarily follows; accordingly, Equation (87) need be solved only for δ_1, reducing the system

to 3 ODE's. A standard 4th order Runge-Kutta integration method has been used to integrate the system, given appropriate initial conditions.

6.4 Numerical Solution - The conditions corresponding to the muzzle blast data of Schmidt and Shear[8] shown in Figure (32) were selected to test the model. The initial conditions were determined from a laminar solution of the heat condition problem:

$$T = \tfrac{1}{2}(T_2-T_1)\ [\,1 + \mathrm{erf}\ y/(2\sqrt{\nu t})\,)] \tag{93}$$

Using $T = 0.995\ (T_2-T_1)$ to define δ_1 gives a laminar solution:

$$\delta_1 = 3.65\sqrt{\nu t} \tag{94}$$

The laminar viscosity, specific heat and Prandtl number were then used to estimate an initial value of k_{T_o}. Consequently, it was only necessary to select arbitrarily the initial value of $\overline{\theta_o^2}$; fortunately, as will be shown, the growth rate of $\overline{\theta_o^2}$ is insensitive to arbitrarily small initial values of $\overline{\theta_o^2}$.

The transition time t at which the turbulent solution should be initiated was estimated at about 400 μsec. using the departure of the experimental data from the inviscid contact surface solution, shown in Figure (32). As demonstrated in Figure (33) the resulting solution for δ_1 is in reasonably good agreement with the experimental observations. (The last two data points represent the limit of the field of view; the arrows indicate that the turbulent front was somewhere beyond this distance.) However, by increasing the transition time to 500 μsec. the solution can be brought into virtually perfect agreement with the data, while by decreasing it to about 200 μsec. the growth of δ_1 is overestimated; note however that the comparison is made on a log-log plot. Fortunately, the dependence on assumed transition time diminishes with increasing time and vanishes asymptotically.

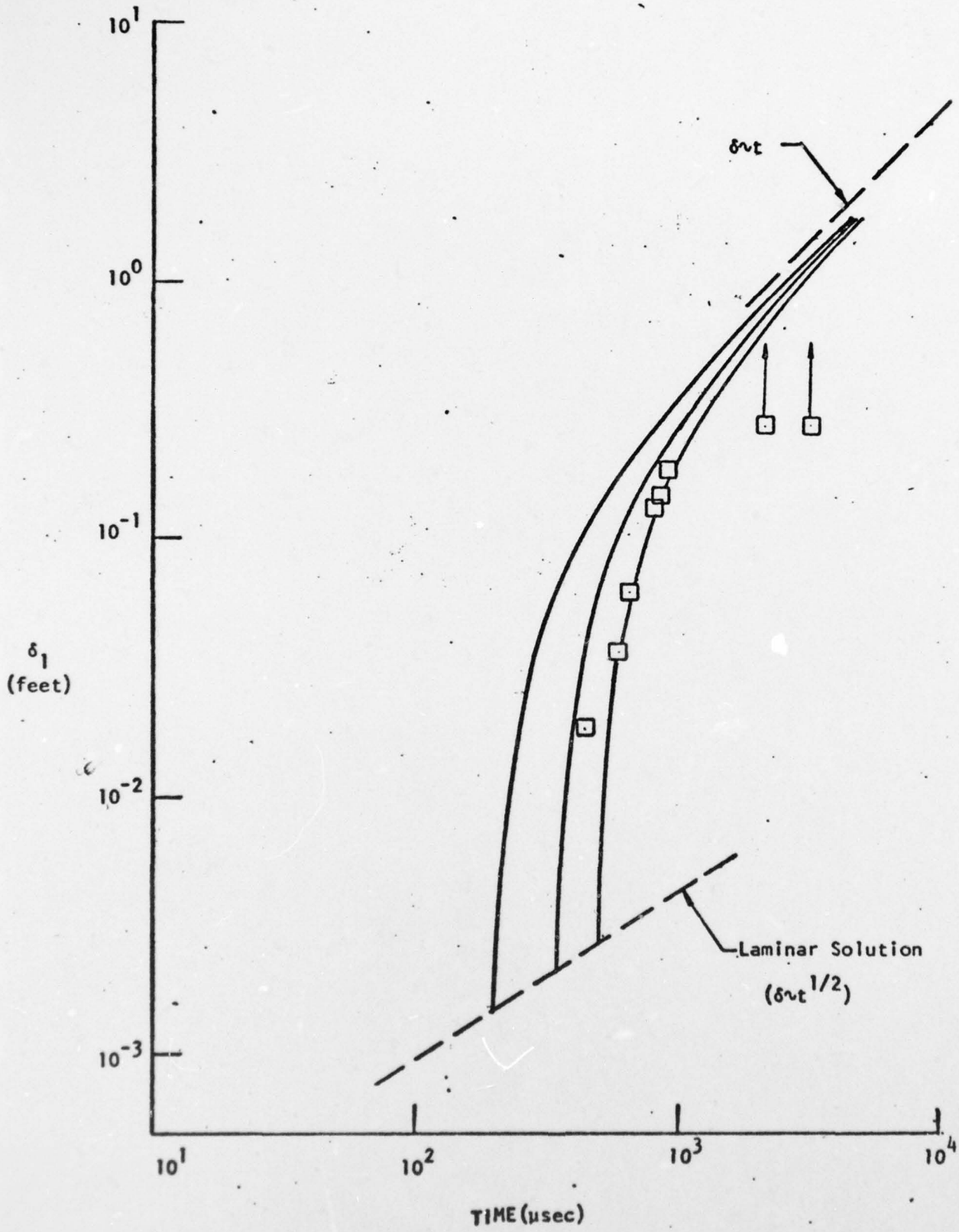

FIGURE 33. GROWTH OF TURBULENT FRONT

It can be seen from Figure (34) that the RMS temperature fluctuation $\sqrt{\theta_0^2}$ predicted by the present two-equation TTE model asymptotes to about 10% of the mean temperature $(T_1+T_2)/2$. Furthermore, the eddy conductivity K_T, as shown in Figure (35), appears to asymptotically approach a slowly varying function of the quantity $\rho(\delta_1-\delta_2)\sqrt{C_\rho(T_2-T_1)}$, which suggests that a classical eddy-viscosity or eddy-conductivity first-order closure model may be adequate (asymptotically) for this problem.

This numerical example and comparison with experimental data is regarded as confirming the validity of the present model. The extension to a chemically reacting mixture could proceed along the following line. Invoking a "turbulent Lewis number" to define the eddy diffusivity of the species, it is only necessary to add the species continuity equation, including the diffusion terms, to the present system. A species distribution function, similar to Equations (85) or (88) must be defined, e.g.,

$$\alpha_i = \alpha_{i_o} \quad (1-\cos 2\pi\eta)/2 + [\alpha_{i_1}\eta + (1-\eta)\alpha_{i_2}] \quad (1+\cos 2\pi\eta)/2 \qquad (95)$$

The species continuity equation need then be evaluated only at y=0, to determine α_{i_o}, requiring one additional ODE to be solved for each species in the reaction model. However, even with the relatively simple mechanism given by Equations (64a) through (64h), some eleven species and accordingly eleven additional equations are involved. Although the present integral method is computationally very efficient compared to, say, a finite difference scheme, it was not considered warranted in view of the exploratory nature of the study and the absence of comparative experimental data, to carry out any nonequilibrium chemistry examples.

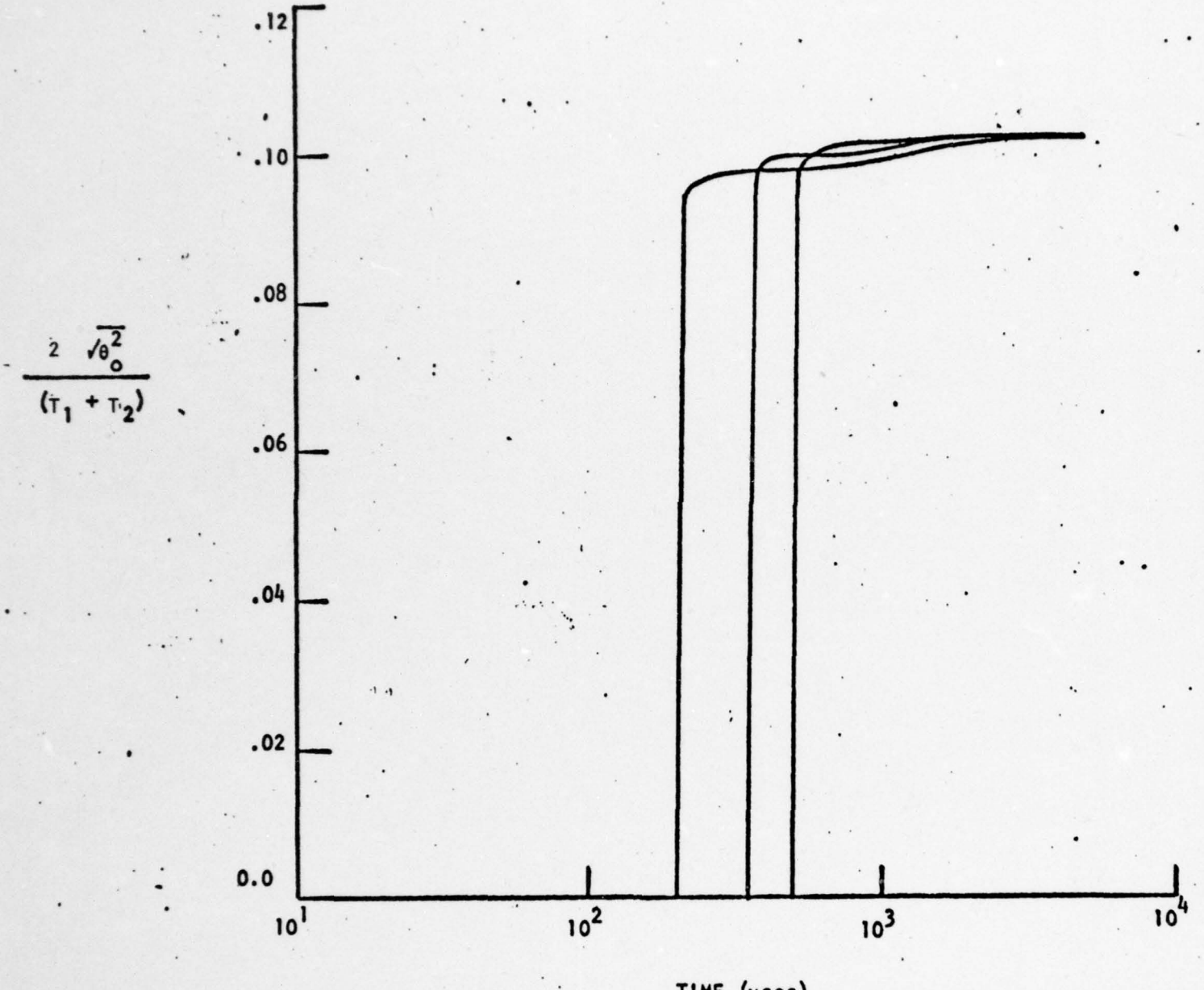

FIGURE 34. GROWTH OF RMS TEMPERATURE FLUCTUATIONS AT INTERFACE

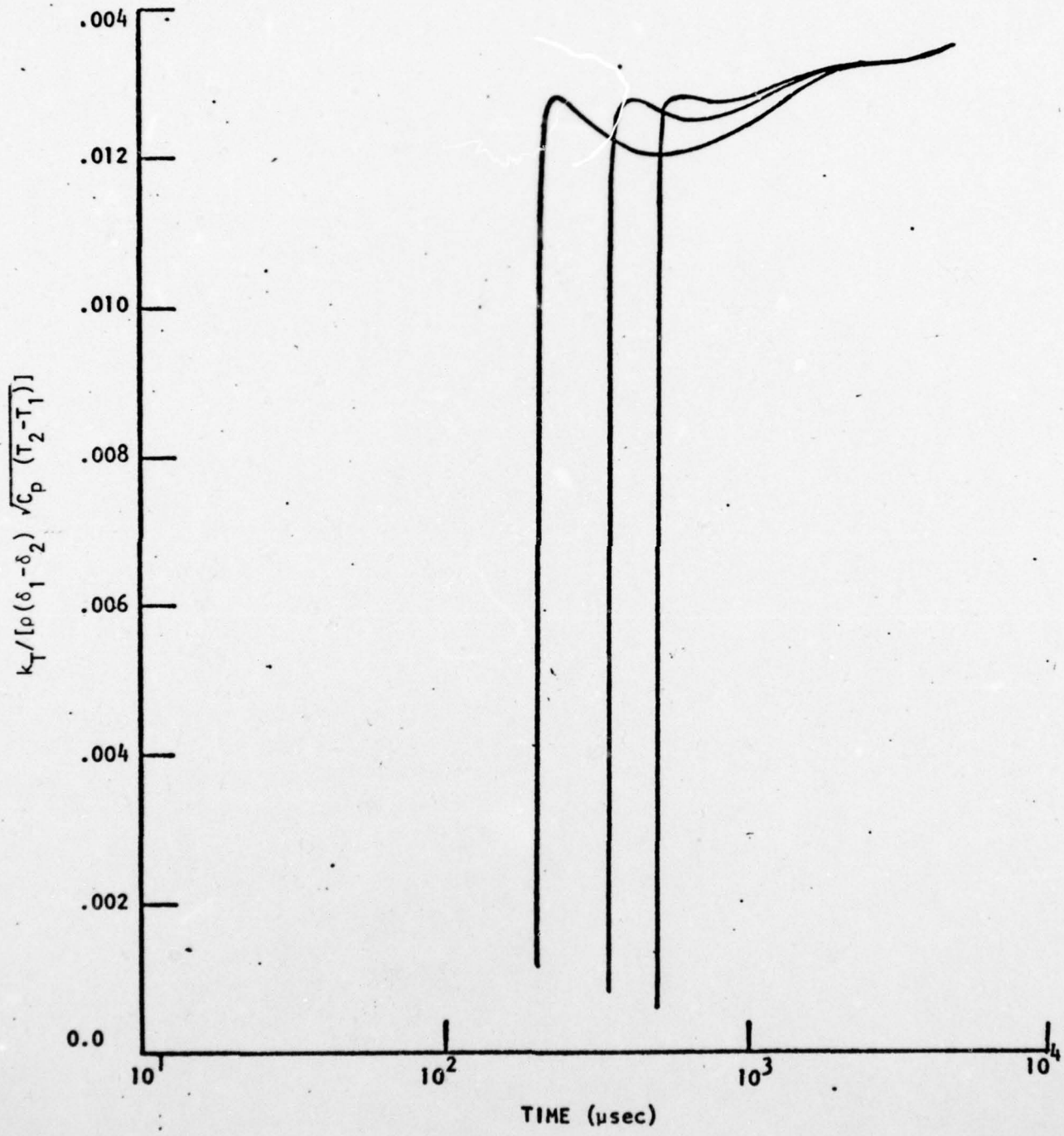

FIGURE 35. GROWTH OF EDDY CONDUCTIVITY

VII. CONCLUSIONS

Formation of an unsteady plume and blast field following ignition of a rocket motor has been described. It is pointed out that the supersonic plume which is believed to form along the ground surface initially expands (i.e., the Mach disc moves outward) as the blast over-pressure decays, but then later collapses (i.e., the Mach disc falls inward toward the origin) as the rate of energy deposition at the ground surface drops off. The rate and duration of energy deposition have been shown to be highly dependent on turbulent mixing in the steady exhaust stream of the rocket motor (prior to impingement on the ground) for low acceleration ($a < 2g$) launches. On the other hand, very simple inviscid flow approximations for the rate and duration of energy deposition appear appropriate for very high acceleration ($a > 20g$) launches. The net effect is to reduce the dependence of energy deposition on vehicle acceleration in the range of intermediate rates ($2g < a < 20g$). This quantitative assessment of viscous effects is, of course, somewhat dependent on the particular example considered which involved a single equivalent nozzle approximation for the exhaust stream of a multi-nozzle engine in the 2×10^6 N thrust category.

The asymptotic behavior of the blast field (for both $M_s \gg 1$ and $M_s \to 1$) has been examined, and the present numerical solution of the inviscid, unsteady flow between the blast wave and Mach disc has been shown to be in excellent agreement with asymptotic theory in both limits. The latter limit ($M_s \to 1$) provides the more stringent test of the numerics. Correlations of numerical solutions for the shock layer over-pressure and density distributions in terms of the Whitham variables are presented, and may in point of fact, be utilized in lieu of the numerical solution for $M_s < 1.1$.

The formulation of the numerical method of solution for the unsteady layers between the blast wave and contact surface and between the contact surface and Mach disc has been presented. Stability of the method subject to wave propagation and chemical rate limitations has been discussed. Interestingly, when both limitations are about equal, the maximum permissible time step is about one-half of that due to either individual limitation; only when the

two are of distinctly different magnitudes does one or the other dominate the stability of the system. An example is presented to characterize the pressure and temperature field. The persistence of a major temperature jump across the contact surface is emphasized, as well as the absence of a velocity jump. The possibility that the temperature jump, or more specifically the associated density jump, could produce a Taylor instability of the contact surface is pointed out.

Extension of the fluid dynamic model to include nonequilibrium chemical reactions has been discussed. Several numerical examples are presented to illustrate the thermochemical characteristics of the flow field. The assumption of a freeze out of chemical reactions from the nozzle exit to the ground surface plume Mach disc has been shown to be suspect. In the absence of mixing across the contact surface, the reactions may be expected to equilibrate on the time scale of the subject problem. However, vigorous afterburning of the propellant gases may be anticipated as turbulent mixing entrains shock-heated air into the propellant gas cloud. The afterburning (and attendant optical flash) will, therefore, probably be mixing-controlled, but the possibility of chemical non-equilibrium in the mixing layer in its early stages should be considered.

An unsteady turbulent mixing layer analysis has been developed to describe conduction and diffusion across the contact surface. The temperature gradient is assumed to be the driving mechanism for the production of turbulent thermal energy (RMS temperature fluctuations). A two-equation closure model for the turbulent thermal energy (TTE) is proposed, by analogy with Spaulding's two-equation model for the turbulent kinetic energy (TKE) equation. A two strip integral method solution for the mixing layer has been developed. Growth of the mixing layer thickness is found to be in excellent agreement with experimental observations of a muzzle blast flow field. Extension of the method to a chemically reacting system has been outlined.

A complete description of the unsteady plume and blast field evolution following ignition and (vertical) launch of a rocket has been presented. The methodology for quantitative analysis of the blast over-pressure, afterburning

of the propellant gases, and associated optical flash, subject to the principal assumption of spherical symmetry, has been developed. However, the considered processes represent only the initial formation of the propellant gas cloud at the ground surface following lift-off. The ultimate motion and dispersion of this propellant gas cloud will result from the combined effects of buoyancy and winds, which have not been considered in this study.

VIII. ACKNOWLEDGEMENT

The author is pleased to acknowledge the assistance of Mr. John Ranlet, now with the Brookhaven National Laboratories, in the conduct of this study and in particular for the rapid but careful development of the necessary computer codes.

Capt. Lloyd R. Lawrence, Jr., USAF, served as Program Manager at the inception of this study, and Major Thomas C. Meier, USAF, continued as Program Manager through its completion. The guidance, encouragement and patience of these gentlemen has been deeply appreciated, and is acknowledged with pleasure.

REFERENCES

1. Erdos, J. I. and Del Guidice, P. D., "Calculation of Muzzle Blast Flowfields," AIAA Journal, Vol. 13, August 1975, pp. 1048-1055.

2. Ranlet, J. and Erdos, J., "Muzzle Blast Flowfield Calculations," BRL-CR-207, U. S. Army Ballistics Research Laboratory, April 1976.

3. Dabora, E. K., "Variable Energy Blast Waves," AIAA Journal, Vol. 10, No. 10, pp. 1384-1385, October 1972.

4. Whitham, G. B., "The Propagation of Spherical Blast," Proc. Roy. Soc. (London) A203, pp. 571-581.

5. Kooker, D. E. and Zinn, B. T., "Triggering Axial Instabilities in Solid Rockets: Numerical Predictions," AIAA Paper No. 73-1298, November 1973.

6. Sterrett, J. R. and Barber, J. B., "A Theoretical and Experimental Investigation of Secondary Jets in a Mach 6 Free Stream with Emphasis on the Structure of the Jet and Separation Ahead of the Jet," AGARD Conf. Proc. No. 4, Separated Flows, May 1966.

7. Dash, S., Boccio, J. and Weilerstein, G., "A Computational System for the Prediction of Low Altitude Rocket Plume Flowfields," GASL TR 239, December 1976.

8. Schmidt, E. M. and Shear, D. D., "Optical Measurement of Muzzle Blast," AIAA Journal, Vol. 13, pp. 1088-1093, August 1975.

9. MacCormack, R. W., "Numerical Solution of the Interaction of a Shock Wave with a Laminar Boundary Layer, " Lecture Notes in Physics, Vol. 8, Springer-Verlag, pp. 151-163, (1971).

10. Cheng, S. I., "Numerical Integration of Navier-Stokes Equations," AIAA Journal, Vol. 8, No. 12, pp. 2115-2122, December 1970.

11. Anderson, J. D., Jr., "A Time-Dependent Analysis for Vibrational and Chemical Nonequilibrium Nozzle Flows," AIAA Journal, Vol. 8, No. 3, pp. 545-550, March 1970.

12. Bahn, G. S., Reaction Rate Compilation for the H-O-N System, Gordon and Breach Science Publ. NY (1968).

13. Baulch, D.L., Drysdale, D. D. and Lloyd, A. C., "Critical Evaluation of Rate Data," University of Leeds, May 1968 through July 1970.

14. Moretti, G., "A New Technique for the Numerical Analysis of Non-equilibrium Flows," AIAA Journal, Vol. 3, No. 2, pp. 223-229, February 1965.

15. McBride, B. J., Heimel, S., Ehlers, J. G. and Gordon, S., "Thermodynamic Properties to 6000°K for 210 Substances Involving the First 18 Elements," NASA SP-3001, (1963).

REFERENCES (Continued)

16. Woodroffe, J. A., "One-dimensional Model for Low Altitude Rocket Exhaust Plumes," AIAA Paper No. 75-244, January 1975.

17. Taylor, G. I., "The Instability of Liquid Surfaces When Accelerated in a Direction Perpendicular to Their Planes," Proc. Royal Society, A, Vol. CCI, pp. 192-196, (1950).

18. Mellor, G. L. and Herring, H. H., "A Survey of the Mean Turbulent Field Closure Models," AIAA J. 11, 5, pp. 590-599, (1973).

19. Baronti, P. and Miller, G., "Integral Solution of the Turbulent Energy Equation," AIAA J. 12, 1, pp. 108-110, (1974).

20. Telionis, D. P., "Calculations of Time-dependent Boundary Layers," Proc. Conf. on Unsteady Aerodynamics, University of Arizona, March 18-20, 1975.

21. Launder, B. E., Morse, E., Rodi, W. and Spalding, D. B., "Prediction of Free Shear Flows - A Comparison of the Performance of Six Turbulence Models," published in Free Turbulent Shear Flows, Volume 1 - Conference Proceedings, NASA SP-321, July 1972.

22. Corrsin, S., "Heat Transfer in Isotropic Turbulence," Journal Appl. Phys. Vol. 23, pp. 113-118, (1952).

23. Johnson, D. S., "Velocity and Temperature Fluctuation Measurements in a Turbulent Boundary Layer Downstream of a Stepwise Discontinuity in Wall Temperature," J. Appl. Mech. 325-336, September 1959.